

ออกซีเดทีฟดีไฮโดรจีเนชันของเอทานอลบนตัวเร่งปฏิกิริยาคอปเปอร์ ซิลเวอร์และลิเทียมบนอะลูมินา



บทคัดย่อและแฟ้มข้อมูลฉบับเต็มของวิทยานิพนธ์ตั้งแต่ปีการศึกษา 2554 ที่ให้บริการในคลังปัญญาจุฬาฯ (CUIR)
เป็นแฟ้มข้อมูลของนิสิตเจ้าของวิทยานิพนธ์ ที่ส่งผ่านทางบัณฑิตวิทยาลัย

The abstract and full text of theses from the academic year 2011 in Chulalongkorn University Intellectual Repository (CUIR)
are the thesis authors' files submitted through the University Graduate School.

วิทยานิพนธ์นี้เป็นส่วนหนึ่งของการศึกษาตามหลักสูตรปริญญาวิศวกรรมศาสตรมหาบัณฑิต
สาขาวิชาวิศวกรรมเคมี ภาควิชาวิศวกรรมเคมี
คณะวิศวกรรมศาสตร์ จุฬาลงกรณ์มหาวิทยาลัย
ปีการศึกษา 2559
ลิขสิทธิ์ของจุฬาลงกรณ์มหาวิทยาลัย

OXIDATIVE DEHYDROGENATION OF ETHANOL OVER Cu-AgLi/Al₂O₃ CATALYSTS

Miss Nasrada Sukarawan



A Thesis Submitted in Partial Fulfillment of the Requirements
for the Degree of Master of Engineering Program in Chemical Engineering

Department of Chemical Engineering

Faculty of Engineering

Chulalongkorn University

Academic Year 2016

Copyright of Chulalongkorn University

ณัฐรดา ศุภรธรรม : ออกซิเดทีฟดีไฮโดรจิเนชันของเอทานอลบนตัวเร่งปฏิกิริยาคอปเปอร์ซิลเวอร์และลิเทียมบนอะลูมินา (OXIDATIVE DEHYDROGENATION OF ETHANOL OVER Cu-AgLi/Al₂O₃ CATALYSTS) อ.ที่ปรึกษาวิทยานิพนธ์หลัก: ศ. ดร.บรรเจิด จงสมจิตร, 111 หน้า.

ในงานวิจัยนี้ได้ทำการศึกษาผลของอัตราส่วนโดยน้ำหนักของคอปเปอร์และซิลเวอร์ (คอปเปอร์ต่อซิลเวอร์ เท่ากับ 100:0, 70:30, 50:50, 30:70, 0:100) บนเฟสผสมของอะลูมินาตัวรองรับอะลูมินาซึ่งประกอบด้วยเฟสแกมมาและไคโนอัตราส่วนที่เท่ากันถูกเตรียมด้วยวิธีโซลโวลเทอรัมอล ตัวรองรับที่เตรียมได้ถูกนำมาเติมด้วยคอปเปอร์ ซิลเวอร์ (อัตราส่วนโดยน้ำหนัก 5 เปอร์เซ็นต์) และลิเทียม (อัตราส่วนโดยน้ำหนัก 0.7 เปอร์เซ็นต์) เพื่อเตรียมตัวเร่งปฏิกิริยาผ่านวิธีการเคลือบฝังแบบเปียก ความสามารถในการเร่งปฏิกิริยาของตัวเร่งปฏิกิริยาถูกวินิจฉัยผ่านปฏิกิริยาดีไฮโดรจิเนชันและออกซิเดทีฟดีไฮโดรจิเนชันของเอทานอลในเครื่องปฏิกรณ์แบบเบดที่อุณหภูมิ 200 ถึง 400 องศาเซลเซียส ณ ความดันบรรยากาศ ประสิทธิภาพในการเร่งปฏิกิริยาพบว่าตัวเร่งปฏิกิริยา Cu(0)Ag(100)Li/M-Al ให้ปริมาณอะเซทัลดีไฮด์สูงสุดและค่าการเกิดปฏิกิริยาของเอทานอลมากที่สุดในทุกอุณหภูมิการทำปฏิกิริยาผ่านปฏิกิริยาดีไฮโดรจิเนชันเพราะพื้นที่ผิวของตัวเร่งปฏิกิริยามีมากที่สุดและยังมีค่าความเป็นเบสทั้งหมดที่มาก โดยเฉพาะอย่างยิ่งค่าปริมาณอะเซทัลดีไฮด์มากที่สุดเกิดขึ้น ณ อุณหภูมิ 350 องศาเซลเซียสเท่ากับ 81 เปอร์เซ็นต์ ตัวเร่งปฏิกิริยานี้ยังแสดงค่าที่ดีเยี่ยมของการให้อะเซทัลดีไฮด์ผ่านปฏิกิริยาออกซิเดทีฟดีไฮโดรจิเนชันสูงสุด ณ อุณหภูมิ 300 องศาเซลเซียสเท่ากับ 92 เปอร์เซ็นต์ นอกเหนือจากนี้ตัวเร่งปฏิกิริยา Cu(30)Ag(70)Li/M-Al แสดงค่าการให้ปริมาณอะเซทัลดีไฮด์ที่อุณหภูมิต่ำที่สุดของอุณหภูมิที่ศึกษา ณ 250 องศาเซลเซียสโดยมีค่าการให้ปริมาณอะเซทัลดีไฮด์เท่ากับ 59 เปอร์เซ็นต์ ตลอดจนการศึกษาความเสถียรภาพของตัวเร่งปฏิกิริยาผ่านการทำปฏิกิริยานาน 10 ชั่วโมง ผลเปรียบเทียบระหว่างการเกิดปฏิกิริยาดีไฮโดรจิเนชันและออกซิเดทีฟดีไฮโดรจิเนชันแสดงถึงการเพิ่มแก๊สออกซิเจนสามารถป้องกันการเสื่อมสภาพของตัวเร่งปฏิกิริยาจากการเกิดคาร์บอนและการหลอมตัวของโลหะ ตัวเร่งปฏิกิริยา Cu(0)Ag(100)Li/M-Al ซึ่งทำปฏิกิริยาผ่านออกซิเดทีฟดีไฮโดรจิเนชัน ณ อุณหภูมิ 300 องศาเซลเซียสมีปริมาณการเกิดคาร์บอนน้อยที่สุดเมื่อเทียบกับตัวมันเองที่ทำปฏิกิริยาผ่านดีไฮโดรจิเนชัน ณ อุณหภูมิ 350 องศาเซลเซียสและตัวเร่งปฏิกิริยา Cu(30)Ag(70)Li/M-Al ที่ทำปฏิกิริยาผ่านออกซิเดทีฟดีไฮโดรจิเนชัน ณ อุณหภูมิ 250 องศาเซลเซียส

ภาควิชา วิศวกรรมเคมี ลายมือชื่อนิสิต

สาขาวิชา วิศวกรรมเคมี ลายมือชื่อ อ.ที่ปรึกษาหลัก

ปีการศึกษา 2559

5770173421 : MAJOR CHEMICAL ENGINEERING

KEYWORDS: COPPER / SILVER / ACETALDEHYDE PRODUCTION

NASRADA SUKARAWAN: OXIDATIVE DEHYDROGENATION OF ETHANOL OVER Cu-AgLi/Al₂O₃ CATALYSTS. ADVISOR: PROF. BUNJERD JONGSOMJIT, Ph.D., 111 pp.

In this research, the effect of copper and silver weight ratio (Cu:Ag of 100:0, 70:30, 50:50, 30:70, 0:100) supported on mixed-phase of Al₂O₃ catalysts was investigated. The mixture of equal phase between gamma- and chi-Al₂O₃ support was synthesized via the solvothermal method. The support was brought to loading with copper, silver (5 wt%), and lithium (0.7 wt%) that was prepared via incipient wetness impregnation technique. The catalytic activity was identified through the ethanol dehydrogenation and oxidative dehydrogenation reactions in packed-bed reactor at 200 to 400°C under atmospheric pressure. The performance in the reaction was found that Cu(0)Ag(100)Li/M-Al showed the highest acetaldehyde yield and ethanol conversion in all reaction temperatures of dehydrogenation reaction study because of its high specific surface area and the large amount of total basicity. Especially, the highest acetaldehyde yield of 81% existed at 350°C. This catalyst also displayed the excellent value of acetaldehyde yield in oxidative dehydrogenation that given the highest yield at 300°C of 92%. In addition, Cu(30)Ag(70)Li/M-Al showed the greatest yield at the lowest temperature of studied reaction temperature, 250°C with acetaldehyde yield of 59%. Along the stability test in time-on-stream for 10 hr, the comparison result between dehydrogenation and oxidative dehydrogenation revealed that the addition of oxygen can prevent the deactivation of catalysts via coke formation and metal sintering. Cu(0)Ag(100)Li/M-Al, which was reacted in oxidative dehydrogenation of ethanol at 300°C had the lowest coke deposition on catalyst surface compared to itself reacted in dehydrogenation at 350°C and Cu(30)Ag(70)Li/M-Al reacted in oxidative dehydrogenation at 250°C.

Department: Chemical Engineering Student's Signature

Field of Study: Chemical Engineering Advisor's Signature

Academic Year: 2016

ACKNOWLEDGEMENTS

The author would like to express the gratefulness and appreciation to her advisor, Professor Dr. Bunjerd Jongsomjit for his best suggestion, useful knowledge and counsel, and invaluable encouragement along this research. This thesis would not be have been completed without all the support and guidance that the author has always received from her advisor. In addition, she is also grateful to thank Associate Professor Dr. Muenduen Phisalaphong, as the chairman of the thesis committee, Dr. Chutimon Satirapipathkul and Assistant Professor Dr. Ekrachan Chaichana for their dedicated in spending the time for her research suggestion.

Moreover, the author would like to thank for the Thailand Research Fund (TRF) and Department of Chemical Engineering, Chulalongkorn University for the financial support of this research.

Most of all, the author would like to evince the greatest acknowledge to her parent, family member for support, encouragement all the time, and all her friends both in Center of Excellence on Catalysis and Catalytic Reaction Engineering and others for their useful help, advice, and encouragement throughout the time of the research.

CONTENTS

	Page
THAI ABSTRACT	iv
ENGLISH ABSTRACT	v
ACKNOWLEDGEMENTS	vi
CONTENTS	vii
TABLE CONTENTS	xi
FIGURE CONTENTS.....	xiii
CHAPTER I INTRODUCTION	16
1.1 General introduction	16
1.2 Research objectives.....	20
1.3 Research scopes.....	20
1.4 Research methodology.....	21
CHAPTER II THEORY.....	23
2.1 Acetaldehyde.....	23
2.1.1 Acetaldehyde production.....	24
2.1.2 Acetaldehyde applications and market trend.....	26
2.2 Ethanol conversion.....	29
2.2.1 Dehydrogenation reaction of alcohol.....	29
2.2.2 Oxidation reaction of alcohol.....	30
2.3 Aluminum oxide.....	30
2.3.1 Synthesis of alumina: The solvothermal method	33
CHAPTER III LITERATURE REVIEW.....	35
3.1 Ethanol conversion to acetaldehyde.....	35

CHAPTER IV EXPERIMENTAL.....	41
4.1 Catalyst preparation.....	41
4.1.1 Chemicals for synthesis of the alumina support and Cu-AgLi/M-Al catalysts	41
4.1.2 Synthesis of mixed γ - and χ -crystalline phase alumina support.....	41
4.1.3 Preparation of copper, silver and lithium loaded on mixed phase alumina catalysts	42
4.1.4 Catalysts nomenclature.....	43
4.2 Catalyst characterization	43
4.2.1 X-ray diffraction (XRD)	43
4.2.2 Nitrogen physisorption	43
4.2.3 X-ray fluorescence (XRF).....	44
4.2.4 Carbon dioxide Temperature-Programmed Desorption (CO ₂ -TPD).....	44
4.2.5 Temperature programmed reduction (TPR).....	44
4.2.6 Fourier transform infrared spectroscopy (FT-IR).....	44
4.2.7 UV-visible spectroscopy (UV-vis).....	45
4.2.8 X-ray photoelectron spectroscopy (XPS).....	45
4.2.9 Scanning electron microscopy (SEM) and energy dispersive X-ray spectroscopy (EDX).....	45
4.2.10 Transmission electron microscopy (TEM).....	45
4.2.11 Thermogravimetric Analysis (TGA).....	45
4.3 Reaction study in dehydrogenation and oxidative dehydrogenation of ethanol.....	46
4.3.1 Dehydrogenation reaction of ethanol.....	46

	Page
4.3.1.1 Chemicals used in the reaction.....	46
4.3.1.2 Reaction testing procedure	46
4.3.1.3 Instruments and apparatus.....	47
4.3.2 Oxidative dehydrogenation of ethanol	47
4.3.2.1 Chemicals used in the reaction.....	47
4.3.2.2 Reaction testing procedure	47
4.3.2.3 Instruments and apparatus.....	48
CHAPTER V RESULTS AND DISCUSSION	50
5.1 Characteristics of Cu, Ag, and Li loading into mixed-phase Al ₂ O ₃	50
5.1.1 X-ray diffraction pattern (XRD)	50
5.1.2 Scanning electron microscope and energy dispersive X-ray spectroscopy (SEM/EDX)	51
5.1.3 X-ray fluorescence (XRF).....	56
5.1.4 Transmission electron microscopy (TEM)	57
5.1.5 Nitrogen physisorption	58
5.1.6 Fourier transform infrared spectroscopy (FT-IR).....	60
5.1.7 UV-vis spectroscopy (UV-vis).....	61
5.1.8 Temperature programmed reduction (TPR).....	62
5.1.9 X-ray photoelectron spectroscopy (XPS).....	64
5.1.10 Carbon dioxide Temperature-Programmed Desorption (CO ₂ -TPD).....	69
5.2 Activity testing by temperature programmed during 200-400°C	70
5.2.1 Dehydrogenation reaction of ethanol	71
5.2.2 Oxidative dehydrogenation reaction of ethanol.....	77

	Page
5.3 The catalytic stability with time-on-stream testing	83
5.4 Characterization of spent catalysts after reaction.....	86
5.4.1 Thermogravimetric analysis (TGA).....	86
CHAPTER VI CONCLUSIONS AND RECOMMENDATION	89
6.1 Conclusions	89
6.2 Recommendations.....	91
REFERENCES	92
APPENDIX A CALCULATION OF PHASE COMPOSITION OF ALUMINA.....	99
APPENDIX B CALCULATION OF CATALYST PREPARATION.....	100
APPENDIX C CALIBRATION CURVES.....	103
APPENDIX D CALCULATION OF TOTAL BASIC SITES OF CATALYSTS	108
APPENDIX E CALCULATION OF CONVERSION, SELECTIVITY AND YIELD	110
VITA.....	111

TABLE CONTENTS

Table 2. 1 Physical properties of acetaldehyde.....	24
Table 4. 1 Detail of different ratios of metal (copper, silver and lithium) loading and nomenclature.....	42
Table 4. 2 The operating condition of 2 types of gas chromatographer.	49
Table 5. 1 Chemical composition on surface determined by EDX of alumina support and all catalysts in the unit of weight% and atomic%.....	56
Table 5. 2 The amount of metals in bulk catalysts from XRF technique.....	56
Table 5. 3 The physical properties of Al ₂ O ₃ and catalysts with various Cu:Ag ratios...	58
Table 5. 4 The amount of basicity of catalysts with different Cu:Ag ratios.....	70
Table 5. 5 The selectivity of acetaldehyde and other byproducts in dehydrogenation of ethanol of different weight content of copper and silver catalysts.....	74
Table 5. 6 The yield of acetaldehyde and other byproducts in dehydrogenation of ethanol of different weight content of copper and silver catalysts.	74
Table 5. 7 The selectivity of acetaldehyde and other byproducts in oxidative dehydrogenation of ethanol of different weight content of copper and silver catalysts.....	80
Table 5. 8 The yield of acetaldehyde and other byproducts in oxidative dehydrogenation of ethanol of different weight content of copper and silver catalysts.....	82
Table 5. 9 The ethanol conversion of chosen catalysts in temperature programmed and time-on-stream system.....	85
Table 5. 10 The amount of coke formation of spent catalysts after 10 hr.....	88

Table C. 1 The individual retention times of the reactant, main product, and byproducts.	103
---	-----



FIGURE CONTENTS

Figure 1. 1 Some oxygenated compound produced at lower cost from biomass.....	16
Figure 1. 2 Some organic molecules produced from ethanol.....	17
Figure 2. 1 Production of acetaldehyde summary over the world.	25
Figure 2. 2 World consumption of acetaldehyde in year 2012.	27
Figure 2. 3 The global acetaldehyde market trends, drivers and projections.	28
Figure 2. 4 Proposed mechanism of dehydrogenation reaction.	29
Figure 2. 5 The calcined temperature of aluminum hydroxide.	31
Figure 2. 6 Water desorption on surface of alumina.....	32
Figure 2. 7 Lewis acid site on surface of alumina.....	32
Figure 2. 8 Solvothermal preparation method in autoclave reactor.	34
Figure 3. 1 Reaction mechanism difference between ethanol oxidation and dehydrogenation into acetaldehyde.	35
Figure 3. 2 A proposed reaction scheme for dehydrogenation reaction of ethanol....	36
Figure 3. 3 A proposed scheme of oxidative dehydrogenation pathway.	37
Figure 3. 4 Proposed mechanism of selective oxidation of ethanol.....	38
Figure 4. 1 Scheme of dehydrogenation reaction of ethanol.....	47
Figure 4. 2 Scheme of oxidative dehydrogenation of ethanol.....	49
Figure 5. 1 XRD patterns of Cu-AgLi supported on γ - χ -Al ₂ O ₃ support.....	50
Figure 5. 2 The SEM images of the catalysts.....	52

Figure 5. 3 EDX mapping of alumina support.....	53
Figure 5. 4 EDX mapping of Cu(0)Ag(100)Li/M-Al.....	53
Figure 5. 5 EDX mapping of Cu(30)Ag(70)Li/M-Al.....	54
Figure 5. 6 EDX mapping of Cu(50)Ag(50)Li/M-Al.....	54
Figure 5. 7 EDX mapping of Cu(70)Ag(30)Li/M-Al.....	55
Figure 5. 8 EDX mapping of Cu(100)Ag(0)Li/M-Al.....	55
Figure 5. 9 TEM micrographs of catalysts.....	57
Figure 5. 10 N ₂ adsorption-desorption isotherm of catalysts.....	59
Figure 5. 11 FT-IR spectra of catalysts.....	60
Figure 5. 12 The UV-visible absorption spectra of the catalysts.....	61
Figure 5. 13 TPR profiles of catalysts.....	63
Figure 5. 14 XPS spectra of the Cu 2p of catalysts.....	65
Figure 5. 15 XPS spectra of the Ag 3d of catalysts.....	66
Figure 5. 16 XPS spectra of the O 1s of catalysts.....	67
Figure 5. 17 XPS spectra of the Li 1s of catalysts.....	68
Figure 5. 18 CO ₂ -TPD profiles of catalysts.....	69
Figure 5. 19 Ethanol conversion of catalysts in dehydrogenation at temperature range of 200-400°C under atmospheric pressure.....	71
Figure 5. 20 Acetaldehyde selectivity of catalysts in dehydrogenation at temperature of 200-400°C under atmospheric pressure.....	72
Figure 5. 21 Acetaldehyde yield of catalysts in dehydrogenation at temperature range of 200-400°C under atmospheric pressure.....	76
Figure 5. 22 Ethanol conversion of catalysts in oxidative dehydrogenation at temperature range of 200-400°C under atmospheric pressure.....	77

Figure 5. 23 Acetaldehyde selectivity of catalysts in oxidative dehydrogenation at temperature range of 200-400°C under atmospheric pressure.....	78
Figure 5. 24 Acetaldehyde yield of catalysts in oxidative dehydrogenation at temperature range of 200-400°C under atmospheric pressure.....	81
Figure 5. 25 Ethanol conversion of 3 excellent activity catalysts in time-on-stream system.....	84
Figure 5. 26 Acetaldehyde yield of 3 excellent activity catalysts in time-on-stream system.....	85
Figure 5. 27 TGA curves in air atmosphere of spent catalysts.....	87
Figure A. 1 The calibration curve of chi-phase alumina obtained by XRD peaks at 2θ of 43°.....	99
Figure C. 1 The calibration curve of ethanol.....	104
Figure C. 2 The calibration curve of acetaldehyde.....	104
Figure C. 3 The calibration curve of ethylene.....	105
Figure C. 4 The calibration curve of acetone.....	105
Figure C. 5 The calibration curve of acetic acid.....	106
Figure C. 6 The calibration curve of carbon monoxide (CO).....	106
Figure C. 7 The calibration curve of carbon dioxide (CO ₂).....	107
Figure D. 1 The calibration curve of carbon dioxide obtained from CO ₂ -TPD profiles.....	109

CHAPTER I INTRODUCTION

1.1 General introduction

Manufacturing bulk chemicals from abundant, renewable, and eco-friendly biomass in place of running out and carbon emission fossil resource are the great importance to sustainable target of the chemical industry nowadays. Ethanol can be produced from biomass and it is called “bioethanol”. As a result, ethanol production from biomass fermentation has become increasingly competitive. Currently, 90% of the ethanol on the market has been obtained from biomass with an annual bioethanol production over 100 billion liters [1]. The USA and Brazil responsible for 84% of the worldwide production [2]. Bioethanol has an advantage compared to other biomass feedstocks, such as lignin, cellulose, hemicellulose and fatty acids: it can be directly converted, in one-pot processes, into drop-in chemicals and could be produced at lower costs from biomass. Indication of relative prices for a range of selected chemicals from either renewable or fossil sources is shown in **Figure 1.1** [2].

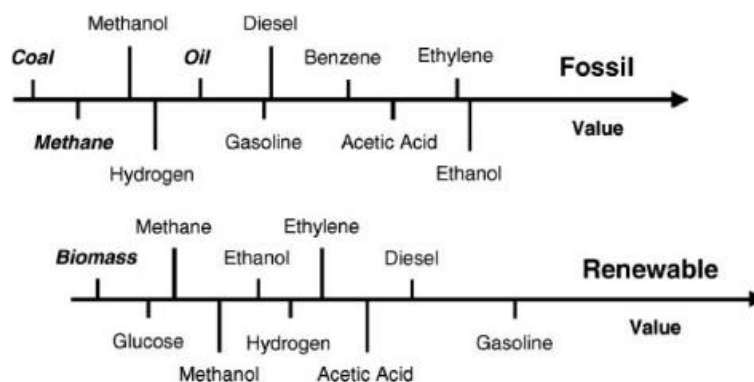


Figure 1. 1 Some oxygenated compound produced at lower cost from biomass.

Ethanol can be used as fuel and fuel additive, but it is also very promising as a platform for the production of value-added chemicals which are attractive growing concern in the last decade. It can be used as a renewable feedstock for both drop-in chemicals, such as ethylene, propylene, diethyl ether, 1,3-butadiene, and hydrocarbons, as well as the production of oxygenated chemicals, such as 1-butanol,

ethyl acetate, acetic acid, acetaldehyde and ketone, because the process is relative simple, non-corrosive, green technology, less toxic and always needs only one feedstock of ethanol (one-pot processes) [3]. **Figure 1.2** is summarized as an ethanol-derived products [2].

The challenges to increase bioethanol using as a chemical feedstock are relate to the development of the novel high performance catalysts and to the cost of replacing well-established processes and products by biomass-derived products. The properties of catalysts have a great influence to the pathway mechanism projected to the desired products. For example, ethanol can be dehydrated into ethylene, diethyl ether using solid acid catalysts. Besides, oxygenated chemicals such as acetaldehyde and ketones can be produced from ethanol by oxidative dehydrogenation reaction with basic catalysts.

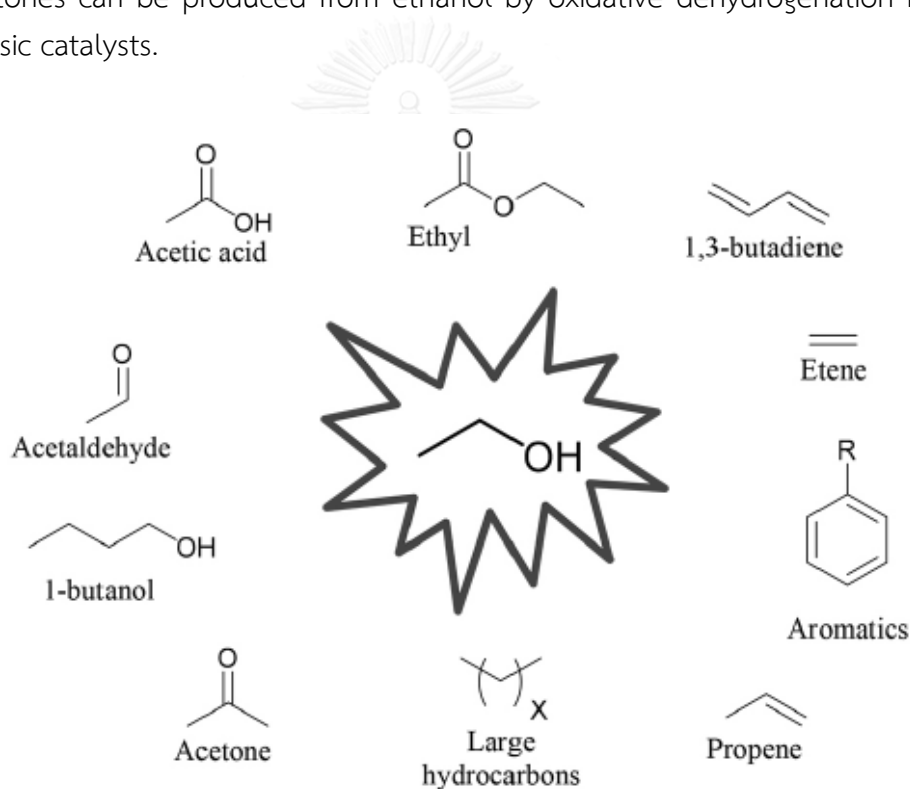


Figure 1. 2 Some organic molecules produced from ethanol.

As previously explain, acetaldehyde comes from ethanol-derived production. Acetaldehyde, CH_3CHO , is one of the most important aldehydes produced and consumed globally for different industrial applications. The market for acetaldehyde is primarily expected to be driven by the downstream markets that use the compound as a key raw material [4]. Acetic acid, acetic anhydride, ethyl acetate, isopropanol, n-butanol, and 2-ethylhexanol are the major products derived from acetaldehyde. The

commercial production processes of acetaldehyde include dehydrogenation and oxidation of ethanol, the hydration of acetylene, the partial oxidation of hydrocarbons, and direct oxidation of ethylene [5] that the equation of these reactions will be described in **section 2.1.1**. With the ever-growing of the world output of bioethanol, the production of acetaldehyde via oxidative dehydrogenation has been gradually considered a feasible process.

In the last few years miscellaneous methods for oxidation of alcohols using heterogeneous catalysts have emerged, especially nanoparticles. Their use of both of molecular oxygen and oxygen donating agents like a hydrogen peroxide as the ultimate stoichiometric oxidant makes these methods attractive and eco-friendly. However, molecular oxygen or even air has been used as a cheap and abundant oxygen source for the oxidation of alcohols in particular [6]. Heterogeneous catalytic systems are kinetically constrained by surface availability and metal–support interactions [1]. Therefore, most research on aerobic oxidations using heterogeneous catalysts has focused mainly on highly active noble metals such as platinum [7, 8], and gold [9]. With this system there was no need for additional base to promote the reaction. This is good in terms of waste minimization and product recovery, but higher loading of the rather expensive noble metal, such as gold, was required to obtain moderate conversion. Hence, more sustainable solutions based on earth abundant, cheap, harmless and stable metals to replace noble metals would be desirable. With this point, application of catalysts based on the relatively inexpensive metals manganese, nickel [10], cobalt [11], copper [12-16], vanadium [17, 18], silver [12, 19-22], and iron [23] has increasingly been explored for oxidative dehydrogenation under ambient conditions. Thus, silver nanoparticles or clusters supported on different metal oxides have been reported to be potential catalysts for the oxidative dehydrogenation of alcohols to carbonyl compounds. Likewise, copper and iron have gained importance in recent years but iron oxides, although harmless, less toxic, and cheaper, are not better catalysts than copper for oxidation reactions of alcohols at low temperatures [24].

Nanocrystalline alumina, Al_2O_3 is an acid, indeed a cheap catalyst and therefore interesting for industrial applications. Mixed γ - and χ -crystalline phases prepared from the thermal decomposition of aluminium isopropoxide (AIP) in organic solvent that has high thermal stability. The studies showed that highly stable nanocrystalline Al_2O_3 with mixed γ - and χ -crystalline phases prepared by the solvothermal method exhibited interesting results [25]. It can be employed as catalyst and catalyst supports in many catalytic reactions such as DME synthesis [26], CO and CO_2 hydrogenation [27, 28], CO

oxidation [8, 22], and propane oxidation [7].

However, alumina has been such a popular catalyst for ethanol dehydration (acid property). In case of using in basic-preferred reaction like dehydrogenation and oxidative dehydrogenation, they are rarely research to publish. One alternative improvement its performance is modify with other basic metal oxides.

In this study, we interested to develop the Cu-AgLi/Al₂O₃ catalysts for ethanol to acetaldehyde. The catalysts were synthesized, characterized and tested at a specified reaction condition. The synthesis parameters and reaction conditions influencing in both dehydrogenation and oxidative dehydrogenation were varied in order to explore the suitable catalysts and conditions for the reaction of ethanol converted to acetaldehyde.



1.2 Research objectives

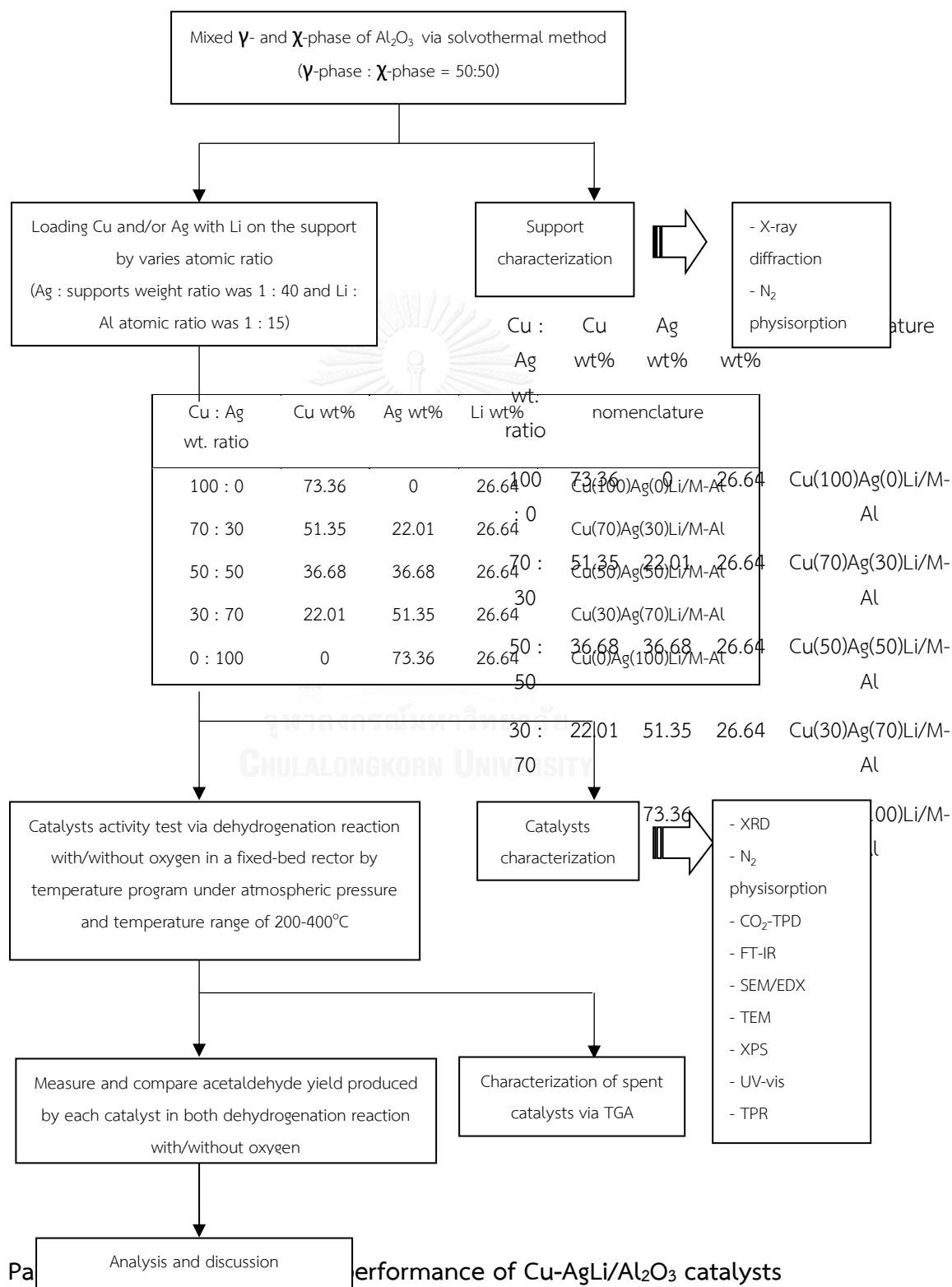
This research is aimed to: develop suitable Cu-AgLi/Al₂O₃ catalysts for ethanol conversion to acetaldehyde. The study focus in the frame of examination of the activity and stability of catalysts by varies the metals, % loading and mechanism with/without oxygen (oxidative dehydrogenation and dehydrogenation, respectively) and analysis of the catalysts properties in term of before and after the reaction for go deeper understanding in mechanism.

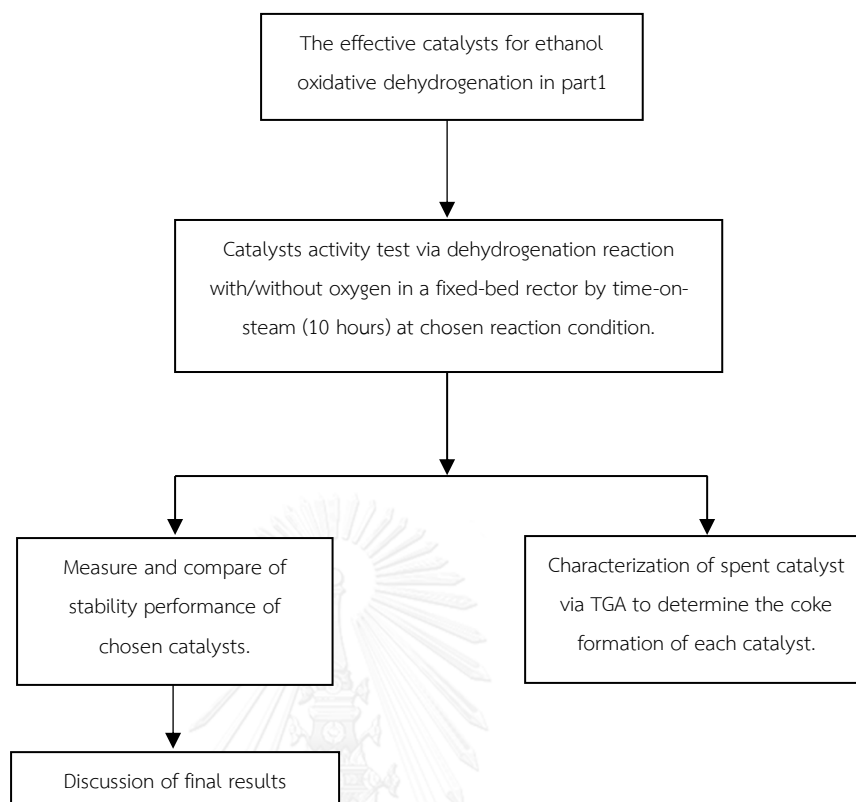
1.3 Research scopes

- Preparation of the gamma-chi alumina support with phase ratio of 1:1 by the solvothermal method.
- Loading the metals (copper and silver) via incipient wetness impregnation method onto mixed-phase alumina support with metals weight ratio of 100:0, 70:30, 50:50, 30:70 and 0:100.
- Analyzing the physiochemical properties of fresh catalysts with several techniques; XRD, N₂ physisorption, XRF, UV-vis, TPR, XPS, SEM-EDX, and TEM and basicity properties via CO₂-TPD and FT-IR techniques.
- Reaction testing the catalysts for ethanol in both oxidative dehydrogenation and dehydrogenation, which are both carried out in a fixed-bed reactor under atmospheric pressure and temperature range of 200-400°C.
- Determining the effective catalysts Cu-AgLi/Al₂O₃ catalysts and reaction condition that gives the excellent yield of acetaldehyde and ethanol conversion.
- Reaction testing of catalysts performance in time-on-stream for 10 hours at their suitable reaction condition.
- Analyzing the thermal stability and coke formation of chosen catalysts after running time-on-stream by using TGA technique.

1.4 Research methodology

Part 1 : The characterization and comparative catalytic activity of Cu-AgLi/Al₂O₃ catalysts.





As mentioned above, it explains about the motivation of the research, the research scopes, and the research methodology. Henceforth, the content of research thesis is arranged as follow:

Chapter II contains basic knowledge of the desired product (acetaldehyde), the ethanol conversion reaction, especially, oxidative dehydrogenation and dehydrogenation reactions, including aluminum oxide catalyst.

Chapter III gives details in the literature review of many studies for finding the suitable catalysts and conditions for dehydrogenation and oxidative dehydrogenation reactions.

Chapter IV describes the procedure for catalysts preparation, procedures for reaction testing, and instrument for characterization techniques.

Chapter V shows the characterization information by various techniques, reaction testing in temperature program, and catalytic performance testing in time-on-stream system.

Chapter VI summarizes the experimental results and recommendations of the research.

CHAPTER II

THEORY

This thesis investigated about ethanol conversion to acetaldehyde via selective oxidation and dehydrogenation reaction. The reaction was declined the activation energy and drive the reaction by using solid catalysts like a mixed γ - and χ -crystalline phase of alumina catalyst. Loading some basic metals such as copper, silver and lithium is the factor that we expect to improve activity and selectivity to produce acetaldehyde from the study. In this chapter, the basic knowledge of acetaldehyde, aluminum oxide and development of catalysts in ethanol converse to acetaldehyde is explained.

2.1 Acetaldehyde

Acetaldehyde, the formula CH_3CHO , is a colorless liquid or gas with a characteristic fruity odor. The other names of acetaldehyde are acetic aldehyde, ethyl aldehyde, and ethanol. Acetaldehyde is a mobile, light molecular weight, low boiling point, flammable substance that these specific physical properties [29-32] are listed below in **Table 2.1**.

Especially, a highly reactive properties, acetaldehyde is often used the most one organic compound, as an intermediate of downstream products and even if a solvent. However, when reaction temperature is higher than 420°C , acetaldehyde decomposes into methane and carbon monoxide [33]. Acetaldehyde is not importance only in chemicals industry, but it also has a large influence in the living thing. It is a mediator in the metabolism of plant and animal organisms that produced by the partial oxidation of ethanol by the liver enzyme called alcohol dehydrogenase. Large amounts of acetaldehyde interfere the biological processes. In alcoholic fermentation, as an intermediate in small amounts of all alcoholic beverage, such as beer, wine, and spirits. Though it also presents in plant juices, essential oils, roasted coffee, and tobacco smoke [34].

About the safety information, this flammable compound from Gas Data Book [35] shows the lower and upper explosive limits of 3.3 to 19.0% by volume, so the selected operating condition should be below or above this range to avoid an

explosion or fire. Flash point and ignition temperature of acetaldehyde is -20°C and 140°C [33], respectively.

Table 2. 1 Physical properties of acetaldehyde.

Properties	Information
Molecular weight	44.054
Normal boiling point	20.16°C
Normal melting point	-123.5°C
Vapor pressure	98 kPa at 20°C
Relative vapor density	1.52 (air = 1)

2.1.1 Acetaldehyde production

Acetaldehyde is typically derived from petroleum and natural gas. In the case of chemical reaction production, the first time of discovery acetaldehyde occurred in 1774 by Carl Wilhelm Scheele during the reaction of black manganese dioxide and sulfuric acid with alcohol and then investigated by Antoine François, comte de Fourcroy and Louis Nicolas Vauquelin in 1800, Johann Wolfgang Döbereiner between 1821 and 1832. Finally, in 1835 Liebig who prepared pure acetaldehyde from the oxidation of ethanol by chromic acid, designated this product "aldehyde". Later that the name was altered to "acetaldehyde", a shortness of the full-word of "aldehyde dehydrogenatus" [30].

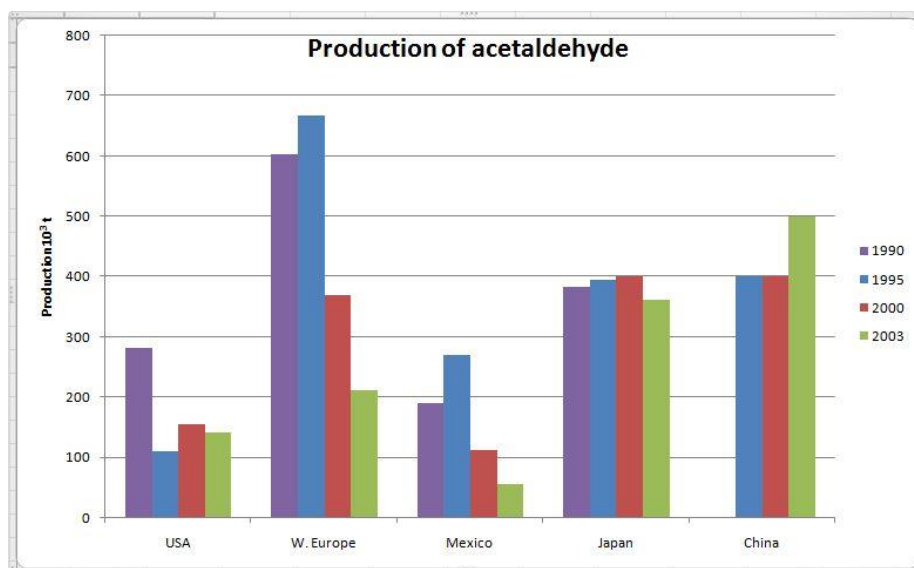
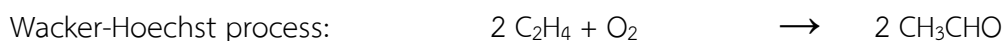
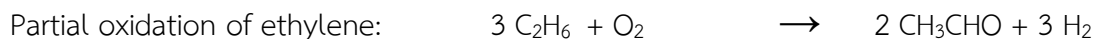
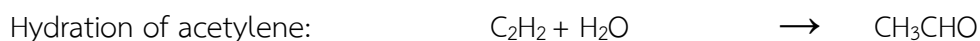
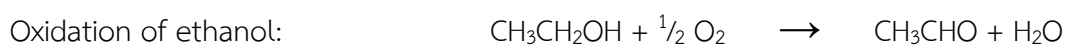
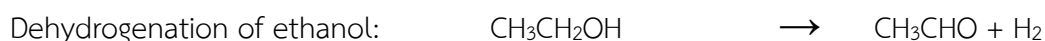


Figure 2. 1 Production of acetaldehyde summary over the world.

Before 1962, ethanol and acetylene were the major sources of acetaldehyde. Since then, ethylene is the dominant feedstock because of the lower cost. In 2003, global acetaldehyde production was about 1 million tones [4]. The commercial production processes include: dehydrogenation and oxidation of ethanol [1, 2, 5, 36, 37], the hydration of acetylene [38], the partial oxidation of hydrocarbons [39, 40], and direct oxidation of ethylene [41, 42] (also known as Wacker-Hoechst process). There are equations of these reactions showed below.



This industrial route was dominant prior to the Wacker process. It is estimated that in 1976, more than 82% of the world's 2.3 megaton per year plant capacity use last one reaction [43]. However, the drawback of Wacker-Hoechst process is the formation of polymerization and condensation products of acetaldehyde. Moreover, it is costly and environmentally problematic, because the catalyst is methylated to give methylmercury during the process.

2.1.2 Acetaldehyde applications and market trend

Acetaldehyde has industrial importance for long times ago. The first commercial usage, occurred between 1914 and 1918, was the production of acetone by acetic acid in Germany (Wacker-Chemie and Hoechst) and in Canada (Shawinigan). The main part applications are using as a starting material in the production of chemical commodities such as acetic acid, acetic anhydride, ethyl acetate, cellulose acetate, vinyl acetate resins, butyl aldehyde, crotonaldehyde, peracetic acid, pentaerythritol, terephthalic acid, and synthetic pyridine derivatives [4, 29, 36, 43]. In addition, acetaldehyde is not only used as an intermediate for the chemicals, but also became downstream itself include: as a solvent in the rubber production, in the silvering of mirrors, in leather tanning, as a denaturant for alcohol, as an additive in fuel mixture, as a hardener for gelatin fibers, as a preservative for fruit and fish, as a synthetic flavoring agent, and in the manufacture of cosmetics, pharmaceutical, plastics, paper, glue and casein products [5].

From Chemical economics handbook (CEH) [32] informed in April 2013 that in the last few years, worldwide acetaldehyde demand has also continuously decreased because of end-use markets and the effects of the economic downturn on these acetaldehyde-derived products. The dearth of demand caused by acetic acid manufacturing, the main product of acetaldehyde industry, shift to more effective technological and lower-cost methanol carbonylation process and even if the minor effect of the plasticizer alcohols industry that completely switched from n-butylaldehyde based on acetaldehyde to the worthwhile process; oxonation of propylene.

However, CEH data in 2012 [44], acetic acid facilities based on acetaldehyde still remain continue to operate mainly in Asia and South America. China is the largest consumer of acetaldehyde in the world, accounting most half of global consumption. Their consumption is heavily weighted toward of acetic acid. Western Europe is the second-largest consumer, accounting for 20% of consumption. The US acetaldehyde market will also rise only minimally, at 1–2% per year during 2012–2018. In contrast,

Japan could be the brightest spot for acetaldehyde consumption in the next five years and this hinges upon the on-purpose production of butadiene from acetaldehyde. The supply of butadiene has been volatile in Japan and the rest of Asia because of the limited availability of naphtha feedstock. Typically, butadiene and other C₄ hydrocarbons are coproduced when naphtha is used as a feedstock for ethylene manufacture. However, the increased production of natural gas from shale gas, particularly in the United States, has caused many ethylene crackers to switch feedstock from naphtha to ethane, which yields lower volumes of coproduct butadiene and other C₄ hydrocarbons. This has spurred the revival of on-purpose production for butadiene and Japan certainly has enough sources of acetaldehyde to support such a project. This new end use should provide a much-needed boost to an otherwise flat acetaldehyde market. The following pie chart in **Figure 2.2** shows worldwide consumption of acetaldehyde that describe previously.

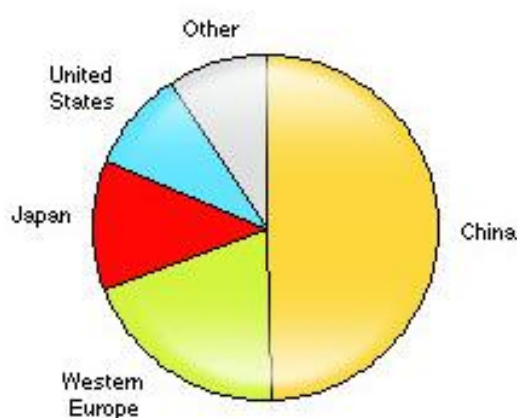


Figure 2. 2 World consumption of acetaldehyde in year 2012.

Other uses such as pyridines and pentaerythritol will grow faster than acetic acid, but the volumes are not large enough to offset the decline in acetic acid. Synthetic pyridine derivatives, peracetic acid, pentaerythritol, and acetate esters accounted for 40% of acetaldehyde demand of 2012 global acetaldehyde consumption. Pyridine and derivatives are important raw materials in agricultural chemicals. Pentaerythritol and acetate esters are both used widely in surface coatings. The other acetaldehyde applications accounted for the remaining global consumption

of acetaldehyde in 2012 includes 1,3-butylene glycol, crotonaldehyde and glyoxal, along with some smaller-volume derivatives.

In 2015, Global Industry Analysts Inc. (GIA) [45] reported about the market trend for acetaldehyde by the year 2022. The demand of acetaldehyde is projected to exceed 1.4 million tons, forced by the rising use as a platform molecule in the production of various organic compounds for wide ranges application including construction, paints and coating, food preservatives, pharmaceuticals and cosmetics, flavoring agent, and food additives in dairy products. Asia-pacific represents the largest region consumption. While a closure of acetic acid based acetaldehyde productions in various parts of the world, China still produced continuously by the same process until recently. Japan represents the large-volume market registering a compound annual growth rate of 3.2% over the forecast period that driven by the commercial scale of butadiene production from acetaldehyde. These data from CEH and GIA summarize in the same way of acetaldehyde future trend. The global acetaldehyde market trends, drivers and projections from GIA is summarized in one picture in **Figure 2.3**.

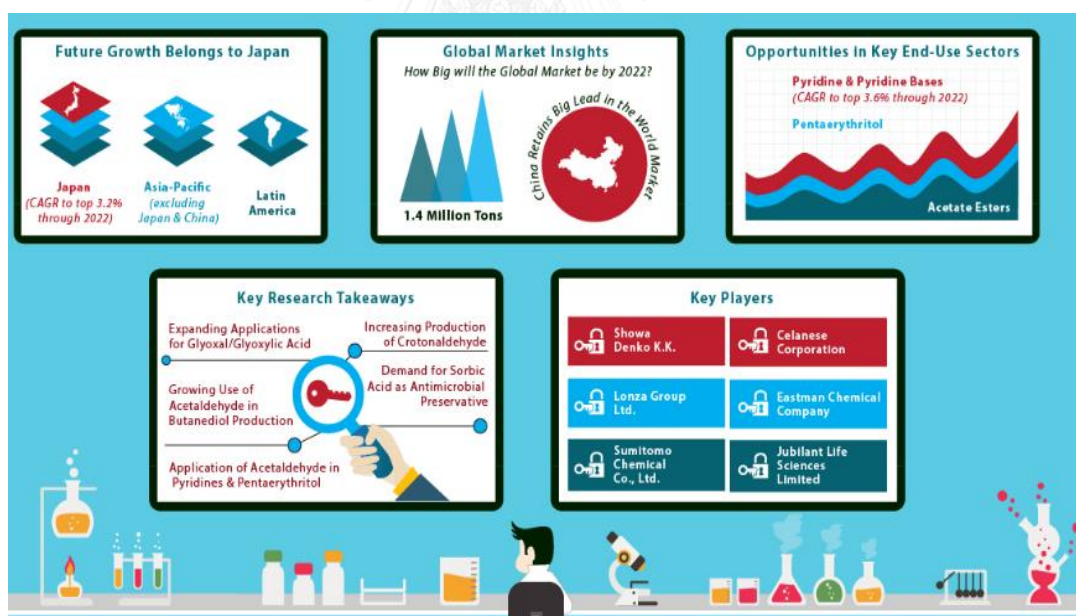


Figure 2. 3 The global acetaldehyde market trends, drivers and projections.

2.2 Ethanol conversion

As described in previous section of introduction that ethanol can produce several chemical pathways. Focusing on the ethanol converted to acetaldehyde product. There are main 2 reactions that currently in the trend of world interesting. Dehydrogenation reaction and oxidation reaction that explained in **section 2.2.1** and **section 2.2.2**, respectively.

2.2.1 Dehydrogenation reaction of alcohol

The definition of dehydrogenation is the reaction that mechanism go by removing a hydrogen from the molecule. It is an endothermic reaction. Dehydrogenation reaction can be converse low molecular weight alkenes (such as ethane and propene) to the corresponding alkane, converse primary alcohol to aldehyde and ketone. During dehydrogenation, nucleophile addition of basic catalysts cause hydrogen removing from the alcohol reactant. Often, primary alcohols can be converted into aldehydes by hydrogen acceptors in the absence of oxygen. **Figure 2.4** summarizes the dehydrogenation of a primary alcohol, secondary alcohol, or amine, respectively from picture left to right [24].

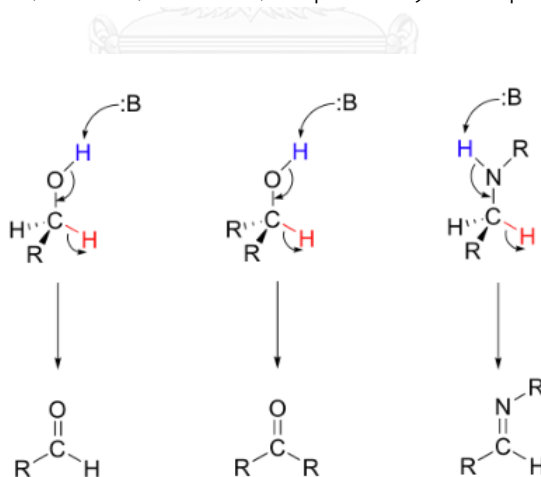
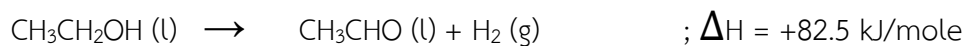


Figure 2. 4 Proposed mechanism of dehydrogenation reaction.

The products yields will be various by the different kind of catalysts and external conditions such as temperature, pressure, retention time, etc. In case of our interesting section of ethanol dehydrogenation, the dehydrogenation of ethanol can

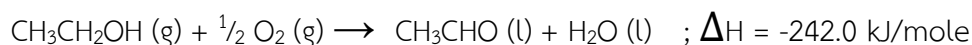
be produce acetaldehyde and hydrogen byproduct and subsequently to ethyl acetate. The first work was reported in 1886, at 260°C.



Catalytic dehydrogenation of ethanol ever used the catalysts such as iron [44], copper [18-19], or oxide of zinc, nickel, or cobalt [12]. In later patents, zinc and chromium catalysts [26], oxides of rare earth metals [27], and mixtures of copper and chromium oxides [28] have been published.

2.2.2 Oxidation reaction of alcohol

Oxidation of ethanol is the oldest and the best laboratory method for preparing acetaldehyde. In the commercial process, ethanol is oxidized catalytically with oxygen (or air) in the vapor phase.



Recently, interest has been growing in the application of supported metal catalysts in gas-phase of oxidation reaction. Many researches have been focused on the use of platinum [12], gold [43], palladium [58], copper [43, 57], and their oxides or alloys [38]. The catalytic performance of supported catalysts for aerobic oxidation usually demonstrate to be superior to non-oxidative ethanol dehydrogenation [55]. The catalytic performance depends on particle size of catalyst and also the acid-base or redox properties of the support.

2.3 Aluminum oxide

Aluminum oxide with the formula of Al_2O_3 , is also known as alumina. Their structure comprise of crystallinity and morphology. The surface areas are approximately about 100 to 600 m^2/g depending on the synthesis method, heat treatment, impurity and water desorption. Alumina is a common catalyst for a various reactions because it have many phases. The phase name remarked with Greek alphabet as follows: beta phase ($\beta\text{-Al}_2\text{O}_3$), gamma phase ($\gamma\text{-Al}_2\text{O}_3$), eta phase ($\eta\text{-Al}_2\text{O}_3$), chi phase ($\chi\text{-Al}_2\text{O}_3$), kappa phase ($\kappa\text{-Al}_2\text{O}_3$), delta phase ($\delta\text{-Al}_2\text{O}_3$), theta phase (θ -

Al_2O_3) and alpha phase ($\alpha\text{-Al}_2\text{O}_3$). Each phase of alumina has a unique crystalline structure with specific properties. The phase depends on the calcine temperatures of aluminum hydroxide (gibbsite, boehmite, and etc.) [30-31]. For example, when gibbsite is calcined at temperature between 280°C and 650°C, it will transform to chi phase. When it is calcined at 750°C to 1150°C, it obtains the kappa phase. Gamma phase alumina can obtain by calcination of boehmite at 480°C to 780°C. Then, when it is calcined at 780°C to 920°C, it gives the delta phase. The temperature transformation sequence of aluminum hydroxide are shown in **Figure 2.5** [29].

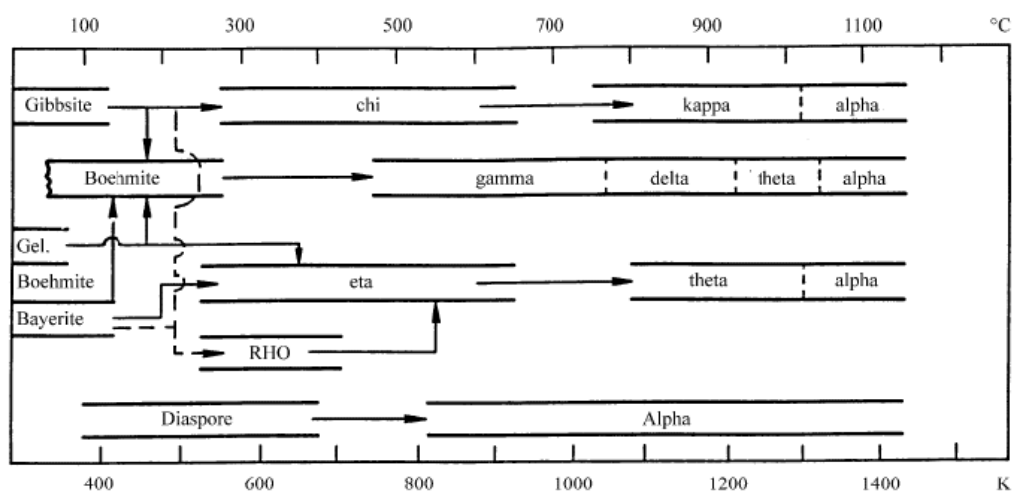


Figure 2. 5 The calcined temperature of aluminum hydroxide.

Phases of alumina can be recognized into two general groups [35]:

1. Alumina with face-centered cubic arrangement of oxygen anions where cubic $\gamma\text{-Al}_2\text{O}_3$ (*gamma*), cubic $\eta\text{-Al}_2\text{O}_3$ (*eta*), monoclinic $\theta\text{-Al}_2\text{O}_3$ (*theta*), and tetragonal (or orthorhombic) $\delta\text{-Al}_2\text{O}_3$ (*delta*) polymorphs are included.
2. Alumina with hexagonal close packed arrangement including trigonal polymorph of $\alpha\text{-Al}_2\text{O}_3$ (*alpha*, *corundum*), orthorhombic $\kappa\text{-Al}_2\text{O}_3$ (*kappa*) and hexagonal $\chi\text{-Al}_2\text{O}_3$ (*chi*).

Another classification of transitional alumina phases defines:

1. Low-temperature alumina phases (γ - and $\eta\text{-Al}_2\text{O}_3$);
2. High-temperature alumina phases (δ - and $\theta\text{-Al}_2\text{O}_3$).

Alumina is widely used as a common catalyst because of its fine particle size, high surface area, surface catalytic activity, excellent thermal stability, high mechanical resistance, and wide range of chemical, physical, and catalytic properties. The surface of alumina contains both of acid and basic sites. The acidity and basicity of alumina can be alternated due to the existence or distinction of hydroxyl group from water molecules. The acidity on surface, which is Lewis and Brønsted acid site, is derived from Al^{3+} cation and water molecule coordinated with cation [32], while the basic site on surface is received from O^{2-} anion and basic hydroxide group [30].

During alumina contacts with humidity, the water molecule adsorb on surface and dried in air at temperature between 100 and 150°C, the water molecule is emitted, but leaves hydroxyl group behind on surface alumina. The role of hydroxyl group is Brønsted acid site as illustrated in **Figure 2.6**. The acid strength and concentration of alumina varied with the calcination temperature. The acid strength and concentration are low when calcined below 300°C, while calcination at 500°C decreases Brønsted acid site. The calcination temperature above 600°C results in adjacent hydroxyl group form into water molecule. Then, the water molecule releases and appears as Al^{3+} cation on alumina surface, which is Lewis acid site [32-33] as shown in **Figure 2.7**.

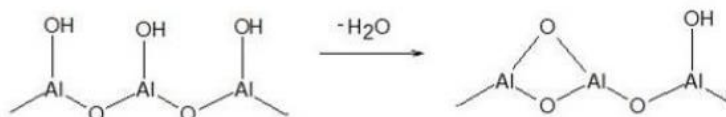


Figure 2. 6 Water desorption on surface of alumina.

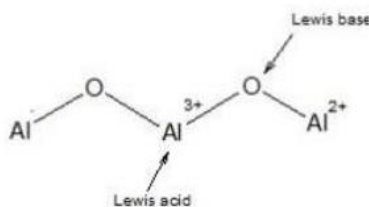


Figure 2. 7 Lewis acid site on surface of alumina.

2.3.1 Synthesis of alumina: The solvothermal method

Alumina can be synthesized by various methods. For instance, flame-hydrolysis, polymeric routes [37], sol-gel process [37-39], hydrothermal and solvothermal methods [30-31, 34]. The pioneer method is flame-hydrolysis and polymeric routes but these methods are not practical. The precipitation method is complex and takes long synthesis times (washing times and aging time) [40]. Metal alkoxide was used as precursors to produce aluminum oxide via the sol-gel method [38-39]. However, the limitation of sol-gel method is long gelation periods and expensive costs of metal alkoxide. The most common method of producing alumina is the hydrothermal technique which the reaction is carried out in water medium. While the hydrothermal technique is very similar to the solvothermal method that it uses different starting precursor in the first step, the water is used in the hydrothermal method while the solvothermal method does not involve water (but this is not always) [34].

Solvothermal process uses an organic compound in place of aqueous solution to synthesize an inorganic compound. The result is the formation of alumina with different characteristics to that produced from the hydrothermal [41]. Solvothermal method operates at temperatures between 200 to 300°C under autogenous pressure of the organics. In order to control the structures, particles size, shape distribution and morphologies, varied process conditions reaction temperature, reaction time, kind of solvent and precursor type were examined. The prefix “solvo-” means any type of solvent. For example, alcohol is used as the reaction media, the reactions are called “alcoholothermal” reactions. Generally, the definition of the solvothermal method is reactions at temperatures higher than the boiling point of the intermediary in liquid or supercritical media. The reaction is carried out in closed system using autoclaves, an apparatus shown in **Figure 2.8** [34].

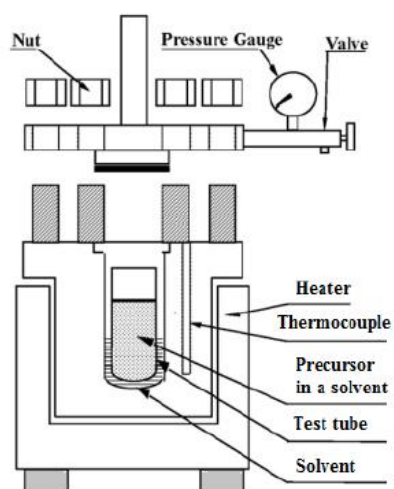


Figure 2. 8 Solvothermal preparation method in autoclave reactor.



CHAPTER III

LITERATURE REVIEW

Focusing on acetaldehyde production from ethanol-based, it can be operated from either dehydrogenation or oxidation by oxygen. For both reactions, catalysts are used in order to decrease activation energy and also raise up the rate of chemical reaction activity. The public studies that seeking suitable catalysts and reaction conditions is described after this.

3.1 Ethanol conversion to acetaldehyde

Gallo *et al.* in 2014 [2] reported a mechanism of ethanol convert to acetaldehyde can be distinguished into two different ways as illustrated in **Figure 3.1** below.

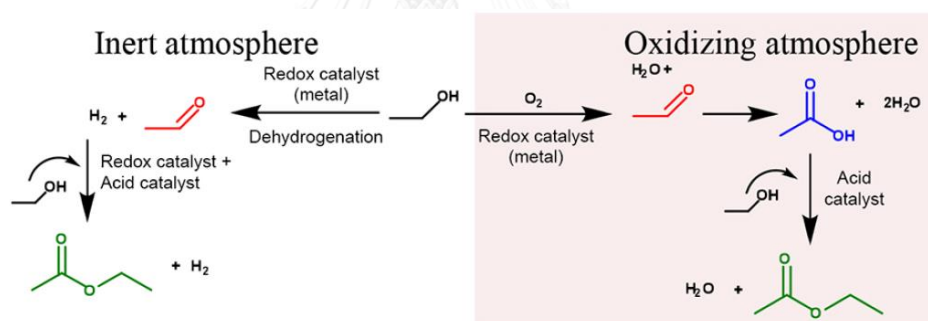


Figure 3. 1 Reaction mechanism difference between ethanol oxidation and dehydrogenation into acetaldehyde.

In an inert atmosphere, ethanol using a redox sites of catalysts can be dehydrogenated to acetaldehyde and also gives valuable byproduct as hydrogen gas. Another pathway is ethanol oxidized to acetaldehyde under aerobic conditions and in the presence of a redox sites of catalysts. Water is a byproduct of the latter. In 2011, the studies of Thuy *et al.* [46] showed that an ethanol oxidation can be carries out at lower temperature and has only one third of the energy consumption and carbon dioxide emission, compared to the dehydrogenation reaction. The reaction of ethanol to acetaldehyde has been studied using mostly basic transition metal based catalysts on different supports. The support, in fact, actually is an important key in the product

distribution of aldehyde or ester.

Volanti *et al.* (2011-12) studies three different controlled copper oxide (CuO) morphologies, urchin-like, fiber-like and nanorods, dispersed in silica and monoclinic zirconia as catalysts in the range of temperature of 225 to 275°C. The report shown that using Cu supported on silica as catalyst obtained 87% acetaldehyde selectivity and only 5.3% selectivity of ethyl acetate with ethanol conversion of 41% at 225°C [47]. While Cu supported on monoclinic zirconia, the selectivity of acetaldehyde and ethyl acetate was found to be 23% and 73%, respectively at 43% ethanol conversion at 200°C [14]. It has found that Cu^+ species were usually over Cu^0 on the metal surface of the Cu/SiO₂ catalyst and the ionic species is more selective to acetaldehyde production. Using Cu/ZrO₂, the support leads to rising in the metal electron density, and therefore its surface is dominated by Cu^0 species. Sato *et al.* reported in 2013, ethanol is activated to $\text{CH}_3\text{CH}_2\text{O}^*$ by Cu^+ sites or on the zirconia surface. When this activation takes place on the Cu^+ sites, the ethanol can be dehydrogenated and transferred to Cu^0 sites as an activated species $\text{CH}_3(\text{C}^*)\text{O}$. This species would undergo coupling reaction with CH_3CHO^* found on the Cu^+ or zirconia sites to be our undesired product, ethyl acetate. As mentioned previously, the copper surface (when supported on zirconia) is poor in Cu^+ , which is mainly involved in dehydrogenation reaction. Therefore it is highly probable that the coupling reaction to ethyl acetate happens on the surface between the metal and support [48]. This is ensured by the fact that if the support does not activate ethanol (such as silica), the whole reaction takes place on the Cu/Cu⁺ species, which causes a poor ethyl acetate selectivity (ca. 5%). **Figure 3.2** shows a scheme of the proposed reaction route of Cu on ZrO₂ and SiO₂ surface.

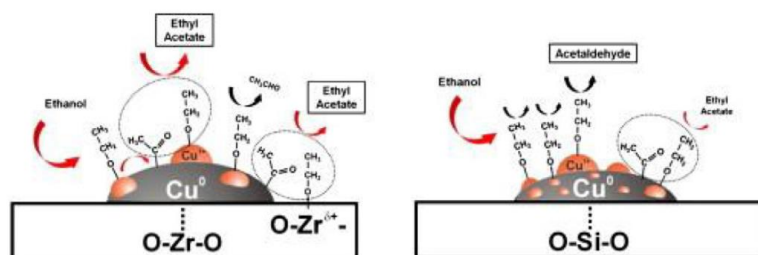


Figure 3. 2 A proposed reaction scheme for dehydrogenation reaction of ethanol.

In 2015, Janlamoon *et al.* [49] published the study of dehydrogenation of ethanol with oxygen. The reaction testing used different phases of alumina; gamma- and chi-phase loading with silver and lithium, operated at reaction temperature of 250

and 400°C. Alumina was synthesized by solvothermal method to produce pure gamma (CHI00), pure chi (CHI100), and equally mixed phases (CHI50) as samples of the study. The different phase composition of alumina, the amount of weak basic sites of AgLi-Al₂O₃, the oxidation state of Ag, and the reduction properties of catalysts also affect the ethanol conversion and acetaldehyde selectivity. AgLi-CHI50 catalyst revealed higher activity than each phase alone, 80% ethanol conversion at temperature below 250°C with good acetaldehyde selectivity. Ethanol oxidative dehydrogenation, the active sites in the oxygen-containing silver including the cycle of hydrogen extraction and the oxygen incorporation as illustrated in **Figure 3.3**. The reduction state of Ag⁺ on CHI50 alumina due to weaker interaction resulting in increased catalytic activity for oxidative dehydrogenation. Furthermore, increased reaction temperature from 250 to 400°C caused a continuous decrease in selectivity of acetaldehyde because of transformation to CO and CO₂.

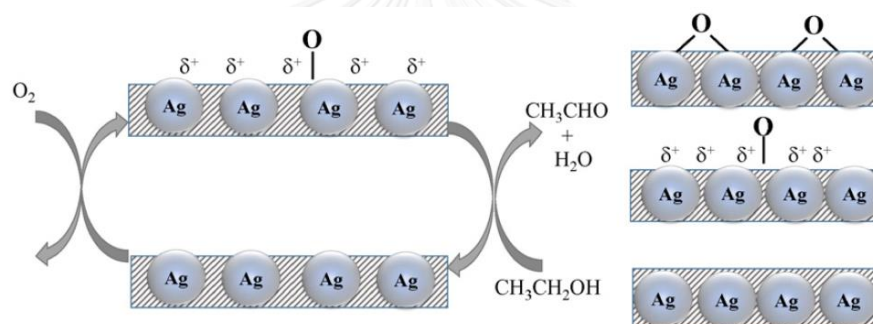


Figure 3. 3 A proposed scheme of oxidative dehydrogenation pathway.

Wach *et al.* [19] proposed a mechanism for the oxidation of methanol on a single crystal Ag(1 1 0), which consists of several reaction steps. The first step, methoxy formation through the activation of O-H bond by adsorbed atomic oxygen ($2\text{CH}_3\text{OH}(\text{g}) + \text{O}^* \rightarrow 2\text{CH}_3\text{O}^* + \text{H}_2\text{O}^*$) at 180 K. Then, next step, C-H bond scission to form formaldehyde and hydrogen ($\text{CH}_3\text{O}^* \rightarrow \text{CH}_2\text{O}^* + \text{H}^*$). After that recombination of a surface hydrogen atom (H^{*}) to form methanol ($\text{CH}_3\text{O}^* + \text{H}^* \rightarrow \text{CH}_3\text{OH}^*$) and the last step of reaction was adsorbed formaldehyde to yield methyl formate and hydrogen via the adsorbed H₂COOCH₃ intermediate. In the presence of excess oxygen, formaldehyde is further oxidized to formate, which subsequently decomposes to CO₂ and H₂O with the assistance of surface oxygen (O^{*}). In addition, a similar reaction mechanism of oxidation of methanol was found on both Ag(1 1 1) and Ag(1 1 0), with exception of the absence of methyl formate product on Ag(1 1 1). Following a similar

way, ethanol on Ag(1 1 0) is first oxidized to surface ethoxy and water upon adsorption at 453°C, and ethoxy subsequently decomposes into acetaldehyde and hydrogen. The recombination of surface hydrogen (H*) with ethoxy to form ethanol is also observed [47].

Xu *et al.* [5] reported an interesting issue in 2016 that produce acetaldehyde from ethanol oxidation by using silver nanoparticles supported on a hydroxyapatite (HAp) foam. In this study, highly dispersed Ag/HAp showed a surprisingly high activity of 1.38 s^{-1} in turnover frequency (TOF), maximum selectivity of approximately 100% and large long durability (approx. 100 hr.) for the oxidative dehydrogenation of ethanol to acetaldehyde. The plausible mechanism for the selective oxidation on Ag/HAp was proposed and divided into two stages by different temperatures; the first step is oxygen molecules (O_2 (g)) are adsorbed on Ag/HAp. Then, atomic oxygen (O) is formed via the dissociation of O_2 . After that $\text{CH}_3\text{CH}_2\text{OH}^*$ is oxidized to CH_3CHO^* mainly by O in the lower temperature range 696–796°C and finally, CH_3CHO^* is further oxidized to CO_2 with oxidant species (OS), including O and hydroxyl species (OH) produced in the reactions at above 796°C. Insight into the mechanism of alcohol dehydrogenation may be potentially used for metal catalysts, such as Au and Cu. **Figure 3.4** illustrates the overall mechanism. Hydrogen, carbon and oxygen atoms are shown in white, grey and red color, respectively. Silver is blue. OS is abbreviated from oxidant species and the symbol * means surface active sites.

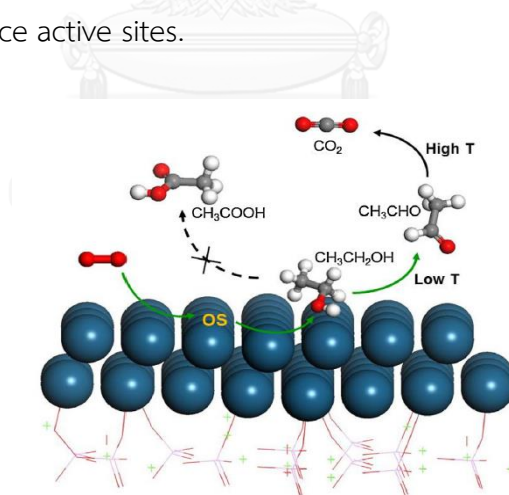


Figure 3. 4 Proposed mechanism of selective oxidation of ethanol.

Liu *et al.* [1] in 2015 showed the interesting result of influence bimetallic Au-Cu and Au-Ir catalysts for gas-phase ethanol oxidation over $\text{MgCuCr}_2\text{O}_4$ support. The catalysts expressed synergy in the aerobic oxidation of ethanol. However, a drawback

of these catalysts is that the higher temperature required for higher ethanol conversion usually results in lower acetaldehyde selectivity and poor stability.

A comparative study of oxidation of methanol on gamma alumina supported group IB metal catalysts was reported in 2009. Lippits *et al.* [50] reported the major role of the support and additives in the activity and selectivity. They researched the dehydrogenation and oxidation of methanol over gamma-alumina supported Cu, Ag, and Au (M) catalysts. All three metals (Cu, Ag, and Au) are active in oxidation of methanol but the most active catalyst is Au/Al₂O₃. 100% conversion were reached at 275, 300, and 350°C for Au, Cu, and Ag/Al₂O₃, respectively. The high activity of these interesting catalysts is relate to the metal-oxugen bond of the support, so the choice of support is very importance for the catalytic performance to increasing the mobility and reactivity of the surface lattice oxygen. The promoting effect of addition of lithium oxide (Li₂O) and ceria (CeO_x) on the dehydrogenation and oxidation have been investigated in the following part. A two-step mechanism is proposed: in the first step, CH₃OH is dehydrogenated on alumina to formaldehyde; in the second step, the formaldehyde reacts on M to produce CO or CO₂. Another mechanism is proposed for good oxidizing catalysts: methanol reacts directly on M and is oxidized to CO₂. The addition of the co-catalyst CeO_x to the catalysts has a beneficial effect on the oxidation of methanol to CO₂ because of its ability to provide oxygen. Alkali metal stabilizes the Au, Cu and Ag nanoparticles and that is a structural promoter. In addition, their hypothesis was Li₂O blocks the adsorption site for methanol on alumina, and hence, decreasing the formation of formaldehyde.

Chua *et al.* [23] discussed the alkali metal effect in hydride-form for improved dehydrogenation on hydrazine borane (N₂H₄BH₃) in 2014. The result showed that a smaller cation radius carries stronger intermolecular forces within the structure and thus possesses a higher melting temperature. Further increasing temperature leads to the release of additional H₂ that demonstrate significantly improved dehydrogenated behavior.

The behavior of nanoparticles of copper and silver on an alumina support in the oxidation and dehydrogenation of ethanol was investigated. In 2010, Lippit *et al.* explained that pure alumina mainly acts as an acidic catalyst and produces diethyl ether and ethylene. Addition of copper and silver nanoparticles results in a direct conversion of ethanol into ethylene oxide. Addition of lithium oxide (Li₂O) influenced the selectivity by suppressing the formation of diethyl ether and ethylene. Using Ag/Li₂O/Al₂O₃ and Cu/Li₂O/Al₂O₃ catalysts, it was possible to obtain high selectivity towards ethylene oxide at a temperature of 200°C. Addition of ceria (CeO_x) results in

higher selectivities towards CO [12]. Furthermore, the behavior of alumina-supported gold catalysts and the effects of addition of Li_2O and CeO_x on the oxidation, dehydrogenation and dehydration reactions of ethanol. Gold particles play an important role in converting ethanol into ethylene oxide and acetaldehyde. Addition of Li_2O influences the selectivity by suppressing the formation of diethyl ether and ethylene. With the $\text{Au}/\text{Li}_2\text{O}/\text{Al}_2\text{O}_3$ catalysts, a high selectivity toward ethylene oxide can be obtained. It is suggested that at low concentrations, the role of oxygen is mainly to prevent coke formation on the catalytic surface [51].

From several above references, it can be hypothesis to develop suitable bimetallic catalysts system and conditions for our research oxidation and dehydrogenation of ethanol to produce acetaldehyde.



CHAPTER IV

EXPERIMENTAL

This chapter explains the experimental procedures, including synthesis of the mixed γ - and χ - crystalline phase alumina catalyst and loading of copper and/or silver with lithium (promoter) as shown in section 4.1. The ethanol dehydrogenation and oxidative dehydrogenation reactions experiment are described in section 4.2 and the catalyst characterization techniques are presented in section 4.3, respectively.

4.1 Catalyst preparation

The equally mixed γ - and χ -phase alumina as the catalyst support was prepared by the solvothermal method in autoclave, and then it was loaded with Cu, Ag, and Li by the incipient wetness impregnation method.

4.1.1 Chemicals for synthesis of the alumina support and Cu-AgLi/M-Al catalysts

1. Aluminium isopropoxide 98 wt% (AIP) available from Aldrich.
2. 1-Butanol (C₄H₉OH) from Merck.
3. Toluene (C₆H₅CH₃) from Fisher Scientific.
4. Silver (I) nitrate 99 wt% (AgNO₃) available from Aldrich.
5. Copper (II) nitrate 99 wt% (Cu(NO₃)₂) available from Aldrich.
6. Lithium (I) nitrate 98 wt% (LiNO₃) available from Aldrich.
7. Methanol (CH₃OH) from Merck.
8. De-ionized water

4.1.2 Synthesis of mixed γ - and χ -crystalline phase alumina support

Crystalline alumina having each phase of gamma- and chi- ratio of 50:50 was prepared by the solvothermal method as reported by Wannaborworn M. *et al.* [52]. First, 25 grams of aluminium isopropoxide was dissolved in 100 ml of solvent (50 ml of 1-butanol mixed with 50 ml of toluene) in the beaker and transfer to a smaller tube of autoclave. Prepared mixed 1-butanol/toluene again for each solvent of 15 ml and poured to a larger tube of autoclave. After that placed a smaller tube into a larger

tube inside the autoclave. The autoclave was purged with N₂, then it was heated up to 300°C at the rate of 2.5°C min⁻¹ and held at this temperature for 2 hours. After the autoclave was cooled down to the room temperature, the white precipitate powder was collected, washed with methanol several times and dried in the oven overnight. Finally, the white powder was calcined in air (flow rate of 100 ml min⁻¹) at the heating rate of 10°C min⁻¹ raised to the desired temperature at 600°C and held at that temperature for 6 hours to eliminate the moisture, impurity and remaining reagent. The obtained alumina supports have to confirm the crystallinity, morphology and the equally of mixed-phase of alumina by X-ray diffractometric (XRD) measurement. Specific surface area, pore volume, pore size can be obtained by N₂ physisorption (BET method) while morphology and element distribution on catalyst surface can be identified by scanning electron microscope and energy dispersive X-ray spectroscopy (SEM/EDX).

4.1.3 Preparation of copper, silver and lithium loaded on mixed phase alumina catalysts

From Meephoka *et al.* reported [8], the incipient wetness impregnation with the loaded metals may give the best value of ethanol conversion and acetaldehyde selectivity. Five different ratios of metal loading are shown in **Table 4.1**. Silver nitrate (AgNO₃), Copper nitrate (Cu(NO₃)₂), and Lithium nitrate (LiNO₃) are used as metal sources in this preparation.

Table 4. 1 Detail of different ratios of metal (copper, silver and lithium) loading and nomenclature.

Sample no.	1	2	3	4	5
Cu : Ag weight ratio	100 : 0	70 : 30	50 : 50	30 : 70	0 : 100
Metal : support weight ratio	1 : 40	1 : 40	1 : 40	1 : 40	1 : 40
Metal : Al atomic ratio	1 : 15	1 : 15	1 : 15	1 : 15	1 : 15
Cu wt%	73.36	51.35	36.68	22.01	-
Ag wt%	-	22.01	36.68	51.35	73.36
Li wt%	26.64	26.64	26.64	26.64	26.64

Mixed γ - and χ -crystalline phase alumina obtained in the previous section was used as a support. 5 wt% of metals (Cu, Ag) and 0.7 wt% Li were mixed with de-ionized water, which its volume equals to pore volume of alumina support. The support was

impregnated with the mixture of metal aqueous-like solution by slow dropping to the support after that. Desired catalysts were dried at temperature of 110°C in the oven for 12 hours, then calcined in air (flow rate of 100 ml min⁻¹) at 400°C for 4 hours at the heating rate of 10°C min⁻¹.

4.1.4 Catalysts nomenclature

After this, 5 catalysts were denoted as the name listed below.

Cu(x)Ag(y)Li/M-Al refers to different weight% of copper, silver and lithium that supported onto 50:50 of γ - and χ -phase alumina. The number in the form of x and y were the weight ratio loading of Cu and Ag, respectively; Moreover, M-Al is abbreviated from mixed-phased alumina.

4.2 Catalyst characterization

4.2.1 X-ray diffraction (XRD)

XRD is the primarily technique using for phase identification of a crystalline sample. This study, the instrument is a SIEMENS D5000 X-ray diffractometer for full control of the XRD analyzer. Data was obtained by using CuK α radiation source ($\lambda = 1.54439 \text{ \AA}$) with Ni filter. The spectra were scanned at a rate of 2.4° min⁻¹ in the 2θ range of 20 to 80° with resolution 0.04°. The standard peak is pure gamma-alumina, pure chi-alumina, copper oxide, silver oxide, and lithium oxide.

4.2.2 Nitrogen physisorption

The catalyst of 1 g for each sample was used to measure specific surface area, pore volume and pore size diameter by N₂ adsorption-desorption at normal boiling point of liquid nitrogen (-196°C) using a Micromeritics ASAP 2000 automated system instrument. Prior to the characterization, all of the samples were degassed at 120°C in nitrogen flow for 3 h to remove the moisture and other adsorbates. The specific surface area, pore volume, and pore size diameter and hysteresis loop of catalysts can be obtained by Brunauer-Emmelt-Teller (BET), BJH method and the gas adsorption-desorption isotherms, respectively.

4.2.3 X-ray fluorescence (XRF)

The chemical compositions of catalysts (Cu, Ag, Al, O) and the weight ratio of Cu:Ag in the catalysts were determined by a X-ray fluorescence (Pana analytical MINIPAL 4 instrument) using 1 g of sample to analysis.

4.2.4 Carbon dioxide Temperature-Programmed Desorption (CO₂-TPD)

The basicity properties of the catalysts was determined by temperature programmed desorption of carbon dioxide (CO₂-TPD) using a Micromeritics Chemisorp 2750 with a computer. In the experiment, about 0.10 g of the sample and 0.03 g of quartz wool were loaded in a glass tube and pretreated at 500°C in a flow of helium. The sample was saturated with pure CO₂ for an hour. Then, the catalyst was purged with helium flow until a constant baseline level was attained. The physisorbed carbon dioxide was desorbed in a gas flow for 2 hours. Then, the sample was heated from 30 to 500°C at a heating rate 10°C min⁻¹. The amount of carbon dioxide in effluent was detected via TCD signal as a function of time.

4.2.5 Temperature programmed reduction (TPR)

For the metal catalysts, temperature programmed reduction (TPR) technique was used to determine the reducibility properties of catalysts. 0.1 g of the sample per each catalyst and 0.03 g of quartz wool were used in this operation and temperature ramping from 30 to 600°C at a ramp rate of 10°C min⁻¹. The carrier gas was 10% hydrogen in argon. During reduction, a cold trap was placed before the detector to remove water produced. A thermal conductivity detector (TCD) measure the amount of hydrogen consumption. The calibration of hydrogen consumption was performed with bulk cobalt oxide (Co₃O₄) at the same conditions.

4.2.6 Fourier transform infrared spectroscopy (FT-IR)

FT-IR was performed on compacted powder disk of 0.5-1 g of each studied catalyst. FT-IR analysis was used to evaluate the functional group as the chemical structure of the catalyst system using a Nicolet 6700 FT-IR spectrometer.

4.2.7 UV-visible spectroscopy (UV-vis)

The oxidation state of metals (copper and silver) was examined by spectroscopic method using UV-visible absorption spectroscopy (Perkin Elmer) at $\lambda = 650$, analysis between wavelength of 200 to 800 nm, and step size of 1 nm.

4.2.8 X-ray photoelectron spectroscopy (XPS)

XPS analysis was used to calculate the surface chemistry of material. For all element, there is a characteristic of binding energy associated with each core atomic orbital. The presence of peaks at particular energies indicates the existence of a specific element in the sample. Moreover, the intensity of the peaks is related to the concentration of the element. So, this technique was performed using the AMICUS spectrometer using $MgK\alpha$ X-ray radiation (1253.6 eV) and $AlK\alpha$ X-ray radiation (1486.6 eV) at voltage 15kV and current of 12 mA. The pressure in the analysis chamber was less than 10^{-5} Pa.

4.2.9 Scanning electron microscopy (SEM) and energy dispersive X-ray spectroscopy (EDX)

The catalyst surface morphology and elemental distribution (mapping) of catalysts were investigated by scanning electron microscopy (SEM) and energy dispersive X-ray spectroscopy (EDX). SEM technique was operated by a model of JEOL mode JSM-6400 and EDX was performed using Link Isis Series 300 program.

4.2.10 Transmission electron microscopy (TEM)

Transmission electron microscopy was used to study the inside morphology and the crystallite size of sample by using JEOL-JEM 200CX transmission electron microscope operated at 100 kV.

4.2.11 Thermogravimetric Analysis (TGA)

TGA measured the amount of weight change of a material after reaction testing and provided the chemical phenomena like a decomposition temperature (finding reaction temperature range), and solid-gas reactions (oxidation). TGA was performed using a TA Instrument SDT Q600 analyzer (USA). The samples of 10–20 mg

and a temperature range between 30 and 400°C at 2°C min⁻¹ were used in the operation with N₂ UHP carrier gas.

4.3 Reaction study in dehydrogenation and oxidative dehydrogenation of ethanol

4.3.1 Dehydrogenation reaction of ethanol

4.3.1.1 Chemicals used in the reaction

1. Absolute ethanol purity 99.99% (C₂H₅OH) available from Merck.
2. Nitrogen gas ultra high purity 99.99% available from Linde.
3. Hydrogen gas ultra high purity 99.999% available from Linde.

4.3.1.2 Reaction testing procedure

Catalytic ethanol reaction was carried out in the fixed-bed continuous flow micro-reactor made from a borosilicate glass with an inside diameter of 0.7 cm. To achieve the reaction study, catalyst 0.15 g. was packed below 0.01 g. of quartz wool layers in the middle of reactor, which located in the furnace. Then, preheated the catalysts at 200°C for 30 min to eliminate the humidity in N₂ as a carrier gas. After finished the preheat step, the catalyst sample was pre-reduced *in situ* in flowing H₂ at 300°C for 1 h before running in dehydrogenation reaction of ethanol. Ethanol was introduced from syringe pump at flow rate of 45 mL/min to the reactor by bubbling N₂ through the vaporizer at 120°C to maintain the partial pressure and hence the composition of the feed. N₂ gas flow rate was kept at 50 mL/min. Ethanol reaction was ranged between 200 to 400°C and pressure at 1 atm total pressure. The effluent was analyzed using 2 kinds of gas chromatography (GC) techniques including, thermal conductivity detector (TCD) and flame ionization detector (FID). Thermal conductivity detector (TCD) was used a Shimadzu GC8A (Porapak-Q and Molecular sieve 5A) that can separate inorganic compositions. For example, N₂ carrier gas, CO, CO₂ and O₂ in air. Flame ionization detector (FID), a Shimadzu GC14B (DB-5) was used for separation of light hydrocarbon products, for example, ethanol (C₂H₅OH), acetaldehyde (C₂H₄O), ethylene (C₂H₄), and acetic acid (CH₃COOH), etc.

4.3.1.3 Instruments and apparatus

Flow diagram of dehydrogenation reaction of ethanol is shown in **Figure 4.1**.

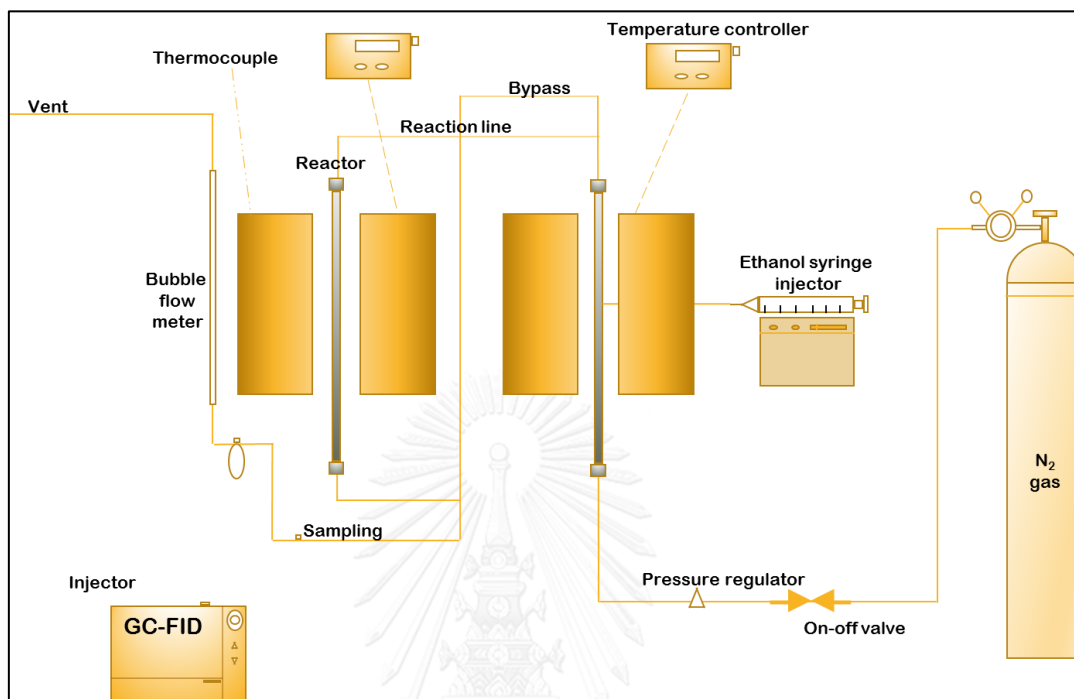


Figure 4. 1 Scheme of dehydrogenation reaction of ethanol.

4.3.2 Oxidative dehydrogenation of ethanol

4.3.2.1 Chemicals used in the reaction

1. Absolute ethanol purity 99.99% (C₂H₅OH) available from Merck.
2. Nitrogen gas ultra high purity 99.99% available from Linde.
3. Hydrogen gas ultra high purity 99.999% available from Linde.
4. Air zero grade balance nitrogen available from Linde.

4.3.2.2 Reaction testing procedure

Catalytic ethanol reaction was carried out in the fixed-bed continuous flow micro-reactor made from a borosilicate glass with an inside diameter of 0.7 cm. To achieve the reaction study, catalyst 0.15 g. was packed below 0.01 g. of quartz wool layers in the middle of reactor, which located in the furnace. Then, preheated the catalysts at 200°C for 30 min to eliminate the humidity in N₂ as a carrier gas. After

finished the preheat step, the catalyst sample was pre-reduced *in situ* in flowing hydrogen gas at 300°C for 1 hour before running in oxidation reaction of ethanol. Ethanol was introduced from syringe pump at flow rate of 45 ml/min to the reactor by bubbling N₂ through the vaporizer at 120°C to maintain the partial pressure and hence the composition of the feed. N₂ gas flow rate was kept at 50 ml/min. Before introducing ethanol to reacted with catalysts in the reactor, oxidative dehydrogenation reaction have to use oxygen, so the flow rate of N₂ carrier gas was decreased to 17.8 ml/min and added air gas to the reactor at the flow rate of 46 ml/min. Catalytic reaction was ranged between temperature of 200 to 400°C and pressure at 1 atm total pressure. The effluent was analyzed using 2 kinds of gas chromatography (GC) techniques including, thermal conductivity detector (TCD) and flame ionization detector (FID). Thermal conductivity detector (TCD) was used a Shimadzu GC8A (Porapak-Q and Molecular sieve 5A) that can separate inorganic compositions, for example, N₂ carrier gas, CO, CO₂ and O₂ in air. Flame ionization detector (FID), a Shimadzu GC14B (DB-5) was used for separation of light hydrocarbon products. For example, ethanol (C₂H₅OH), acetaldehyde (C₂H₄O), ethylene (C₂H₄), acetone (C₃H₆O) and acetic acid (CH₃COOH), etc.

4.3.2.3 Instruments and apparatus

Flow diagram of oxidative dehydrogenation reaction of ethanol is shown in Figure 4.2.

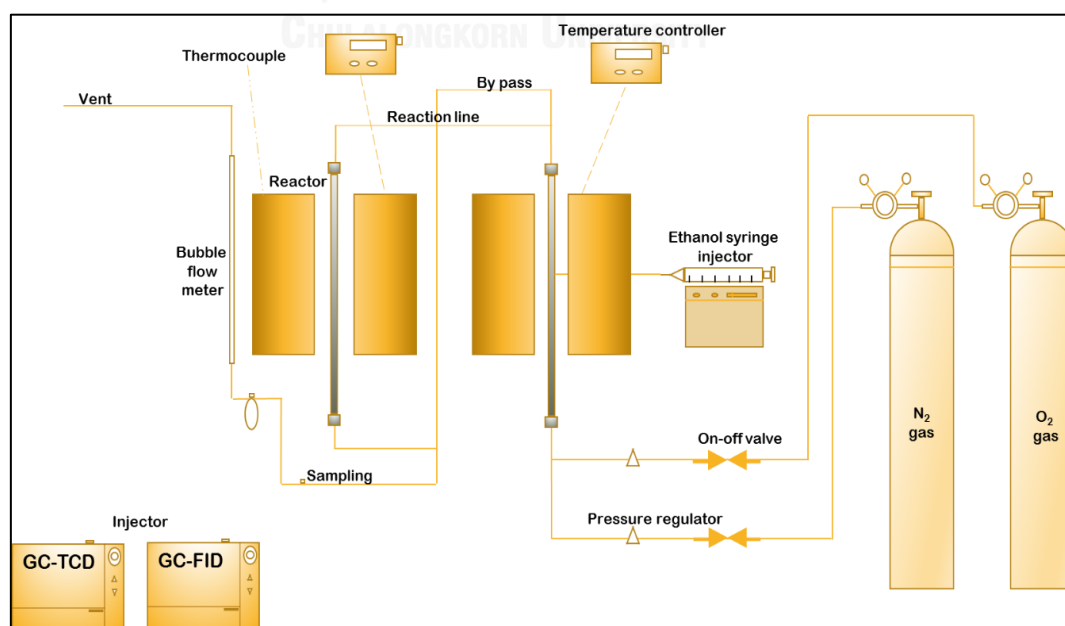


Figure 4. 2 Scheme of oxidative dehydrogenation of ethanol

In the reaction study, 2 kinds of gas chromatography techniques including, thermal conductivity detector (TCD) and flame ionization detector (FID) were used. The composition of light hydrocarbon products were detected by a Shimadzu GC14B (DB-5) gas chromatograph equipped with FID. The composition of inorganic was analyzed by A Shimadzu GC8A (molecular sieve 5A and Parapak Q) gas chromatography equipped with TCD. The operating condition of GC was shown in the **Table 4.2**.

Table 4. 2 The operating condition of 2 types of gas chromatographer.

Gas chromatographer	Shimadzu GC14B	A Shimadzu GC8A	
Detector	FID	TCD	TCD
Column	DB-5	molecular sieve 5A	Parapak Q
Carrier gas	N ₂ (99.999%)	He (99.999%)	He (99.999%)
Column temperature			
- Initial	40°C	60°C	60°C
- Final	40°C	60°C	60°C
Injector temperature	150°C	100°C	100°C
Current	-	80 mA	80 mA
Analyzed composition	Ethanol	Carbon monoxide	Carbon
	Ethylene	Oxygen	dioxide
	Acetaldehyde	Nitrogen	Ethylene

CHAPTER V

RESULTS AND DISCUSSION

This chapter explains the characteristic information from several techniques via X-ray diffraction (XRD), N₂ physisorption, carbon dioxide temperature-programmed desorption (CO₂-TPD), temperature programmed reduction (H₂-TPR), X-ray photoelectron spectroscopy (XPS), scanning electron microscopy (SEM) and energy dispersive X-ray spectroscopy (EDX), UV-visible spectroscopy (UV-vis), Fourier transform infrared spectroscopy (FT-IR), transmission electron microscopy (TEM), X-ray fluorescence (XRF), and thermogravimetric analysis (TGA) of Cu-AgLi catalysts modified with 5 different weight ratios of Cu:Ag (weight ratio of 100:0, 70:30, 50:50, 30:70, and 0:100) system as shown in section 5.1. The catalytic activity of catalysts in dehydrogenation and oxidative dehydrogenation reactions are described in section 5.2, especially, the discussion that showed how these 2 sections connected to each other.

5.1 Characteristics of Cu, Ag, and Li loading into mixed-phase Al₂O₃

5.1.1 X-ray diffraction pattern (XRD)

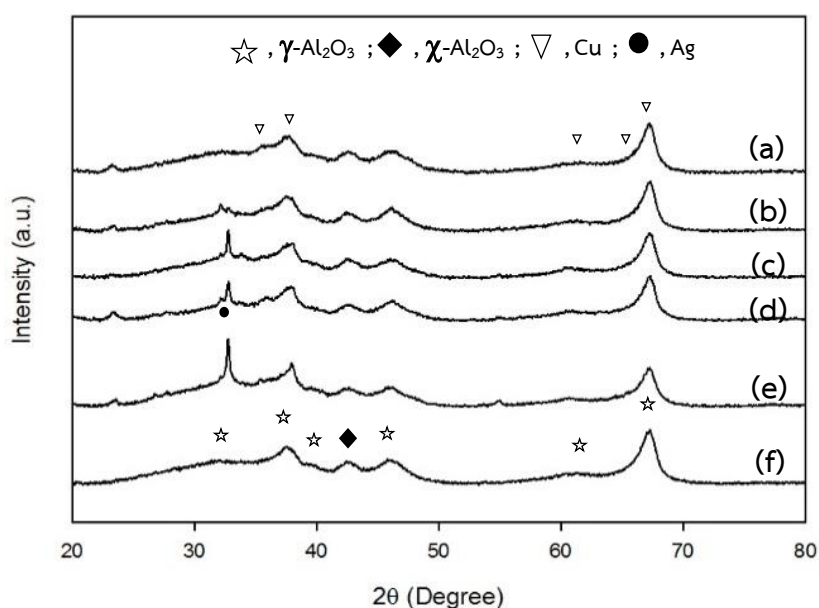


Figure 5. 1 XRD patterns of Cu-AgLi supported on γ - γ -Al₂O₃ support.

The XRD patterns of catalysts are displayed in **Figure 5.1**. In this figure contains XRD pattern of (a) Cu(100)Ag(0)Li/M-Al, (b) Cu(70)Ag(30)Li/M-Al, (c) Cu(50)Ag(50)Li/M-Al, (d) Cu(30)Ag(70)Li/M-Al, (e) Cu(0)Ag(100)Li/M-Al, and (f) mixed-phase γ - χ -Al₂O₃ support. For mixed-phase alumina support, which γ -Al₂O₃ and χ -Al₂O₃ were produced using 1-butanol and toluene as the synthesis solvent, has the XRD crystalline peaks of γ -Al₂O₃ appeared at 2θ of 32, 37, 39, 46, 61, and 67° and χ -Al₂O₃ appeared at 2θ of 37, 39, 43, 46, 61, 67°. The peak at 2θ of 43° showed characteristics of χ -Al₂O₃. The observation is in good agreement with the XRD analysis of Janlamoon *et al.* report [49]. Besides, the mixed-phase Al₂O₃ support in this research focused only at 50% of each phase of γ -Al₂O₃ and χ -Al₂O₃. The composition of alumina was resolved by the area of characteristic peak of χ -Al₂O₃ at 43° that the solution is shown in **Appendix A**.

All of Cu-AgLi on Al₂O₃ catalysts were calcined in air at 600°C before characterization, so Cu, Ag, Li should be in form of metal oxide. The XRD peaks of Cu-AgLi on Al₂O₃ catalysts exhibited similar patterns as seen from those with the presence of additional peaks of metal oxides. The characteristic peaks of CuO observed at 36 and 39° [53]. Typically, Cu₂O cubic phase can be observed at 36 and 42° were assigned to the Cu⁺ specie [14], so in this studied XRD patterns were difficult to identify the peaks that associated with Cu₂O. The characteristic peaks of Ag₂O observed at 34° [54]. Hence, it is difficult to differentiate the metallic Cu, metallic Ag, or other oxidation states of Cu and Ag peaks from the Al₂O₃ peaks in Cu-AgLi/M-Al. While no apparent diffraction peaks of Li or Li₂O species were observed, indicating that Li was present as well dispersion on the Al₂O₃ support or the nanoparticle sizes was lower the detector limitation of instrument (size smaller than 3 nm).

5.1.2 Scanning electron microscope and energy dispersive X-ray spectroscopy (SEM/EDX)

The morphology of catalysts and the elemental distribution on the catalysts surface can be identified by SEM and EDX techniques, respectively.

Figure 5.2 illustrated the morphology of alumina support **(a)**, Cu-AgLi on Al₂O₃ with various loads of Cu:Ag content **(b)** to **(f)**. It can be clearly seen that the addition of copper, silver in different contents and lithium in fixed content led to an increase particles coating on the alumina surface compare with the SEM image of alumina support with unloading metal. However, it can be observed from SEM images that all studied catalysts have similar particle size and agglomerate features on the support

with various amounts of Cu:Ag of each catalyst. It could be said that the loading metals into the alumina did not change the alumina support structure or all of catalysts had no significant difference of surface morphology.

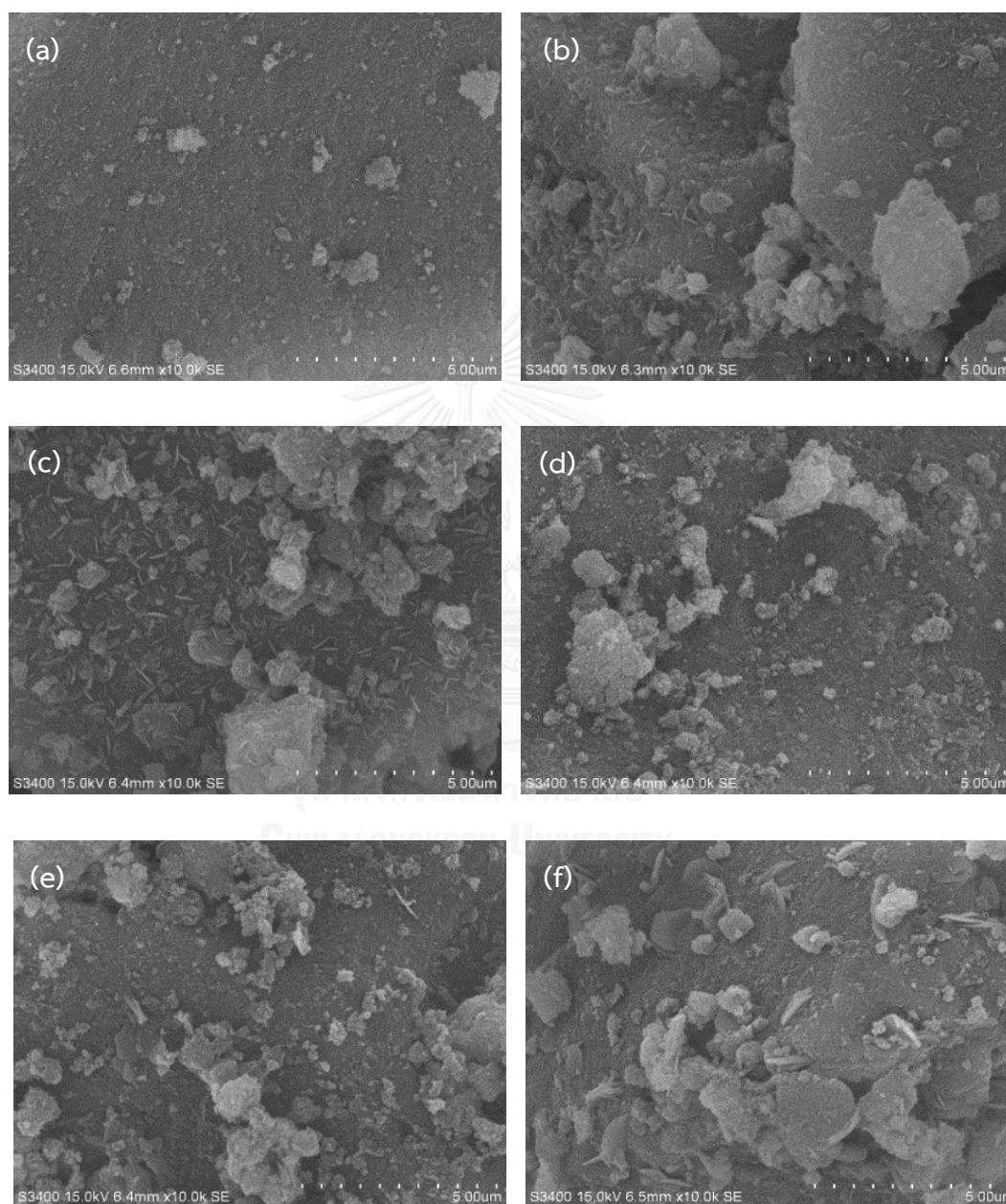


Figure 5. 2 The SEM images of the catalysts.

(a) alumina support, (b) Cu(100)Ag(0)Li/M-Al, (c) Cu(70)Ag(30)Li/M-Al, (d) Cu(50)Ag(50)Li/M-Al, (e) Cu(30)Ag(70)Li/M-Al, and (f) Cu(0)Ag(100)Li/M-Al.

The elemental dispersion of Al_2O_3 support (Al, O) and Cu, Ag, Li metals into the support was analyzed via energy dispersive X-ray spectroscopy. Li metal was also loaded into the support as well, but Li cannot be detected by EDX, so EDX mapping in Figure 5.3 to Figure 5.8 showed only Al, O, Cu, and Ag as follows;

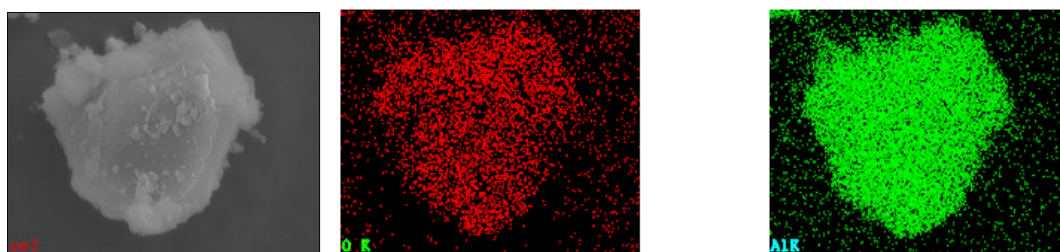


Figure 5. 3 EDX mapping of alumina support.

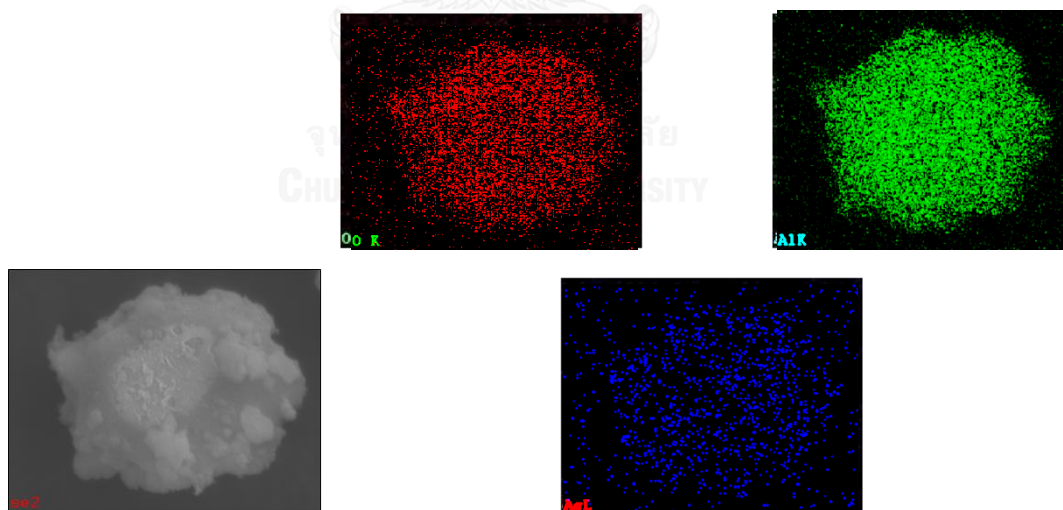


Figure 5. 4 EDX mapping of $\text{Cu}(0)\text{Ag}(100)\text{Li}/\text{M-AL}$.

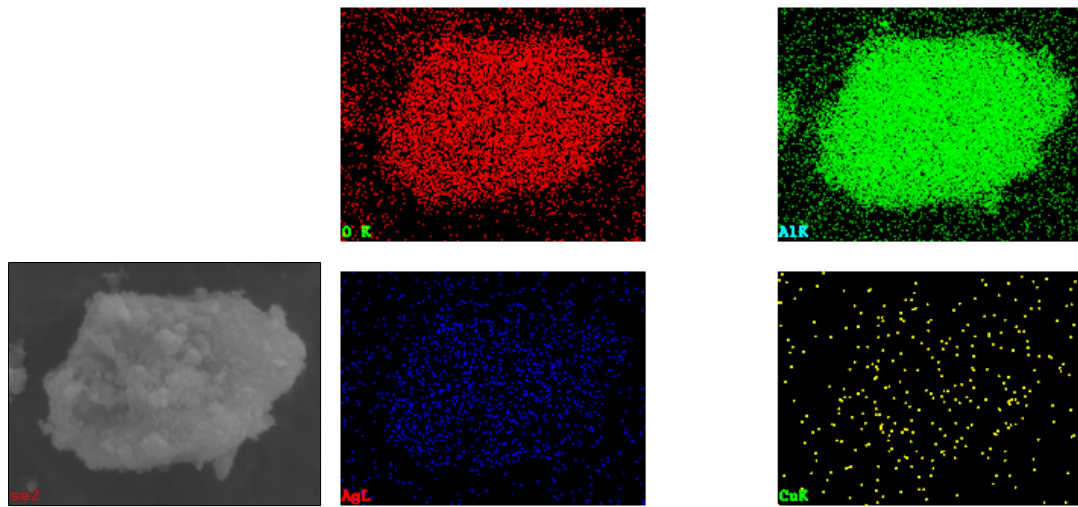


Figure 5. 5 EDX mapping of Cu(30)Ag(70)Li/M-Al.

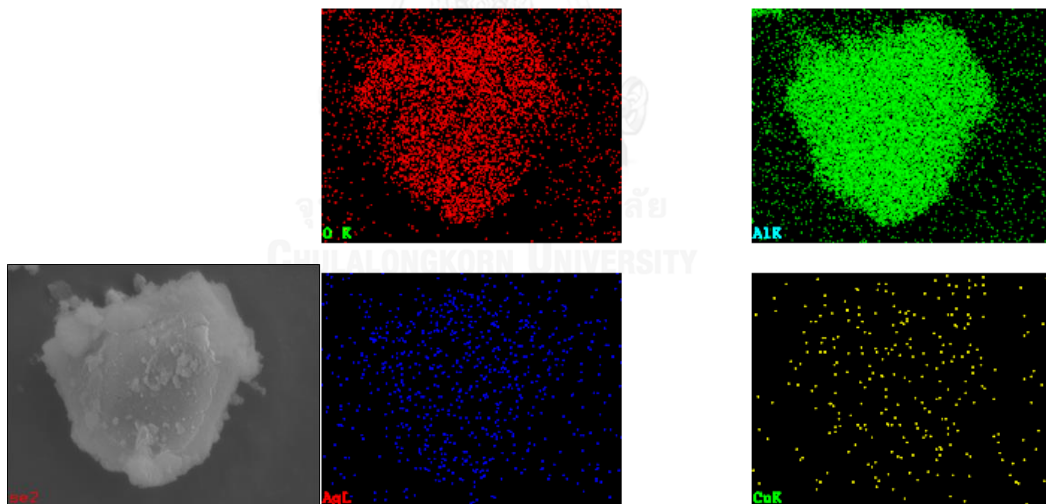


Figure 5. 6 EDX mapping of Cu(50)Ag(50)Li/M-Al.

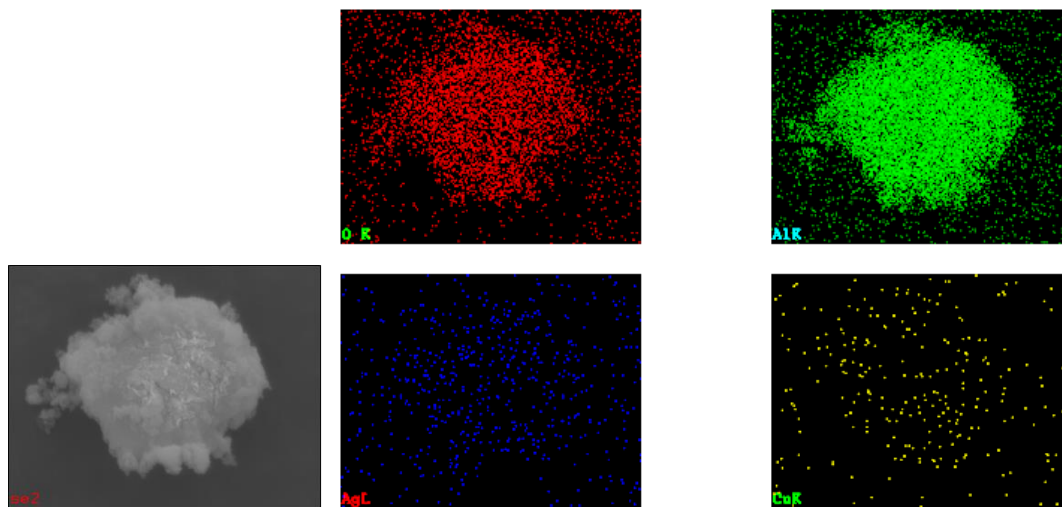


Figure 5. 7 EDX mapping of Cu(70)Ag(30)Li/M-Al.

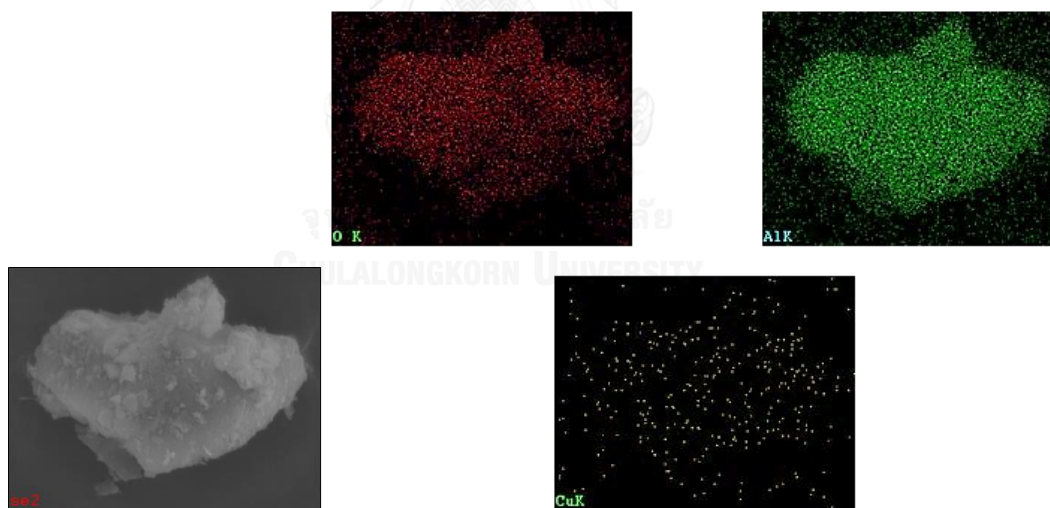


Figure 5. 8 EDX mapping of Cu(100)Ag(0)Li/M-Al.

From all EDX mappings of Al (green color), O (red color), Ag (blue color), and Cu (yellow color) distribution, they showed that these elements disperse on the surface of all catalysts very well. The elemental distribution on catalysts surface can be quantitatively obtained as summarized in **Table 5.1**.

Table 5. 1 Chemical composition on surface determined by EDX of alumina support and all catalysts in the unit of weight% and atomic%.

Catalysts	(wt%)				(at%)			
	Cu	Ag	Al	O	Cu	Ag	Al	O
Alumina support	-	-	56.54	35.79	-	-	47.11	50.29
Cu(100)Ag(0)Li/M-Al	7.22	-	55.39	35.63	2.58	-	46.50	50.44
Cu(70)Ag(30)Li/M-Al	5.28	3.57	54.27	35.11	3.06	0.56	46.11	49.79
Cu(50)Ag(50)Li/M-Al	5.00	3.71	54.54	34.97	1.83	0.79	46.56	50.34
Cu(30)Ag(70)Li/M-Al	1.77	4.07	54.84	37.55	0.63	0.84	45.50	52.55
Cu(0)Ag(100)Li/M-Al	-	5.44	54.43	38.37	-	1.12	44.95	53.44

5.1.3 X-ray fluorescence (XRF)

The quantities of metals in the bulk catalysts were measured by XRF that is shown in **Table 5.2**. The EDX technique measured the amount of element at the depth of approximately 2 μm from the surface.

Table 5. 2 The amount of metals in bulk catalysts from XRF technique.

Catalysts	(wt%)		
	Cu	Ag	Al
Cu(100)Ag(0)Li/M-Al	12.265	-	87.402
Cu(70)Ag(30)Li/M-Al	8.846	3.101	87.73
Cu(50)Ag(50)Li/M-Al	6.685	6.268	86.701
Cu(30)Ag(70)Li/M-Al	3.970	8.308	87.374
Cu(0)Ag(100)Li/M-Al	-	12.713	86.88

From **Tables 5.1** and **5.2**, they compare the amount of species existing between catalysts surface and in bulk obtained from EDX and XRF techniques, respectively. The EDX technique measured the amount of species at the depth of approximately 2 μm from the surface, unlike the XRF that measured the amount of element in the catalyst bulk. The results reveal that the most part of specie in the catalyst is aluminum (Al) that comes from the alumina support (Al_2O_3). Focusing on the metals, copper and silver, the EDX results show that the measured weight ratios are slightly lower than nominal ratios, while the results confirmed by XRF are slightly

higher than the nominal ratios. The difference may be caused by copper being more better dispersed in mixed-phase alumina than silver, which may be observed more obviously comparing Cu:Ag weight ratios of 100:0 and 0:100 from SEM images in **Figure 5.2 (b)** and **(f)**, so that the area with large agglomerate particles contains larger amounts of Ag relative to Cu. Therefore, almost all copper species can be occupied in the pores of alumina support. The result from the weight ratio of copper identified in bulk catalyst was clearly found to be higher than the weight ratio of silver species that almost all silver is identified on catalyst surface.

5.1.4 Transmission electron microscopy (TEM)

The morphology, i.e. shape, size and distribution, of the nanoparticles was usually evaluated with transmission electron microscopy technique which is supplementary to the XRD crystallinity. TEM images in the measurement scale of 0.2 μm of Cu-AgLi supported on alumina with various weight ratios of Cu and Ag (100:0, 70:30, 50:50, 30:70, 0:100) are shown in **Figure 5.9 (a)** to **(e)**.

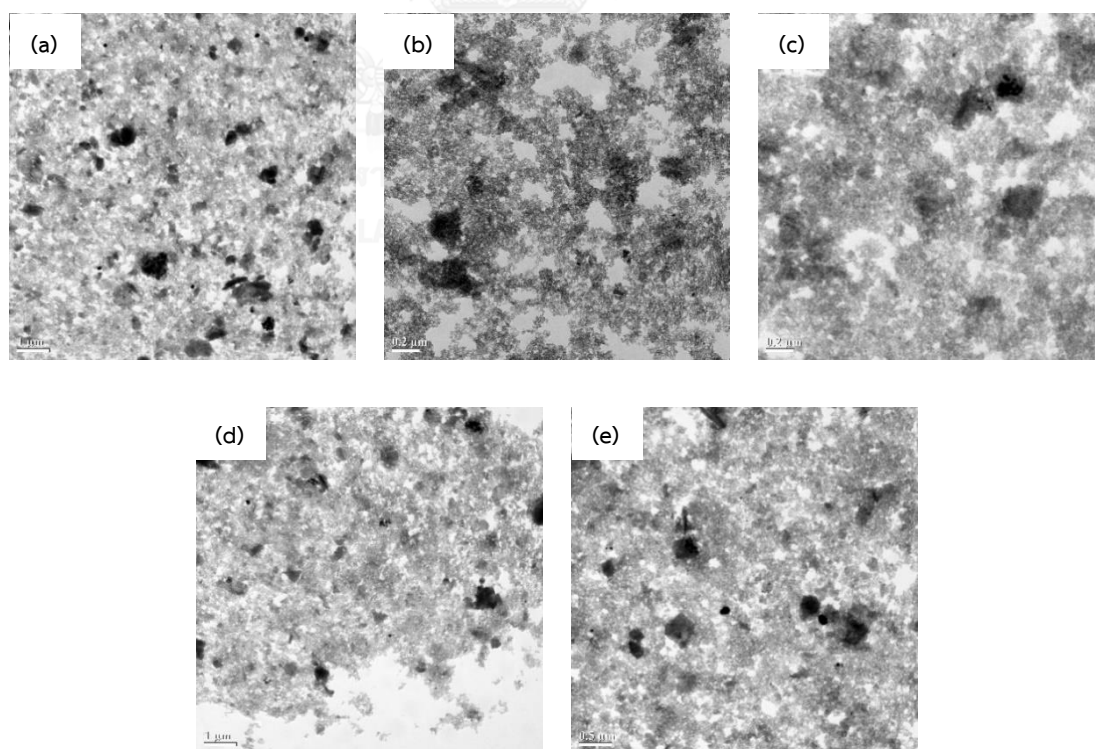


Figure 5. 9 TEM micrographs of catalysts.

(a) Cu(100)Ag(0)Li/M-Al, (b) Cu(70)Ag(30)Li/M-Al, (c) Cu(50)Ag(50)Li/M-Al, (d) Cu(30)Ag(70)Li/M-Al, and (e) Cu(0)Ag(100)Li/M-Al.

From the TEM images, it typically used for determine the structural inside the pore of catalysts. Figure 5.9 shows the TEM micrographs of all Cu-AgLi supported on alumina that can see the pore of alumina (grey color) containing the particles (black color) that can be presumed these particle are metal Cu and Ag from the supported information about % weight appearance of Cu and Ag in EDX and XRF techniques.

5.1.5 Nitrogen physisorption

Table 5. 3 The physical properties of Al₂O₃ and catalysts with various Cu:Ag ratios.

Catalysts	Specific surface area (m ² /g cat)	Average pore volume (cm ³ /g cat)	Average pore diameter (nm)
Mixed-phase Al ₂ O ₃	165	0.546	8.44
Cu(100)Ag(0)Li/M-Al	147	0.490	8.45
Cu(70)Ag(30)Li/M-Al	154	0.502	8.48
Cu(50)Ag(50)Li/M-Al	163	0.510	8.38
Cu(30)Ag(70)Li/M-Al	167	0.513	8.48
Cu(0)Ag(100)Li/M-Al	172	0.536	8.03

BET surface area, BJH pore volume, and BJH pore diameter of CuAgLi on Al₂O₃ catalysts are summarized in **Table 5.3**. The BET surface area comparison between alumina support and Cu-AgLi loaded on alumina catalysts are no significant changed because the amount of metal loading on support is only a small amount (5 wt% of Cu and Ag, and 0.7 wt% Li). However, when compared within the catalysts containing different ratio of Cu and Ag, it was also found that the BET surface areas decreased from 172 to 147 m²/g with an increase in portion of silver. The BJH pore size and BJH pore diameter were rather similar for the Cu-AgLi on Al₂O₃ catalysts and alumina support in the range of 0.5 cm³/g and 8 nm, respectively. It reveals that the high porosity of the γ -Al₂O₃ support was kept after Cu, Ag, and Li loading.

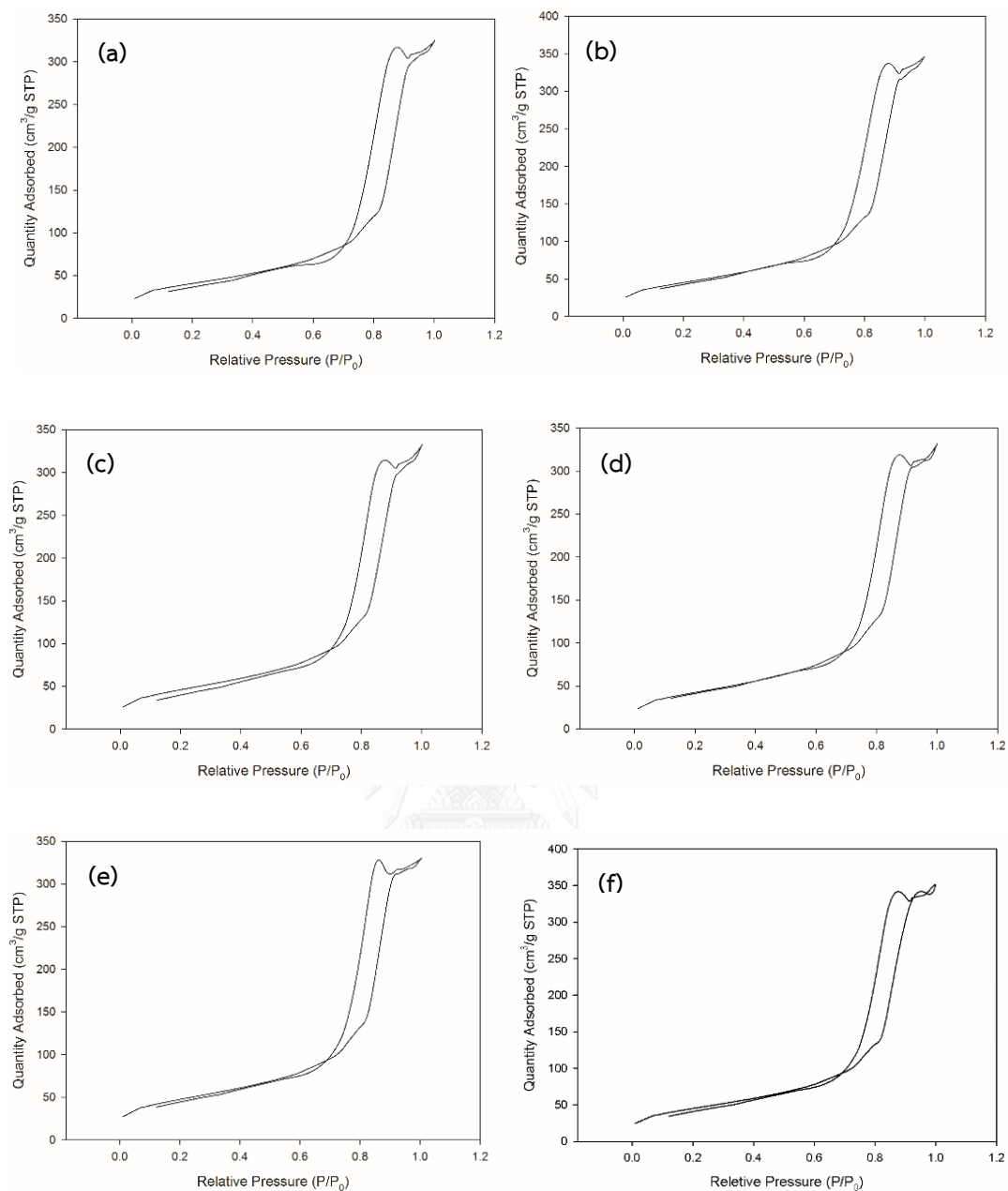


Figure 5. 10 N₂ adsorption-desorption isotherm of catalysts.

(a) Cu(100)Ag(0)Li/M-Al, (b) Cu(70)Ag(30)Li/M-Al, (c) Cu(50)Ag(50)Li/M-Al, (d) Cu(30)Ag(70)Li/M-Al, (e) Cu(0)Ag(100)Li/M-Al, and (f) mixed-phase γ - χ -Al₂O₃ support.

From the BJH pore diameter of 8 nm, it can be said that the type of pores is mesoporous structure (pore diameter of 3-50 nm). The nitrogen adsorption-desorption isotherms in **Figure 5.10** confirm this conclusion. All isotherms illustrate the hysteresis

loop at high relative pressure (P/P_0 more than 0.4) demonstrating that they are mesoporous structure corresponding to type IV of the BDDT classification [55].

5.1.6 Fourier transform infrared spectroscopy (FT-IR)

The functional groups in all catalysts can be determined by FT-IR. The FT-IR spectra that x-axis is the wavenumber in the unit of cm^{-1} and y-axis is %transmittance of Cu-AgLi system on alumina catalysts are displayed in **Figure 5.11**.

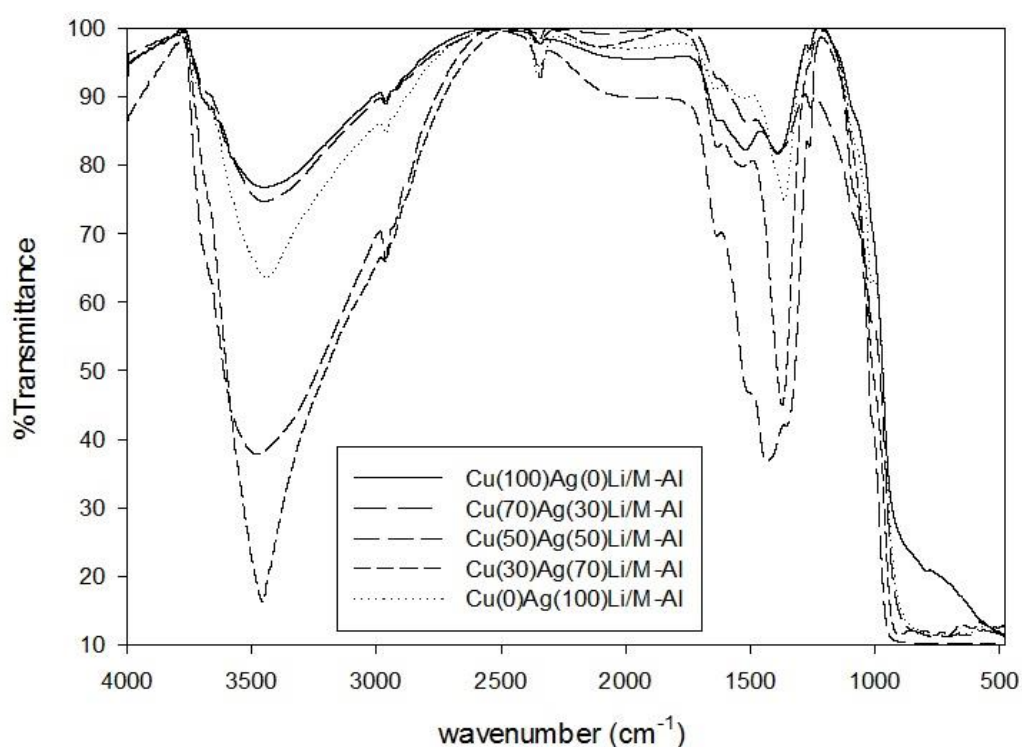


Figure 5. 11 FT-IR spectra of catalysts.

From the FT-IR spectra of different weight ratios of Cu:Ag supported on mixed-phase alumina. The IR bands at 3430 to 3475 cm^{-1} are attributed to the stretching vibration of OH- group for coordinated to Al^{3+} cations (Al-OH-Al) [56], whilst the bands at 1363-1632 cm^{-1} for all samples are assigned to H-OH vibrations of H_2O molecules. The bands at 600-790 cm^{-1} are due to Al-O vibration of Al_2O_3 [57], consistent with the XRD information. No peaks of other species appear in all spectra, which are ordinarily regarded as the evidence of totally reduction of copper and silver by H_2 .

5.1.7 UV-vis spectroscopy (UV-vis)

As explained in chapter 2 (theory) that the dehydrogenation or oxidative dehydrogenation reactions activity strongly depends on basic and redox metal active sites. Prior to the reaction, reduction process is necessary step to convert the oxidation state of Cu and Ag species to metallic forms. The oxidation state of Cu and Ag were determined by UV-visible spectroscopy, and the observed results are shown in **Figure 5.12**.

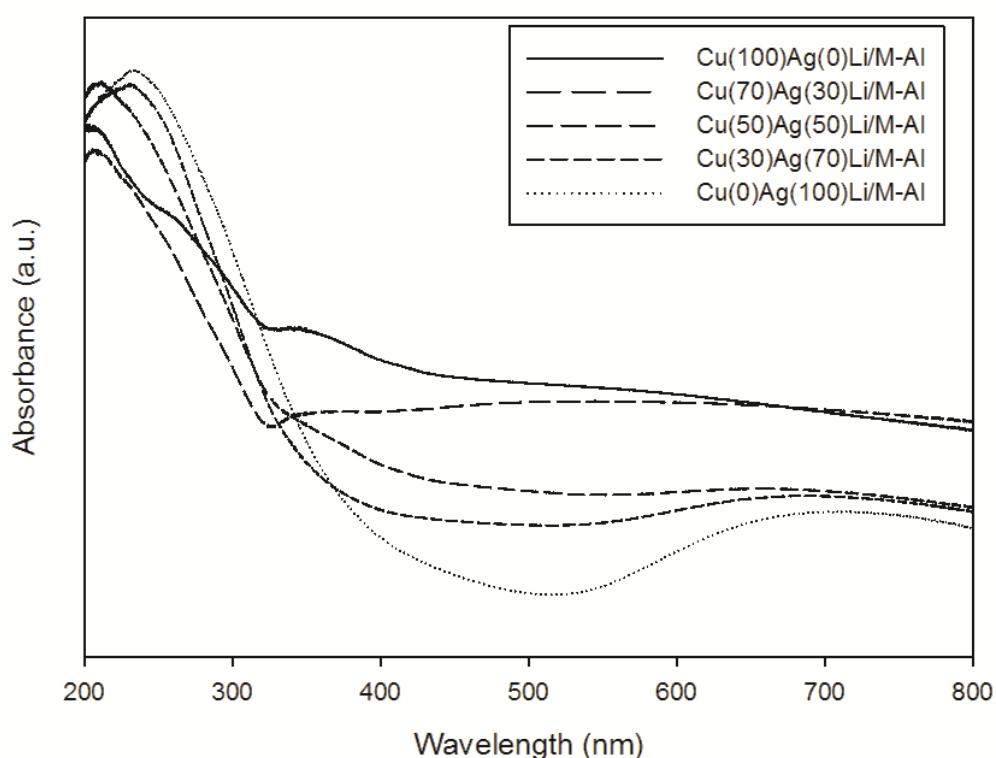


Figure 5. 12 The UV-visible absorption spectra of the catalysts.

The interaction of silver and copper oxides with alumina support probably has strong influence on the oxidation state of Cu and Ag. The UV-visible absorption spectra display the similarly high intensity around 210-240 nm, shoulder peak around 340-450 nm and another broad peak was found for only Cu(0)Ag(100)Li/M-Al at high absorption band around 600-800 nm. Janlamool *et al.* observed that Ag^+ state displayed the absorption at 210 nm and the peak at 430 nm corresponded to Ag^0 metallic particles

[49]. Mamontov *et al.* reported that the absorption band at 332 nm associated with the existence of the charge silver cluster ($\text{Ag}_n^{\delta+}$) [58]. These references are in good agreement with UV-visible profiles of Cu-AgLi/ Al_2O_3 catalysts. The Cu(0)Ag(100)Li/M-Al that contained Cu:Ag weight ratio of 0:100 exhibited the highest intensity of Ag^+ and $\text{Ag}_n^{\delta+}$ clusters peaks, while Cu(70)Ag(30)Li/M-Al exhibited the lowest absorption intensity of both peaks. Intensity of absorption band reveals to the amount of active species. Therefore, when weight ratio of Ag increased, catalysts have more active species promoting the activity for the studied reactions (dehydrogenation and oxidative dehydrogenation reactions). In addition, this catalyst system, the intensity increased in the order of Cu(0)Ag(100)Li/M-Al > Cu(30)Ag(70)Li/M-Al > Cu(50)Ag(50)Li/M-Al > Cu(100)Ag(0)Li/M-Al > Cu(70)Ag(30)Li/M-Al.

5.1.8 Temperature programmed reduction (TPR)

Hydrogen temperature programmed reduction experiments were performed to investigate the reducibility. This technique is suitable for testing low loaded and highly dispersed catalyst samples that characteristics are beyond the limitation of detector by other direct structural analysis methods, like XRD [3]. TPR is a quantitative technique that intensity of peak relate to the amount of each metal species. Monometallic, Cu(100)Ag(0)Li/M-Al and Cu(0)Ag(100)Li/M-Al, and bimetallic, Cu(30)Ag(70)Li/M-Al, Cu(50)Ag(50)Li/M-Al, and Cu(70)Ag(30)Li/M-Al, prepared by the incipient wetness impregnation method were analyzed and the TPR profiles are shown in **Figure 5.13 (left side)** and the Cu(100)Ag(0)Li/M-Al that contained weight ratio of 100% Cu is shown in **the right side of Figure 5.13** to clearly express the existence of copper reduction peak that hard to see in summarized peak profiles.

According to the TPR profiles, the reducibility of monometallic sample is discussed first. The TPR curve of Cu(100)Ag(0)Li/M-Al that disappears of silver specie can be clearly seen in **Figure 5.13** on the right hand side. It could be classified into one broad peak that deconvoluted to show a reduction peak at 100-400°C. The lower peak temperature is corresponded to the reduction of bulk CuO (Cu^{2+}) on surface and the higher peak temperature at the right hand side of this broad peak is likely a consequence of the reduction of core CuO (Cu^{2+}) occurred in alumina pore. From the overlap of peak, the reduction peak of Cu_2O (Cu^+) that it is regularly reduced at high

temperature around 580 to 590°C [53] that cannot be found from this characterized TPR profile.

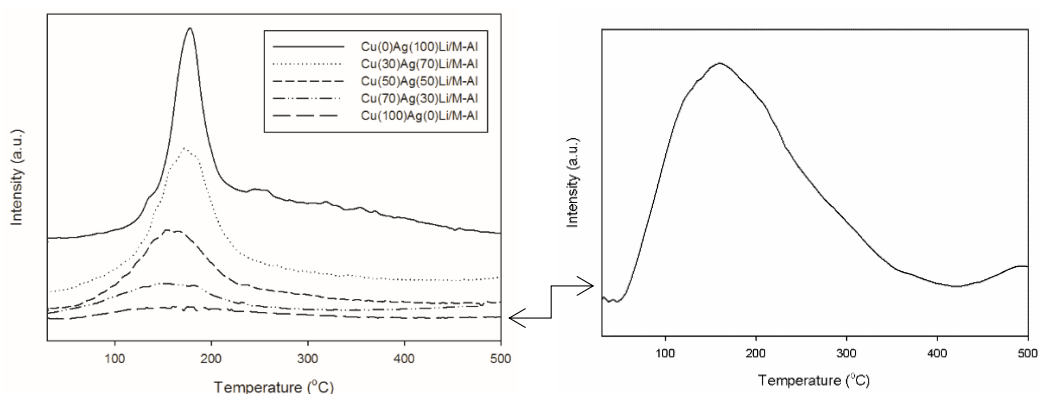


Figure 5. 13 TPR profiles of catalysts.

Cu-AgLi supported on alumina with various weight ratios of copper and silver (left) and TPR profile of only Cu(100)Ag(0)Li/M-Al (right).

The studied silver monometallic catalyst, or Cu(0)Ag(100)Li/M-Al, The TPR profile showed one peak of the reduction peak that has the explanation from Janlamool *et al.* reported that AgLi-CHI50 broad peak of TPR can be attributed to the overlap of two step reduction between Ag^+ to $\text{Ag}_n^{\delta+}$ in the lower temperature and $\text{Ag}_n^{\delta+}$ and Ag^0 in the higher temperature [49]. From characterized TPR profile, the sharp peak at 178°C is related to Ag^+ species and the lower intensity peak at 250 to 330°C is attributed to $\text{Ag}_n^{\delta+}$ species.

Focus on the amount of each species that can be examined from the peak intensity. Cu(0)Ag(100)Li/M-Al showed the highest intensity over the other weight ratio of Cu:Ag catalysts at 178°C and the intensities of TPR peaks decreased when silver loading in the catalysts decreased that Cu(100)Ag(0) showed the lowest intensity of TPR peak. From now, it can be concluded that the amount of Ag active species is much higher than the amount of Cu active species.

Another interesting point to the discussion is the occurrence of shifted peak. From bimetallic catalysts, which contained both copper and silver, the reduction temperature peaks also shifted from the characteristic peak of monometallic copper or monometallic silver samples. From the profiles reveals that the appearance of copper and silver species can decrease the reduction temperature lower than monometallic copper or silver. It could be said that at low temperature, metal species can be easily reduced because of the weak interaction than the strong interaction that

TPR peak appears at higher temperature [3]. The maximum reduction peaks for all bimetallic samples decreased with decreased the Ag weight ratios that have the reduction temperature from 178, 173, 154, and 152°C of Cu(0)Ag(100)Li/M-Al, Cu(30)Ag(70)Li/M-Al, Cu(50)Ag(50)Li/M-Al, and Cu(70)Ag(30)Li/M-Al, respectively. It can conclude that the presence of mixed copper and silver in catalysts system can decrease the electronic interaction between metal (Cu, Ag) and alumina supports that can see from the shifted of reduction peak to the lower temperature. However, the majority effect to the catalytic activity should be from the amount of Ag and Cu species more than the effect of shift peak position. Because of their huge difference between the intensity of Ag and Cu characteristic peak which Ag has a lot of active species but Cu has only a few amount of active species or it could be said that a number of active species involved the reducibility of Cu-AgLi supported on mixed-phase Al₂O₃ catalysts.

5.1.9 X-ray photoelectron spectroscopy (XPS)

The XPS was investigated for the Cu-AgLi supported on Al₂O₃ with different Cu and Ag ratios to confirm the composition at surface of catalyst, the existence of metallic state, and oxidation form of copper, silver, and lithium. The XPS analysis also determined the ability of Cu-AgLi samples to resist oxidation. To eliminate the analysis error, the prepared catalysts were fully dried under thermal overnight. XPS profiles are given in **Figure 5.14** to **Figure 5.17** for Cu 2p, Ag 3d, O 1s, and Li 1s, respectively.

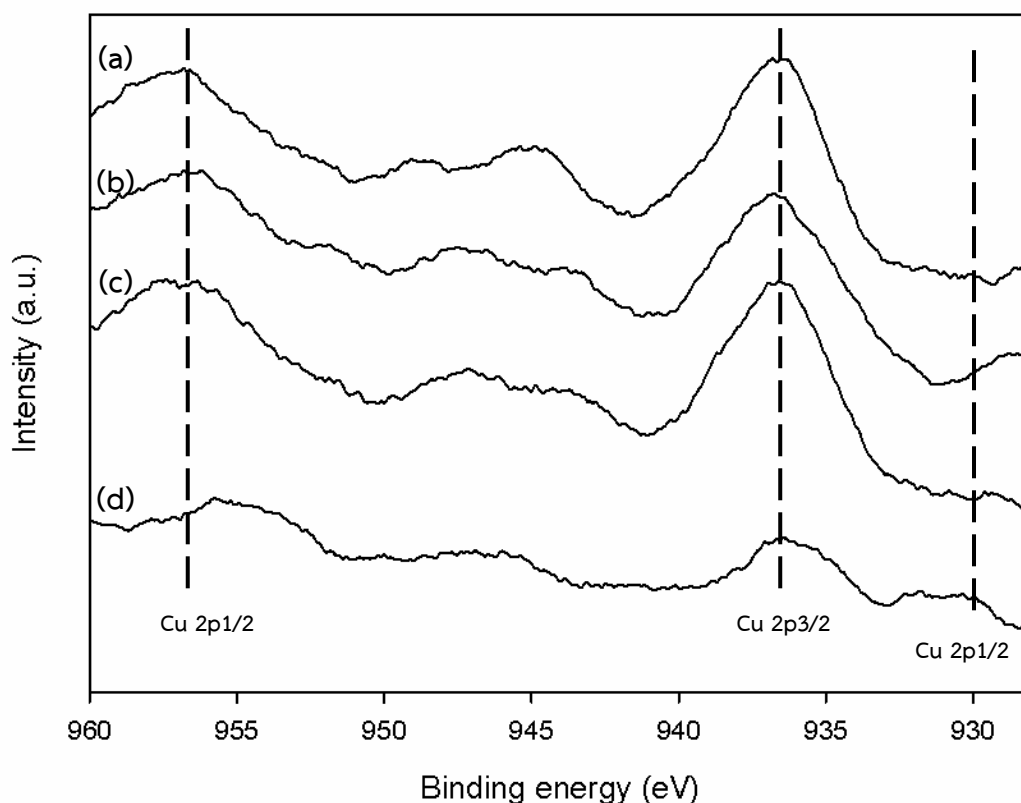


Figure 5. 14 XPS spectra of the Cu 2p of catalysts.

Recorded from (a) Cu(30)Ag(70)Li/M-Al, (b) Cu(50)Ag(50)Li/M-Al, (c) Cu(70)Ag(30)Li/M-Al and (d) Cu(100)Ag(0)Li/M-Al.

For copper nanoparticles catalysts, based on Gaussian curve fitting, the Cu 2p_{3/2}, and Cu 2p_{1/2} peaks are typically observed binding energies at 932.3, 934.0, and 953.6 eV [53, 59], respectively. In **Figure 5.14**, the XPS found the broad peak around 930, 936 and 957 eV for all various Cu:Ag weight ratios attributed to the zerovalent copper (Cu⁰) and Cu²⁺ species. It can be seen that the peaks of CuO at 936 and 957 eV have intensity increased when compared between monometallic Cu in **Figure 5.14 (d)** and bimetallic Cu and Ag in **Figure 5.14 (a) to (c)**. On the other hand, the peak of Cu⁰ at 930 eV decreased when silver was loaded in bimetallic samples, so it can be suggesting that in the case of bimetallic Cu and Ag, copper is easily oxidized. It means copper prefer to exist in the Cu²⁺ form from all possible oxidation state of copper (Cu²⁺, Cu⁺, and Cu⁰). The slight peak shift of Cu 2p was probably caused by the interaction between copper species and alumina support [60]. Hensen *et al.* reported that XPS of Cu 2p_{3/2} cannot differentiate between Cu⁺ and metallic Cu (Cu⁰) [1]. It can

confirm the direct reduction of surface Cu^{2+} to Cu^0 with a little transfer through Cu^+ species from XRD and H_2 -TPR techniques in the previous sections.

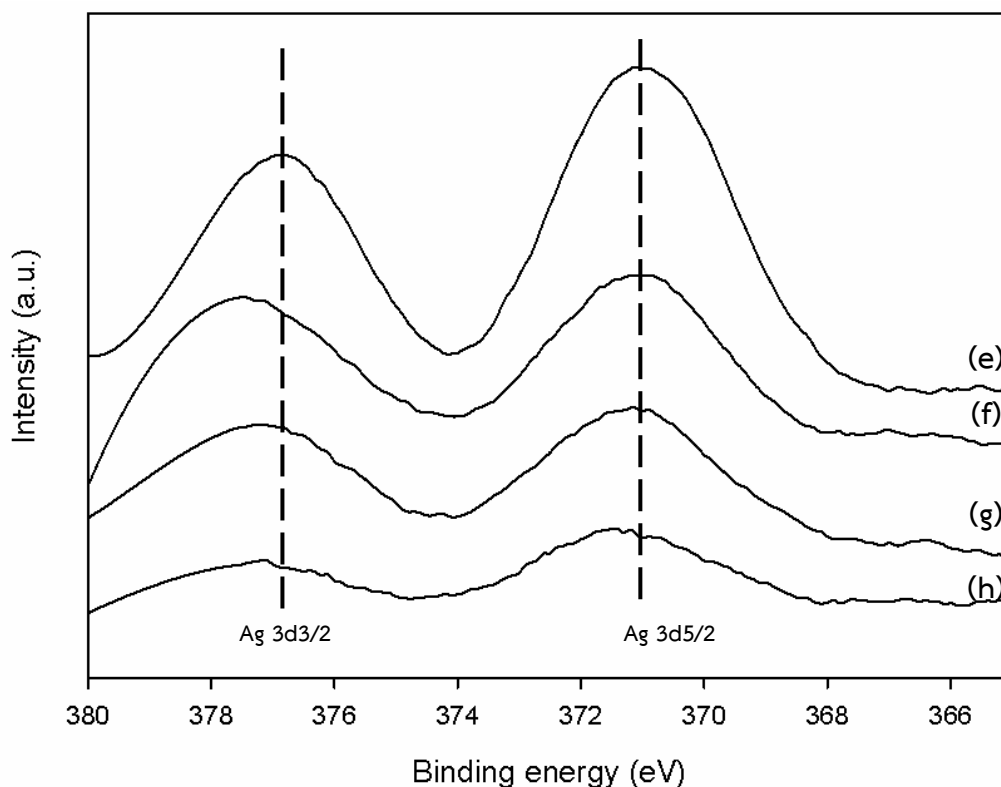


Figure 5. 15 XPS spectra of the Ag 3d of catalysts.

Recorded from (e) $\text{Cu}(0)\text{Ag}(100)\text{Li}/\text{M-Al}$, (f) $\text{Cu}(30)\text{Ag}(70)\text{Li}/\text{M-Al}$, (g) $\text{Cu}(50)\text{Ag}(50)\text{Li}/\text{M-Al}$ and (h) $\text{Cu}(70)\text{Ag}(30)\text{Li}/\text{M-Al}$.

The Ag 3d peaks are observed approximately at 371 and 377 eV in the XPS profiles. These 2 peaks are 3d5/2 and Ag 3d3/2, respectively which are in agreement with metallic silver (Ag^0) [1, 5]. It can be clearly noticed that the intensity of Ag 3d peaks increased when Ag weight ratio enlarged and $\text{Cu}(0)\text{Ag}(100)\text{Li}/\text{M-Al}$ has the highest intensity of both XPS peaks. Another point that discovered from XPS of Ag is when increased copper content for the bimetallic catalyst samples in **Figure 5.15 (f) to (h)**, the peak position shift to higher binding energy compared with monometallic sample in **Figure 5.15 (e)**. Ag 3d5/2 shifted from 370.8 to 371.6 eV and Ag 3d3/2 shifted from 376.5 to 377.9 eV that there were an intimate contact between copper and silver, and the interaction with each other also enable Ag to exhibit a greater tendency to lose electrons [57]. In other words, peaks of both Ag 3d5/2 and Ag 3d3/2 shifted to higher

binding energy means to facilitate oxidation of Ag^0 to Ag^+ states, agree with Hensen *et al.* report [1].

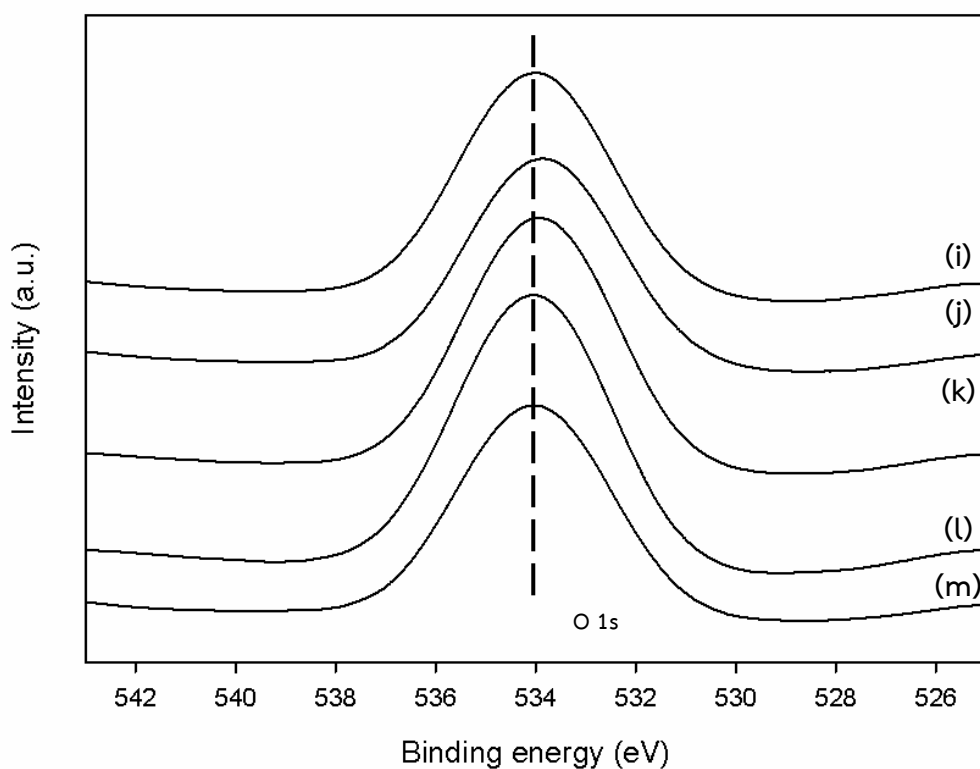


Figure 5. 16 XPS spectra of the O 1s of catalysts.

Recorded from (i) Cu(0)Ag(100)Li/M-Al, (j) Cu(30)Ag(70)Li/M-Al, (k) Cu(50)Ag(50)Li/M-Al, (l) Cu(70)Ag(30)Li/M-Al, and (m) Cu(100)Ag(0)Li/M-Al.

The existence of the oxide forms were confirmed by the presence of the oxygen peak of O 1s at 534 eV for all catalysts. Lee *et al.* reported that the lattice O exhibits a binding energy between 529 and 530 eV. These 2 peaks can be attributed to the lattice O and chemisorbed O_2 on the surface, respectively [59]. Studied catalysts found to be a broad peaks at 534 eV, maybe comes from the overlap and shift peak interaction. From O 1s XPS spectra, it can support the observation of CuO (Cu^{2+}) and Ag_2O (Ag^+) species in the prepared Cu-AgLi supported on mixed-phase Al_2O_3 catalysts.

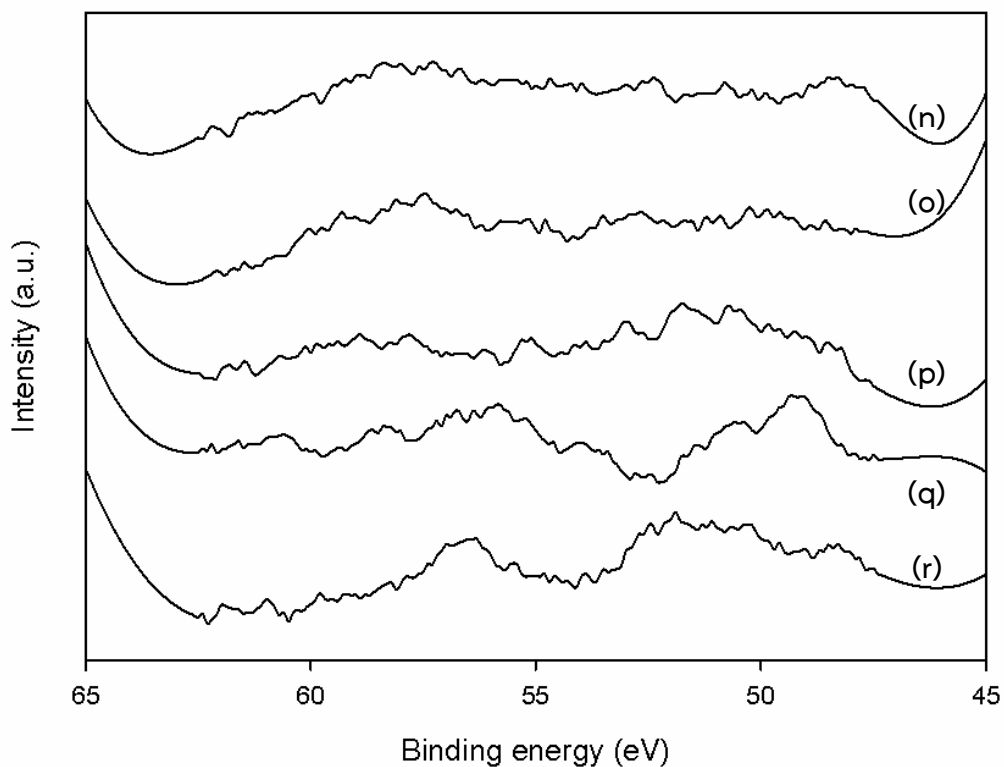


Figure 5. 17 XPS spectra of the Li 1s of catalysts.

Recorded from (n) Cu(0)Ag(100)Li/M-Al, (o) Cu(30)Ag(70)Li/M-Al, (p) Cu(50)Ag(50)Li/M-Al, (q) Cu(70)Ag(30)Li/M-Al, and (r) Cu(100)Ag(0)Li/M-Al.

Using the surface-sensitive analytical technique XPS to analyze the oxidation states of Li species, it is difficult to find the binding energy peak of lithium. However, the EDX technique can show the existence and dispersion of lithium in the studied Cu-AgLi on mixed-phase alumina catalysts.

5.1.10 Carbon dioxide Temperature-Programmed Desorption (CO₂-TPD)

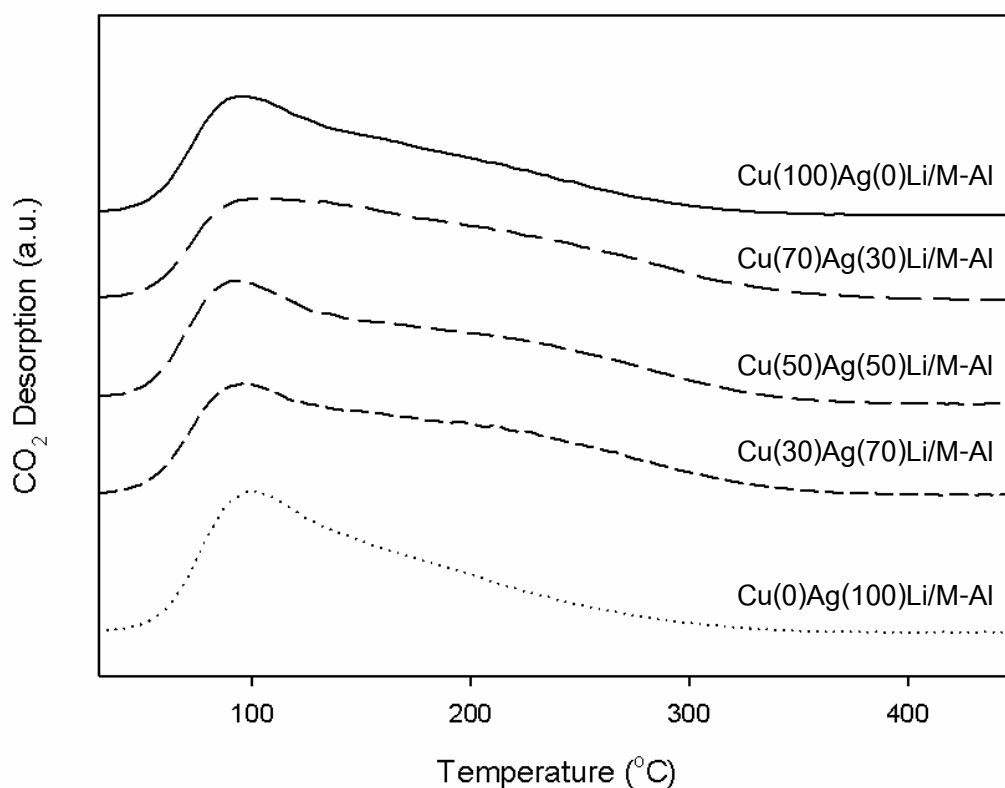


Figure 5. 18 CO₂-TPD profiles of catalysts.

The surface basicity of catalysts was determined by TPD of CO₂ technique that their profiles are shown in **Figure 5.18**. The CO₂-TPD profiles had the main desorption peaks for the Cu-AgLi supported on Al₂O₃ catalysts appearing at low desorption temperature between 90 and 100°C, revealing that all studied catalysts had weak-strength basic sites and involved OH- functional group. Medium-strength (150°C) peaks are about M-O²⁻ pair that carbon dioxide molecules interact in the medium level. The peaks at temperature above 250°C involve O²⁻ ions that CO₂ interaction on strong. Additionally, the existence of χ -phase of Al₂O₃ support causes the increase of more medium and strong basic sites, so the shoulder peak above 120°C is observed in all represented profiles. The main desorption peaks occur at low to medium desorption temperature. Hence, the determination about quantitative measurement of the basic sites will be separated into 2 regions; weak-to-medium and strong. The total, weak-to-medium and strong evolved CO₂ was calculated by integration of TPD curves as the result summarized in **Table 5.4** in the unit of $\mu\text{mole CO}_2$ per g. catalyst.

Table 5. 4 The amount of basicity of catalysts with different Cu:Ag ratios.

Catalysts	Weak-to-moderate basicity ($\mu\text{mole CO}_2 \text{ g}^{-1}$)	Strong basicity ($\mu\text{mole CO}_2 \text{ g}^{-1}$)	Total basicity ($\mu\text{mole CO}_2 \text{ g}^{-1}$)
Cu(100)Ag(0)Li/M-Al	211	6	217
Cu(70)Ag(30)Li/M-Al	224	9	233
Cu(50)Ag(50)Li/M-Al	250	7	257
Cu(30)Ag(70)Li/M-Al	276	10	285
Cu(0)Ag(100)Li/M-Al	221	7	228

The oxidative dehydrogenation and dehydrogenation reactions both are well-known as favorite basic site catalytic reactions. The more basicity of catalyst can catalyze the forward reaction to gain more conversion and activity. The amount of CO_2 consumed from **Table 5.4** can be arranged the total basicity from highest to lowest in order of: Cu(30)Ag(70)Li/M-Al > Cu(50)Ag(50)Li/M-Al > Cu(70)Ag(30)Li/M-Al > Cu(0)Ag(100)Li/M-Al > Cu(100)Ag(0)Li/M-Al that the values are 286, 257, 233, 228, and 217 $\mu\text{mole CO}_2 / \text{g cat}$. According to the TPD results, the existence of both copper and silver has the higher basicity than single copper or silver alone. In other words, these bimetallic catalysts have the synergistic effect.

5.2 Activity testing by temperature programmed during 200-400°C

The catalytic performance of the mixed phase alumina loading with copper, silver, and lithium catalysts conversing ethanol to acetaldehyde was studied in both of dehydrogenation and oxidative dehydrogenation reactions. Before the reaction, the prepared catalysts were reduced *in situ* in flowing H_2 at 300°C for 1 hour. The reaction testing begins when 0.15 g of catalyst was added into the fixed-bed reactor, then vaporized ethanol having flow rate of 45 ml/min was flowed through the reactor. The reaction was carried out in the temperature ranging from 200 to 400°C.

The catalytic activity depends on various parameter such as the operating temperature [3, 52, 60, 61], the type and amount of metals loading [3, 10, 28, 53, 61], and effect of the atmosphere conditions [6]. Besides, the reaction temperature is usually a driving force to improve catalytic conversion of endothermic reaction, the

catalyst basicity and redox properties are the important factor influencing on the reaction activity. Dewilde *et al.* [62] found that the dehydrogenation of ethanol over basic catalyst produces acetaldehyde as a main product. The reaction testing is discussed within 2 reactions, which are the catalytic activity in dehydrogenation of ethanol in **section 5.2.1** and the catalytic activity in oxidative dehydrogenation of ethanol in **section 5.2.2**. The reaction results were reported in terms of ethanol conversion, acetaldehyde selectivity, and yield with respect to temperature profile. The definition and calculation of conversion, selectivity, and yield are already shown in **Appendix E**.

5.2.1 Dehydrogenation reaction of ethanol

The Cu-AgLi/M-Al catalyst system was also brought to evaluate the catalytic activity in ethanol dehydrogenation reaction at specific reaction temperature of 200, 250, 300, 350, and 400°C under atmospheric pressure. The ethanol conversion, acetaldehyde selectivity, and yield were all investigated and described in **Figure 5.19** to **Figure 5.21**, respectively.

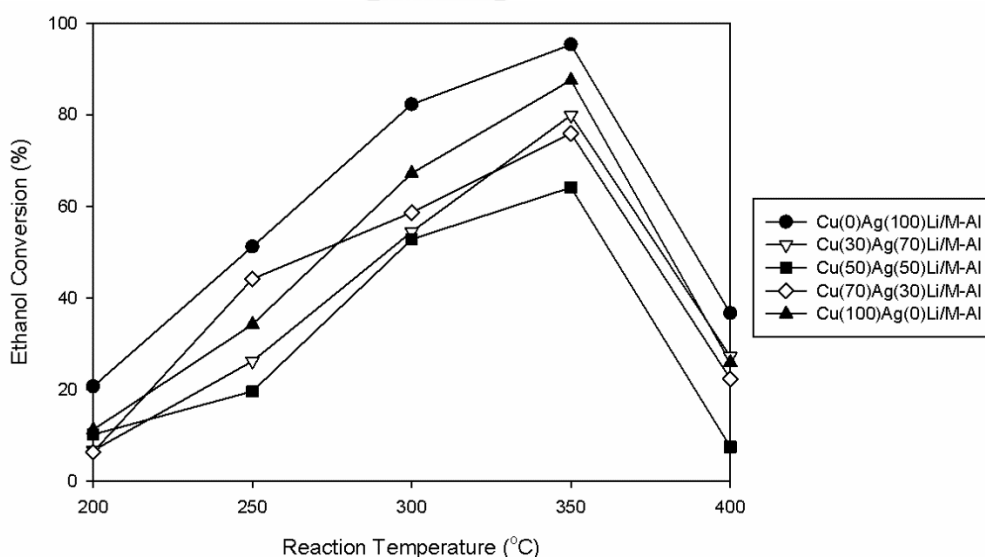


Figure 5. 19 Ethanol conversion of catalysts in dehydrogenation.

In **Figure 5.19**, the temperature dependence of ethanol conversion of the Cu-AgLi/M-Al catalyst system is presented for dehydrogenation conditions. Starting the reaction temperature of 200°C, the conversion was continuously escalated as the

raising in temperature from 200 to 350°C that gave the highest ethanol conversion in all catalysts. The increasing of conversion associated with the endothermic behavior of dehydrogenation reaction that favored of high temperature. The sharp decrease in ethanol conversion occurred in a temperature range of 350 to 400°C because of the deactivation of catalysts by coke formation that can be proven by TGA technique (discussed in **section 5.4**).

At 350°C, the temperature that gave the highest conversion in all catalysts, the conversion can be arranged in order of: Cu(0)Ag(100)Li/M-Al > Cu(100)Ag(0)Li/M-Al > Cu(30)Ag(70)Li/M-Al > Cu(70)Ag(30)Li/M-Al > Cu(50)Ag(50)Li/M-Al with the ethanol conversion of 95, 88, 80, 76, and 64%, respectively.

So, it seems that monometallic catalysts can be converted to the products more than bimetallic copper and silver catalysts. The ethanol conversion agrees with the characterization results from UV-visible, H₂-TPR, and XPS that the more amount of active species of Ag⁺ and Ag_n^{δ+} cluster can improve the catalytic activity in this reaction. However, as discussed in the theory of dehydrogenation reaction (chapter 2), not only the redox properties that effect to the activity, the properties of basicity also have the strong influence of reaction. So, it is the synergistic effect of both redox sites and basic sites to achieve quite high ethanol conversion performance.

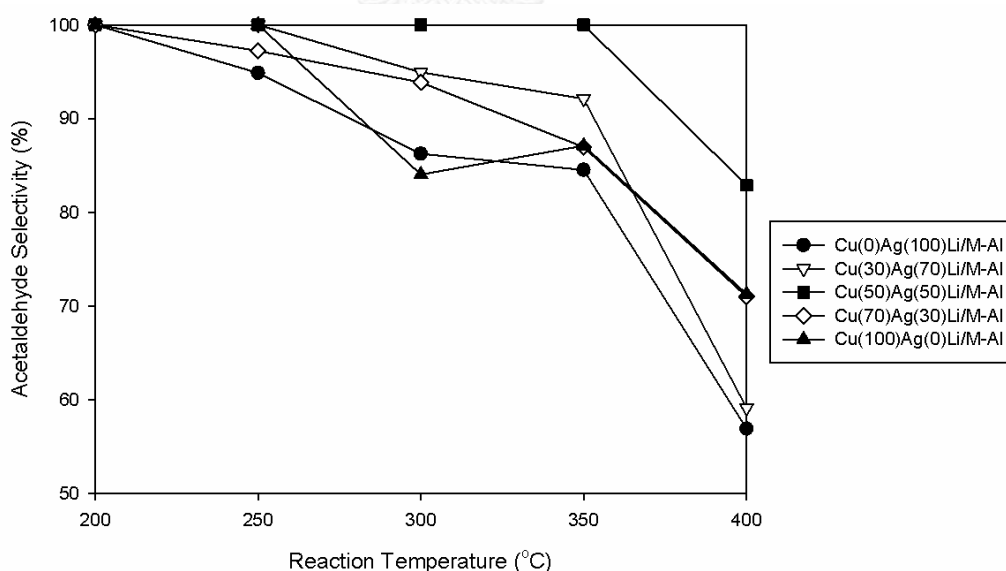


Figure 5. 20 Acetaldehyde selectivity of catalysts in dehydrogenation.

Figure 5.20 displays acetaldehyde selectivity among all studied catalyst samples. According to the results, the selectivity towards acetaldehyde of all catalysts

found to be continuously decreased as the rising in reaction temperature of 200 to 400°C excepting for Cu(50)Ag(50)Li/M-Al that can be converted ethanol to only acetaldehyde product until 350°C. This trend of selectivity can say that the bimetallic can be produced more amount of the desired product, acetaldehyde, than monometallic catalysts. From the selectivity at lower than 100% completely converted to acetaldehyde, the other byproducts are produced in the meantime. The undesired byproducts of dehydrogenation of ethanol in this study compose of acetic acid and ethylene that measured and summarized in **Table 5.5**. No observation of CO and CO₂ as a byproduct from TCD detector.



Table 5. 6 The selectivity of acetaldehyde and other byproducts in dehydrogenation of ethanol of different weight content of copper and silver catalysts.

Catalysts	Selectivity (%)														
	Acetaldehyde						Acetic acid						Ethylene		
	200	250	300	350	400	200	250	300	350	400	200	250	300	350	400
Temperature (°C)	200	250	300	350	400	200	250	300	350	400	200	250	300	350	400
Cu(0)Ag(100)Li/M-Al	100	94.8	86.2	84.5	56.9	-	5.2	13.7	15.5	0.7	-	-	-	-	42.4
Cu(30)Ag(70)Li/M-Al	100	100	94.9	92.1	59.1	-	-	5.1	7.9	3.1	-	-	-	-	37.8
Cu(50)Ag(50)Li/M-Al	100	100	100	100	82.9	-	-	-	-	-	-	-	-	-	17.1
Cu(70)Ag(30)Li/M-Al	100	97.2	93.9	86.9	71.0	-	2.8	6.1	13.0	4.9	-	-	-	0.1	23.8
Cu(100)Ag(0)Li/M-Al	100	100	84.0	87.1	71.3	-	-	16.0	12.9	0.5	-	-	-	-	28.2

Table 5. 8 The yield of acetaldehyde and other byproducts in dehydrogenation of ethanol of different weight content of copper and silver catalysts.

Catalysts	Yield (%)																
	Acetaldehyde							Acetic acid							Ethylene		
	200	250	300	350	400	200	250	300	350	400	200	250	300	350	400		
Temperature (°C)	200	250	300	350	400	200	250	300	350	400	200	250	300	350	400		
Cu(0)Ag(100)Li/M-Al	20.6	6.7	10.2	6.3	11.2	-	2.6	11.3	14.5	0.26	-	-	-	-	15.5		
Cu(30)Ag(70)Li/M-Al	48.6	26.2	19.6	42.9	34.2	-	-	2.8	6.3	0.85	-	-	-	-	10.3		
Cu(50)Ag(50)Li/M-Al	70.9	51.7	52.8	55.0	56.4	-	-	-	-	-	-	-	-	-	1.3		
Cu(70)Ag(30)Li/M-Al	80.5	72.5	64.1	66.0	76.2	-	1.2	3.6	9.8	1.2	-	-	-	0.1	5.3		
Cu(100)Ag(0)Li/M-Al	20.8	16.1	16.2	15.8	18.4	-	-	10.7	11.3	0.1	-	-	-	-	7.3		

As seen the selectivity of acetic acid and ethylene in **Table 5.5**, acetic acid can be detected by FID detector from starting reaction temperature, 200°C, until 400°C less than 16% selectivity for overall catalysts. The mechanism of acetic acid production comes from the further reaction of ethanol to acetaldehyde, and acetaldehyde to acetic acid. Sun *et al.* said that its includes base-catalyzed dehydrogenation of ethanol to form acetaldehyde, followed by further oxidation of acetaldehyde to acetic acid [63]. In the case of ethylene, its selectivity presents only at the high thermal condition at 400°C with a large amount of ethylene. Ethylene produced via ethanol dehydration reaction [55]. Overall selectivity of ethylene can be determined around 20-40%. It can be noticed that the monometallic samples, which are Cu(0)Ag(100)Li/M-Al and Cu(100)Ag(0)Li/M-Al gave the higher selectivity of ethylene than the bimetallic catalysts, which are Cu(30)Ag(70)Li/M-Al, Cu(50)Ag(50)Li/M-Al, and Cu(70)Ag(30)Li/M-Al. The finding of ethylene byproduct because the support alumina has acid sites that the ethanol conversion favors forming ethylene at the high reaction temperature.

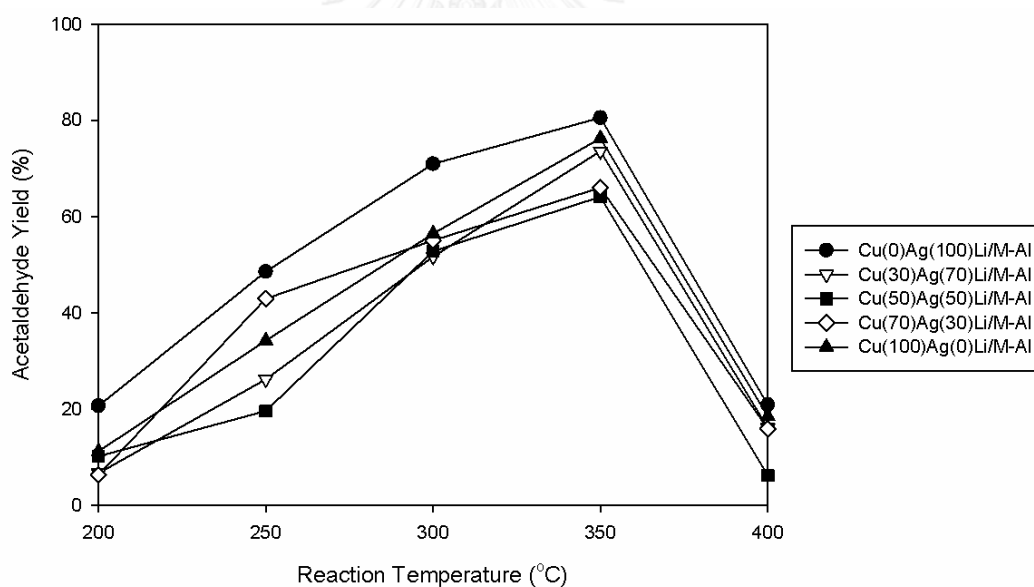


Figure 5. 21 Acetaldehyde yield of catalysts in dehydrogenation.

According to the acetaldehyde yield that depended on both conversion and selectivity results, which is shown in **Figure 5.21** above. The yields of acetaldehyde have the same trend in all catalysts. Lowest reaction temperature at 200°C, the yield of all catalysts is around 10%, excepting for Cu(0)Ag(100)Li/M-Al that gave 20% yield. In addition, Cu(0)Ag(100)Li/M-Al shows the outstanding results that give the highest %yield in all reaction temperature of this study. It is interesting to select this sample

to further investigate the stability property at specific temperature in the time-on-stream that was described in **section 5.3**.

5.2.2 Oxidative dehydrogenation reaction of ethanol

The catalytic performance of the Cu-AgLi/M-Al catalysts was studied in the effect of addition of oxygen as a co-feed reactant. So, the dehydrogenation reaction in aerobic conditions was also studied in the same temperature range and pressure. The aerobic condition is also well-known in the name of “oxidative dehydrogenation” reaction or “oxidation” reaction that has 2 reactants; ethanol and oxygen. The ethanol conversion, acetaldehyde selectivity, and yield of oxidative dehydrogenation reaction is shown in **Figure 5.22** to **Figure 5.24**. About the anaerobic dehydrogenation was already shown the results including ethanol conversion, acetaldehyde selectivity and yield in **Figure 5.20** to **Figure 5.22** in previous section, respectively.

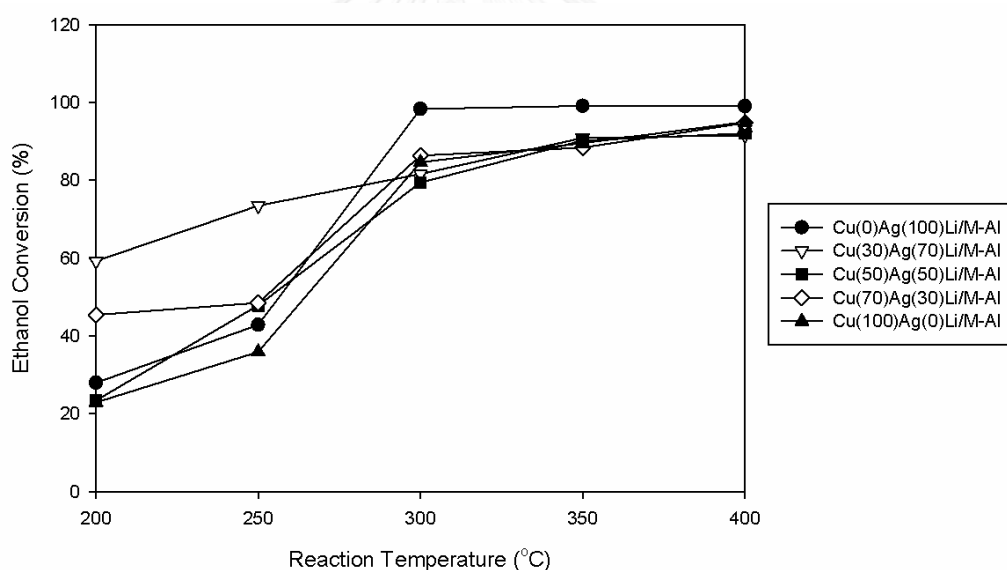


Figure 5. 22 Ethanol conversion of catalysts in oxidative dehydrogenation.

Figure 5.22 illustrates the ethanol conversion of oxidative dehydrogenation reaction obtained from Cu(0)Ag(100)Li/M-Al, Cu(30)Ag(70)Li/M-Al, Cu(50)Ag(50)Li/M-Al, Cu(70)Ag(30)Li/M-Al, and Cu(100)Ag(0)Li/M-Al. In the effect of reaction temperature, the ethanol conversion was elucidated when increased temperature from 200 to 400°C.

Consider the low reaction temperature region, Cu(30)Ag(70)Li/M-Al interestingly

expresses the highest ethanol conversion of 59.27 and 73.50% at 200 and 250°C, respectively. The conversion can be arranged in the order of: Cu(30)Ag(70)Li/M-Al > Cu(70)Ag(30)Li/M-Al > Cu(50)Ag(50)Li/M-Al > Cu(0)Ag(100)Li/M-Al > Cu(100)Ag(0)Li/M-Al. This result reveals that bimetallic demonstrated the easily oxidized when compared with monometallic copper or silver (correspond with TPR profiles in characterization part). In the high reaction temperatures that consist of 300 to 400°C, the ethanol conversion of all catalysts is quite similar around 80-85%, 88-90%, and 92-94% at 300, 350, and 400°C reaction temperature, respectively. Except for Cu(0)Ag(100)Li/M-Al that gave the highest value with closely complete ethanol conversion (ca. 98-99%) in the high-temperature range. Hence, in the oxidative dehydrogenation reaction, basic properties of bimetallic Cu and Ag play the key role to enhance the activity in the low reaction temperature region but in the high-temperature range, redox properties play the key role to reaction activity instead.

Unlike the anaerobic dehydrogenation, no drop of activity was observed from oxidative dehydrogenation reaction. It can be said that the presence of oxygen in the reaction improves the thermal resistance to slower deactivation via coke formation. This discussion is in good agreement with the report by Riisager *et al.* in the oxidative dehydrogenation of benzyl alcohol to benzaldehyde. The report observed that atmospheric oxygen can regenerate the catalytic metal site cycle [6].

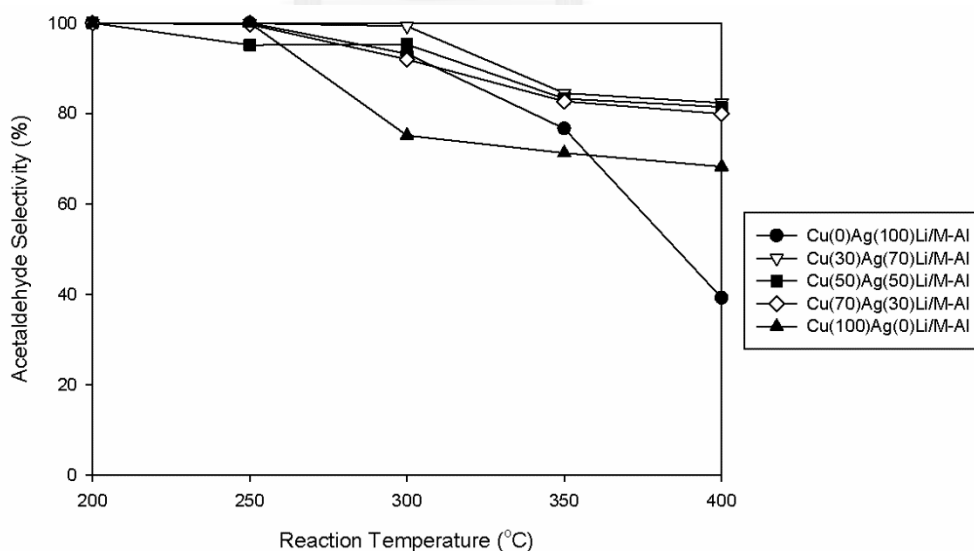


Figure 5. 23 Acetaldehyde selectivity of catalysts in oxidative dehydrogenation.

The selectivity towards acetaldehyde of all studied catalysts is shown in **Figure 5.23**. The results demonstrated the entirely acetaldehyde produced from ethanol oxidative dehydrogenation at 200°C and the acetaldehyde selectivity of all catalysts found to be slightly diminished as the raising in reaction temperature of 250 to 350°C. Focusing on the monometallic catalysts, after 250°C the acetaldehyde selectivity drops sharply from 100 to 39.19% of Cu(0)Ag(100)Li/M-Al and from 99.98 to 68.22% of Cu(100)Ag(0)Li/M-Al. Difference from the bimetallic catalysts, Cu(30)Ag(70)Li/M-Al, Cu(50)Ag(50)Li/M-Al, and Cu(70)Ag(30)Li/M-Al, they still remain higher acetaldehyde selectivity than 80%. This trend of selectivity can be said that the bimetallic can produce the amount of the desired product, acetaldehyde more than the monometallic catalysts. It is a good news and get the same trend with dehydrogenation reaction in the previous section. From the selectivity uncomplete converted to acetaldehyde, the other byproducts are produced in the meantime. The undesired byproducts of oxidative dehydrogenation of ethanol in this study consist of acetic acid, ethylene, carbon monoxide, and carbon dioxide. The amount of each products can be detected in both FID and TCD detectors and summarized in **Table 5.7** below.

Table 5. 10 The selectivity of acetaldehyde and other byproducts in oxidative dehydrogenation of ethanol of different weight content of copper and silver catalysts.

Catalysts	Selectivity (%)														
	Acetaldehyde					Acetic acid					Ethylene				
	Temperature (°C)	200	250	300	350	400	200	250	300	350	400	200	250	300	350
Cu(0)Ag(100)Li/M-Al	100	100	93.2	76.6	39.2	-	-	1.1	2.0	0.8	-	-	0.3	0.6	3.9
Cu(30)Ag(70)Li/M-Al	99.9	99.9	99.3	84.5	82.3	0.1	0.1	0.6	4.5	0.9	-	-	-	2.1	4.9
Cu(50)Ag(50)Li/M-Al	100	95.1	95.3	83.3	81.4	-	4.9	1.6	3.6	-	-	-	1.5	3.9	4.3
Cu(70)Ag(30)Li/M-Al	100	99.7	91.9	82.7	79.9	-	-	1.5	3.5	2.4	-	0.3	4.1	3.4	4.8
Cu(100)Ag(0)Li/M-Al	100	100	75.1	71.2	68.2	-	-	-	-	-	-	-	8.3	8.1	6.4

Catalysts	Selectivity (%)														
	Carbon monoxide (CO)					Carbon dioxide (CO ₂)									
	Temperature (°C)	200	250	300	350	400	200	250	300	350	400				
Cu(0)Ag(100)Li/M-Al	-	-	5.2	20.0	49.9	-	-	-	0.7	6.0					
Cu(30)Ag(70)Li/M-Al	-	-	-	7.1	5.9	-	-	-	1.8	5.8					
Cu(50)Ag(50)Li/M-Al	-	-	-	6.5	10.8	-	-	1.5	2.7	3.5					
Cu(70)Ag(30)Li/M-Al	-	-	-	8.1	10.8	-	-	2.4	2.4	2.1					
Cu(100)Ag(0)Li/M-Al	-	-	12.8	15.4	19.6	-	-	3.8	5.2	5.8					

As seen the selectivity of acetic acid, ethylene, CO, and CO₂ in **Table 5.7**, the acetic acid selectivity of all catalysts is less than 5%, while ethylene selectivity is less than 5% except Cu(100)Ag(0)Li/M-Al that present ethylene selectivity of 6-8%. The amount of acetic acid and ethylene detected from oxidative dehydrogenation reaction were lower than dehydrogenation reaction, this suggested that the addition of oxygen co-feed will improve the mechanism control to route ethanol converted to form acetaldehyde product. Unlike the dehydrogenation reaction, this oxidative dehydrogenation observed the CO and CO₂ as the byproducts and their selectivity increased following the rise of temperature. It can be noticed that the monometallic samples which are Cu(0)Ag(100)Li/M-Al and Cu(100)Ag(0)Li/M-Al gave higher selectivity of carbon monoxide than the bimetallic catalysts which are Cu(30)Ag(70)Li/M-Al, Cu(50)Ag(50)Li/M-Al, and Cu(70)Ag(30)Li/M-Al in the temperature range of 300-400°C. The formation of CO and CO₂ byproducts results from the appearance of oxygen as a co-feed reactant in this oxidative dehydrogenation reaction.

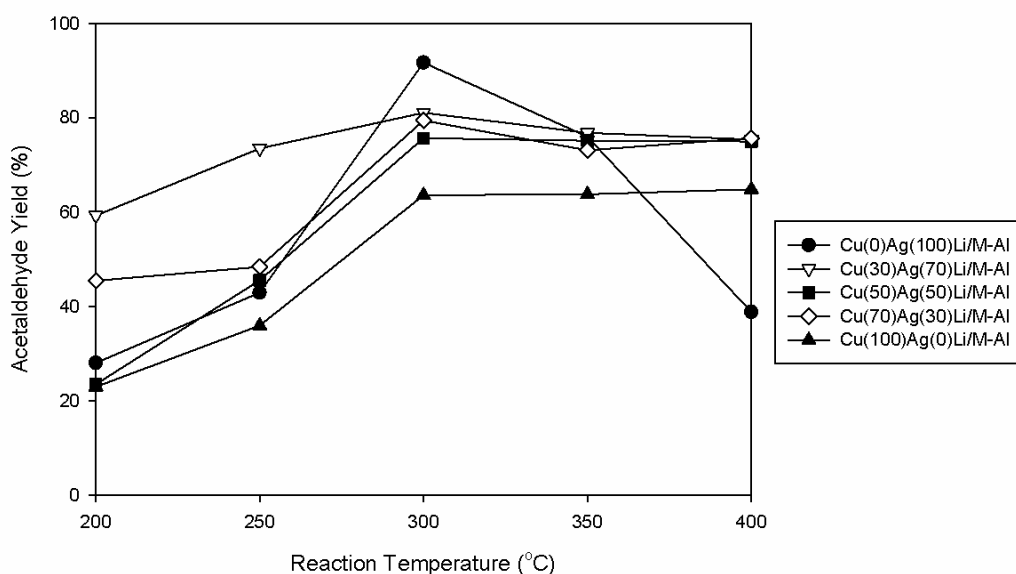


Figure 5. 24 Acetaldehyde yield of catalysts in oxidative dehydrogenation.

Table 5. 12 The yield of acetaldehyde and other byproducts in oxidative dehydrogenation of ethanol of different weight content of copper and silver catalysts.

Catalysts	Yield (%)															
	Acetaldehyde						Acetic acid						Ethylene			
Temperature (°C)	200	250	300	350	400	400	200	250	300	350	400	200	250	300	350	400
Cu(0)Ag(100)Li/M-Al	28.0	59.2	23.5	45.4	22.9	-	-	-	1.1	2.0	0.9	-	-	0.3	0.6	3.8
Cu(30)Ag(70)Li/M-Al	42.9	73.5	45.5	48.4	35.9	-	-	0.5	4.1	0.9	-	-	-	-	1.9	4.5
Cu(50)Ag(50)Li/M-Al	91.6	81.0	75.6	79.4	63.5	-	2.3	1.2	3.3	-	-	-	-	1.2	3.5	4.0
Cu(70)Ag(30)Li/M-Al	75.9	76.8	75.1	73.1	63.8	-	-	1.3	3.1	2.3	-	0.2	3.6	3.0	4.5	4.5
Cu(100)Ag(0)Li/M-Al	38.8	75.4	74.9	75.7	64.8	-	-	-	0.1	0.1	-	-	-	7.1	7.3	6.0

Catalysts	Yield (%)											
	Carbon monoxide (CO)						Carbon dioxide (CO ₂)					
Temperature (°C)	200	250	300	350	400	400	200	250	300	350	400	
Cu(0)Ag(100)Li/M-Al	-	-	5.1	19.8	49.4	-	-	-	-	0.7	6.0	
Cu(30)Ag(70)Li/M-Al	-	-	-	6.4	5.5	-	-	-	-	1.6	5.3	
Cu(50)Ag(50)Li/M-Al	-	-	-	5.8	9.9	-	-	-	1.2	2.4	3.2	
Cu(70)Ag(30)Li/M-Al	-	-	-	7.1	10.2	-	-	-	2.1	2.1	2.0	
Cu(100)Ag(0)Li/M-Al	-	-	10.8	13.8	18.6	-	-	-	3.2	4.6	5.5	

According to the acetaldehyde yield that depended on both conversion and selectivity results, it is shown in **Figure 5.24**. The yields of acetaldehyde accrue in the temperature of 200 to 300°C in order of Cu(30)Ag(70)Li/M-Al (59% rise to 81%) > Cu(70)Ag(30)Li/M-Al (45% rise to 79%) > Cu(0)Ag(100)Li/M-Al (28% rise to 92%) > Cu(50)Ag(50)Li/M-Al (24% rise to 76%) > Cu(100)Ag(0)Li/M-Al (23% rise to 64%). From all catalysts, Cu(0)Ag(100)Li/M-Al displays the outstanding results that give highest value at 300°C of 92% acetaldehyde yield. Focusing on the low temperature condition to reduce the thermal supply, the Cu(30)Ag(70)Li/M-Al shows the excellent yield at 200°C of 59% acetaldehyde yield. It is interesting to select these samples to further investigate the stability property at specific temperature in the time-on-stream that will be discussed in **section 5.3**.

5.3 The catalytic stability with time-on-stream testing

From dehydrogenation reaction, Cu(0)Ag(100)Li/M-Al was chosen as the representative catalyst having the highest acetaldehyde yield of 81% at 350°C that was discussed in **section 5.2.1**. On the oxidative dehydrogenation catalytic results, Cu(0)Ag(100)Li/M-Al was also chosen as the representative catalyst producing the highest yield of 92% at 300°C and Cu(30)Ag(70)Li/M-Al was chosen as the highest acetaldehyde yield at lowest temperature zone; 59% at 200°C that was discussed in **section 5.2.2**. Therefore, these 3 catalysts were brought to compare the characteristics and thermal stability properties with time-on-stream programmed for 10 hr. The studied of spent catalyst characteristics explained in **section 5.4**. The catalytic activity of time-on-stream testing showed the results in the form of ethanol conversion and acetaldehyde yield in **Figure 5.25** and **Figure 5.26**, respectively.

In **Figure 5.25** below, the ethanol conversion of Cu(0)Ag(100)Li/M-Al running in dehydrogenation at 350°C and in oxidative dehydrogenation reaction at 300°C and Cu(30)Ag(70)Li/M-Al running in oxidative dehydrogenation reaction at 200°C were examined via time-on-stream system for 10 hr. The results were found that the reaction study of dehydrogenation of Cu(0)Ag(100)Li/M-Al at 350°C gave a quite stable of ethanol conversion around 72-77%. While the oxidative dehydrogenation reaction of both Cu(0)Ag(100)Li/M-Al at 300°C and Cu(30)Ag(70)Li/M-Al at 200°C had the increasing of ethanol conversion at the beginning of reaction time and became more stable after 5 hr of Cu(0)Ag(100)Li/M-Al and after 2 hr of Cu(30)Ag(70)Li/M-Al. This observation is mentioned that the oxidative dehydrogenation reaction takes longer

time than dehydrogenation to reach the steady state. The comparison of ethanol conversion between temperature programmed and time-on-stream system is shown in Table 5.9.

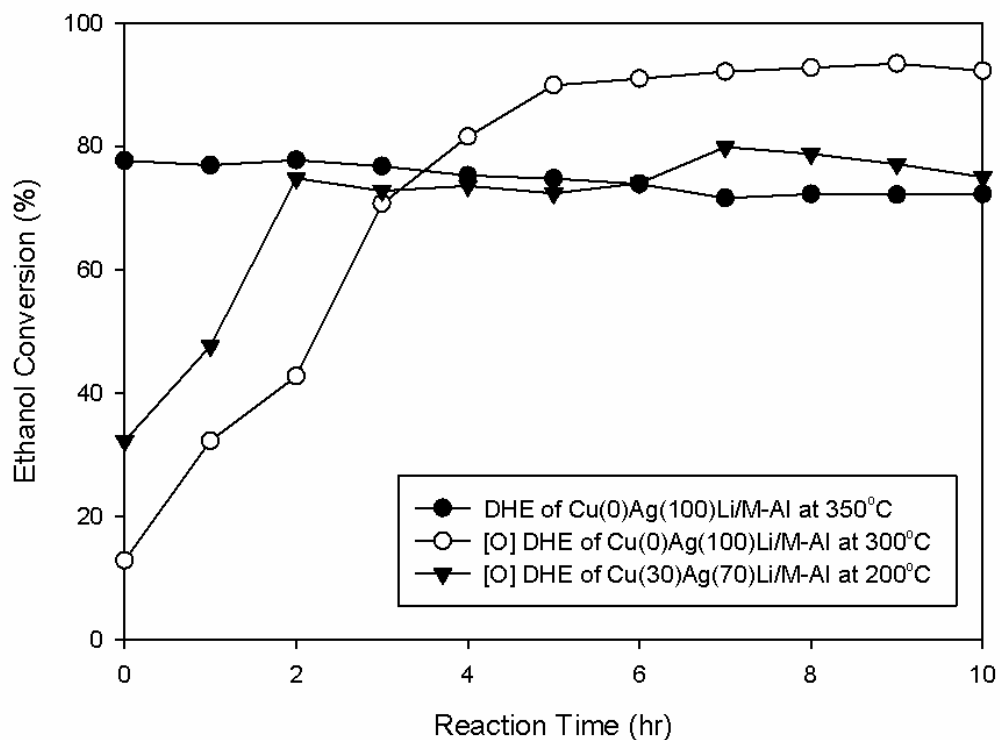


Figure 5. 25 Ethanol conversion of 3 excellent activity catalysts in time-on-stream system.

As the calculated ethanol conversion, only Cu(30)Ag(70)Li/M-Al that studied in oxidative dehydrogenation reaction at 200°C gave the ethanol conversion of time-on-stream system greater than of temperature programmed system. This discovery may be associated with temperature dependence. In other words, Cu(0)Ag(100)Li/M-Al in both oxidative dehydrogenation at 300°C and dehydrogenation at 350°C depends on the reaction time parameter stronger than reaction temperature parameter.

Table 5. 13 The ethanol conversion of chosen catalysts in temperature programmed and time-on-stream system.

Catalysts	Ethanol conversion (%)	
	Temperature programmed	Time-on-stream
Cu(0)Ag(100)Li/M-Al in DHE at 350°C	95.26	74.63
Cu(0)Ag(100)Li/M-Al in [O] DHE at 300°C	98.32	71.92
Cu(30)Ag(70)Li/M-Al in [O] DHE at 200°C	59.27	68.89

The acetaldehyde yield of each catalysts through time-on-stream testing was selected as the most interesting consideration, which is displayed in **Figure 5.26**.

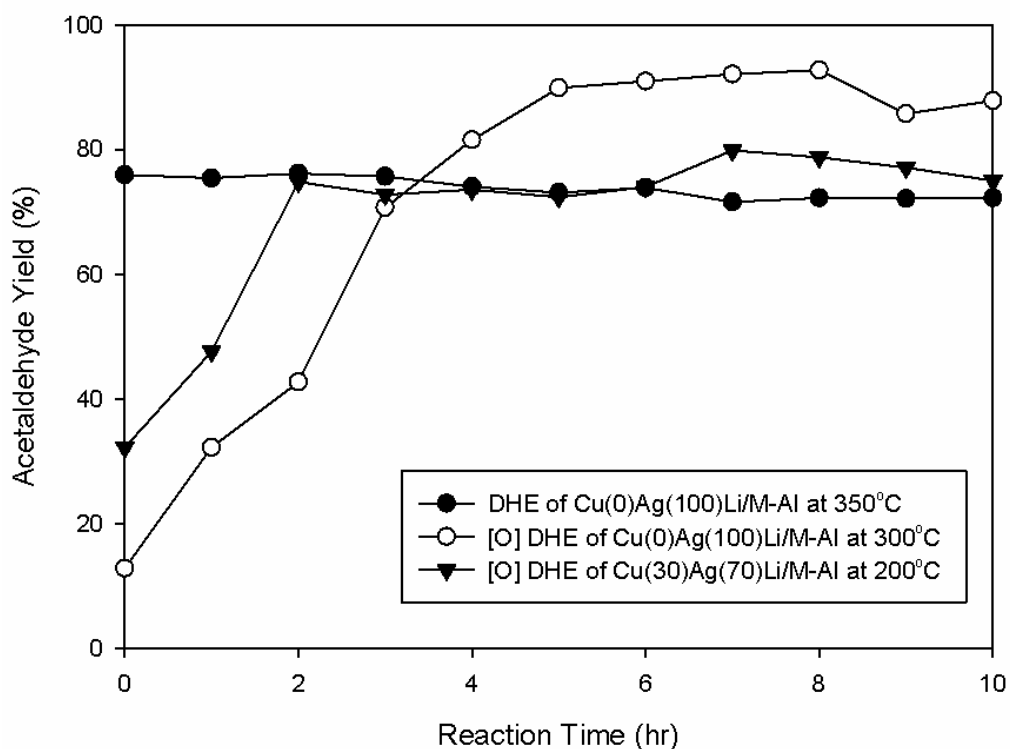


Figure 5. 26 Acetaldehyde yield of 3 excellent activity catalysts in time-on-stream system.

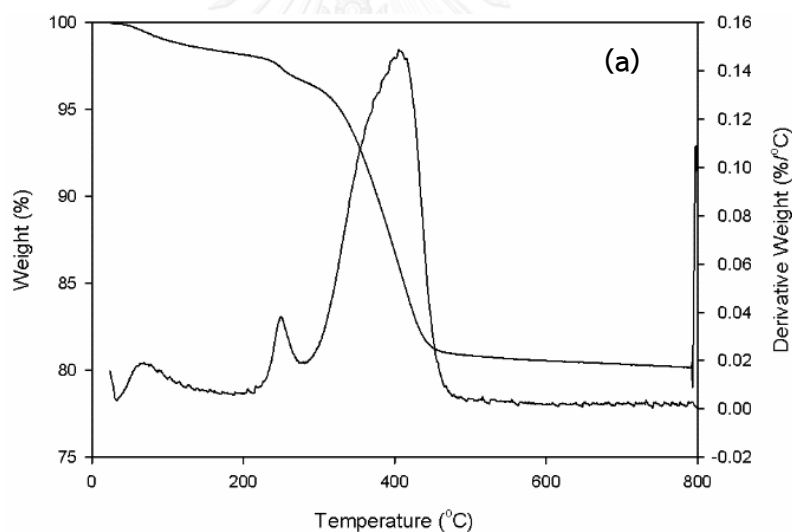
With thoroughly 10 hr of time-on-stream testing, these 3 chosen catalysts at its suitable temperature gave almost 100% acetaldehyde selectivity. Hence, the %yield of acetaldehyde was similar to value of %ethanol conversion. As depicted in **Figure 5.26**, acetaldehyde yield was reported as the function of time. From the results, it can

be considered that Cu(0)Ag(100)Li/M-Al, which reacting in oxidative dehydrogenation at 300°C demonstrated the greatest acetaldehyde yield since using through the reaction for 5 hr and reached 89.90% of acetaldehyde yield (the average yield of reaction time 5 to 10 hr) when it was used for 10 hr.

5.4 Characterization of spent catalysts after reaction

5.4.1 Thermogravimetric analysis (TGA)

The thermal decomposition of chosen catalysts after being used in the dehydrogenation and oxidative dehydrogenation reactions for continuous 10 hr has been examined through thermogravimetric analysis (TGA). The decomposition trend of each catalyst is depicted in **Figure 5.27**.



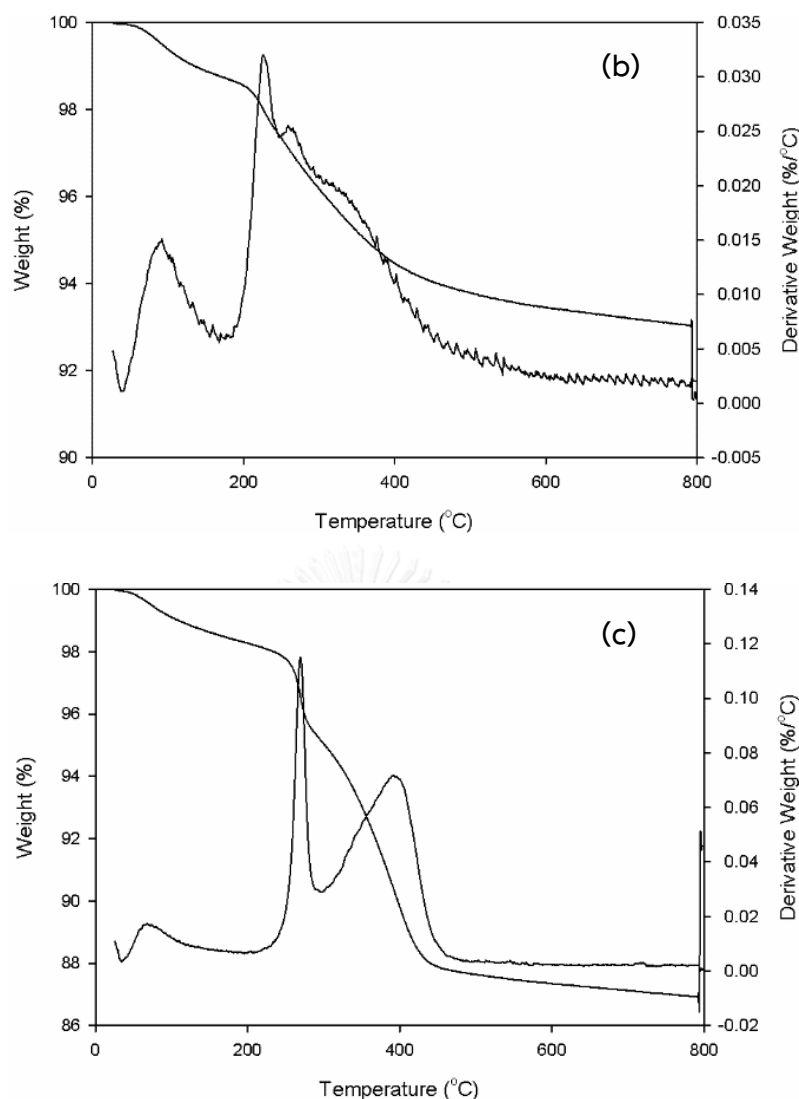


Figure 5. 27 TGA curves in air atmosphere of spent catalysts.

- (a) Cu(0)Ag(100)Li/M-Al in dehydrogenation reaction at 350°C,
 (b) Cu(0)Ag(100)Li/M-Al in oxidative dehydrogenation at 300°C, and
 (c) Cu(30)Ag(70)Li/M-Al in oxidative dehydrogenation at 200°C.

As seen in **Figure 5.27**, the slight weight loss of all spent catalysts below 200°C was due to the removal of physically adsorbed water and moisture in each catalyst. The weight loss at higher temperature (ca. 200 to 800°C) found that all TGA curves consisting 2 stages of decomposition via coke formation. Moreover, the amount of coke found on catalyst surface can be examined in **Table 5.10** as follows;

Table 5. 14 The amount of coke formation of spent catalysts after 10 hr.

Catalysts and their conditions	Temperature (°C)	Weight (%)	The amount of coke formation (%)
Cu(0)Ag(100)Li/M-Al in dehydrogenation at 350°C	200	98.15	17.98
Cu(0)Ag(100)Li/M-Al in oxidative dehydrogenation at 300°C	800	80.17	
Cu(0)Ag(100)Li/M-Al in oxidative dehydrogenation at 300°C	200	98.55	5.51
Cu(30)Ag(70)Li/M-Al in oxidative dehydrogenation at 200°C	800	93.04	
Cu(30)Ag(70)Li/M-Al in oxidative dehydrogenation at 200°C	200	98.27	11.35
Cu(30)Ag(70)Li/M-Al in oxidative dehydrogenation at 200°C	800	86.92	

At this point, the amount of coke formation on spent catalysts can be ordering from high to low coke found of: Cu(0)Ag(100)Li/M-Al in dehydrogenation reaction at 350°C > Cu(30)Ag(70)Li/M-Al in oxidative dehydrogenation at 200°C > Cu(0)Ag(100)Li/M-Al in oxidative dehydrogenation at 300°C. This result is could be said that Ag-contained catalysts can prevent the coke formation that conclude from lowest coke formation of only 5.5% of Cu(0)Ag(100)Li/M-Al catalyst in oxidative dehydrogenation reaction.

However, these coke formation of catalysts from TGA profiles can be compared between oxidative dehydrogenation that oxygen is involved and dehydrogenation without oxygen. From the comparison, it can be confirmed that the presence of oxygen in oxidative dehydrogenation improves the resistance ability of the thermal decomposition by carbon blocking the active surface that has already been discussed in **section 5.2.2**.

CHAPTER VI

CONCLUSIONS AND RECOMMENDATION

6.1 Conclusions

In the present study, the effect of bimetallic copper and silver with various weight ratios (Cu:Ag of 100:0, 70:30, 50:50, 30:70, 0:100) supported on mixed-phase of γ - and χ - Al_2O_3 prepared via thermal decomposition method of synthesis support and incipient wetness impregnation method of metal loading catalysts was studied. The characterization techniques were used to investigate the physiochemical properties, basicity and redox behaviors of Cu-AgLi supported on alumina catalysts. Moreover, to study the effect of oxygen as a co-feed reactant that presented by reaction testing of ethanol dehydrogenation in both anaerobic and aerobic conditions at the same temperature range of 200 to 400°C and pressure of 1 atm. The ethanol conversion, acetaldehyde selectivity, and acetaldehyde yield were all calculated and used to find the highest catalytic activity catalysts for further stability study. Hence, the stability of the chosen catalysts in the long reaction time were studied by running the reaction in time-on-stream for 10 hr at the specific conditions of each excellent activity catalysts. The deactivation of spent catalysts from coke formation after running time-on-stream were measured via TGA technique. Therefore, the research studied can be summarized the results that concluded as follows:

- 1) A number of active species (Ag^+ , $\text{Ag}_n^{\delta+}$, and Cu^{2+}) directly affect the performance of the catalysts in dehydrogenation for both with/without oxygen co-feed. The results are catalytic activity increased when Cu:Ag weight ratio decreased. Because of the amount of the active species in copper metal are much lower than in Ag metal (Cu species appeared lower intensity in H_2 -TPR, UV-vis, and XPS profiles) so Cu-AgLi/ Al_2O_3 had more active sites when increased Ag loading. However, the advantage of bimetallic Cu-Ag catalysts is the weaker interaction between metal and alumina support or easily charge transfer that is the good redox properties.

- 2) The excellent performance catalysts are Cu(0)Ag(100)Li/M-Al that given the highest %yield and ethanol conversion at all reaction temperatures of dehydrogenation reaction study (the highest acetaldehyde yield was existed at 350°C of 81%). Cu(0)Ag(100)Li/M-Al also displays the highest value of acetaldehyde yield in oxidative dehydrogenation that gives the highest value at 300°C of 92%.
- 3) Focusing on the low-temperature condition to reduce the thermal supply, bimetallic copper and silver that represent in Cu(30)Ag(70)Li/M-Al, it showed the outstanding yield at 250°C of 59% acetaldehyde yield compared with other weight ratios of Cu and Ag in catalysts. The excellent catalytic performance because of its highest basicity that can be detected by the CO₂-TPD technique of 285 μmole CO₂ g⁻¹ cat. But not only the basicity that effect to the activity, but the concentration of active sites still has effects to promote the reaction result, too.
- 4) Ag-contained catalysts can prevent the coke formation compared with the bimetallic Cu and Ag that is concluded from the lowest coke formation of only 5.5% via TGA technique of Cu(0)Ag(100)Li/M-Al catalyst. In addition, oxygen presence in the reaction can regenerate active sites of metal in the catalysts.

6.2 Recommendations

- 1) IR of carbon dioxide should be further characterized to deeper understand the surface structures of basic sites. CO₂ is adsorbed on catalysts in different forms: bidentate carbonate, unidentate carbonate, and bicarbonate [64] that different type of basic catalysts can be distinguish CO₂ interaction form.
- 2) The IR of pyrrole should be analyzed for measurement of the strength of the basic sites.
- 3) The high resolution TEM, including selected-area electron diffraction (SAED) should be verified to confirm the morphologies observed by SEM and TEM.
- 4) In order to apply this research to industry scale, the bioethanol is an interesting resource for studied in oxidative dehydrogenation reaction.
- 5) The reduction prior the reaction should be further studied, in the point of temperature effect and chemical reduction, to finding the optimum condition for this catalysts system.
- 6) The catalytic stability should be further investigated more than 10 hr in order to apply the good activity and stability catalysts to the commercial usage.

REFERENCES

1. Liu, P., et al., On the metal-support synergy for selective gas-phase ethanol oxidation over $\text{MgCuCr}_2\text{O}_4$ supported metal nanoparticle catalysts. *Journal of Catalysis*, 2015. **331**: p. 138-146.
2. Gallo, J.M.R., J.M.C. Bueno, and U. Schuchardt, Catalytic Transformations of Ethanol for Biorefineries. *JOURNAL OF THE BRAZILIAN CHEMICAL SOCIETY*, 2014. **25**: p. 2229-2243.
3. Freitas, I.C., et al., Effect of Cu content on the surface and catalytic properties of Cu/ZrO_2 catalyst for ethanol dehydrogenation. *Journal of Molecular Catalysis A: Chemical*, 2014. **381**: p. 26-37.
4. Research, T.M., Acetaldehyde Market - Global Industry Analysis, Size, Share, Trends and Forecast 2015 - 2023. 2015.
5. Xu, J., et al., Silver/hydroxyapatite foam as a highly selective catalyst for acetaldehyde production via ethanol oxidation. *Catalysis Today*, 2016.
6. Poreddy, R., C. Engelbrekt, and A. Riisager, Copper oxide as efficient catalyst for oxidative dehydrogenation of alcohols with air. *Catalysis Science & Technology*, 2015. **5**: p. 2467-2477.
7. Glinrun, T., et al., Improvement of propane oxidation activity over $\text{Pt/Al}_2\text{O}_3$ by the use of MIXED γ - and χ - Al_2O_3 supports. . *Reaction Kinetics, Mechanisms and Catalysis* 2010. **100**: p. 441-448.
8. Meephoka, C., et al., Effect of phase composition between nano γ - and χ - Al_2O_3 on $\text{Pt/Al}_2\text{O}_3$ catalyst in CO oxidation. *Catalysis Communications*, 2008. **9**(4): p. 546-550.
9. Sun, X., et al., $\text{Au/Cu-Fe-La-Al}_2\text{O}_3$: A highly active, selective and stable catalysts for preferential oxidation of carbon monoxide. *Applied Catalysis A: General*, 2016. **527**: p. 19-29.

10. Almukhlifi, H.A. and R.C. Burns, Oxidative dehydrogenation of isobutane to isobutene by pyrovanadates, $M_2V_2O_7$, where $M(II) = Mn, Co, Ni, Cu$ and Zn , and Co_2VO_4 and ZnV_2O_4 : The effect of gold nanoparticles. *Journal of Molecular Catalysis A: Chemical*, 2015. **408**: p. 26-40.
11. Ochoa-Hernández, C., et al., Hydrocarbons production through hydrotreating of methyl esters over Ni and Co supported on SBA-15 and Al-SBA-15. *Catalysis Today*, 2013. **210**: p. 81-88.
12. Lippits, M.J. and B.E. Nieuwenhuys, Direct conversion of ethanol into ethylene oxide on copper and silver nanoparticles Effect of addition of CeO_x and Li_2O . *catalysis today*, 2010. **154**: p. 127-132.
13. Cowell, J.J., et al., Bonding and reactivity of styrene on Cu(110): heterogeneous alkene epoxidation without the use of silver. *Surface Science*, 1999. **437(1-2)**: p. 1-8.
14. Sato, A.G., et al., Site-selective ethanol conversion over supported copper catalysts. *Catalysis Communications*, 2012. **26**: p. 122-126.
15. Salker, A.V. and M.S.F. Desai, CO-NO/O₂ redox reactions over Cu substituted cobalt oxide spinels. *Catalysis Communications*, 2016. **87**: p. 116-119.
16. Reina, T.R., et al., WGS and CO-PrOx reactions using gold promoted copper-ceria catalysts: "Bulk $CuOCeO_2$ vs. $CuOCeO_2/Al_2O_3$ with low mixed oxide content". *Applied Catalysis B: Environmental*, 2016. **197**: p. 62-72.
17. Hidalgo, J.M., et al., (V)/Hydrotalcite, (V)/ Al_2O_3 , (V)/ TiO_2 and (V)/SBA-15 catalysts for the partial oxidation of ethanol to acetaldehyde. *Journal of Molecular Catalysis A: Chemical*, 2016. **420**: p. 178-189.
18. Pereira, S.C., et al., Vanadium-lithium alumina a potential additive for coke oxidation by CO_2 in the presence of O_2 during FCC catalyst regeneration. *Applied Catalysis B: Environmental*, 2016. **196**: p. 117-126.
19. WACHS, I.E. and R.J. MADIX, THE OXIDATION OF METHANOL ON A SILVER (110) CATALYST *Surface Science*, 1978. **76**: p. 531-558.

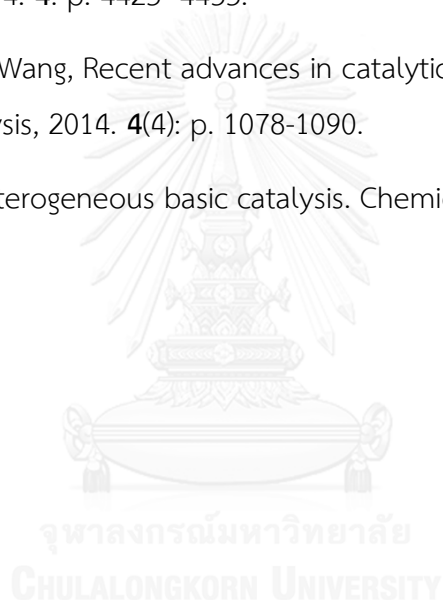
20. Kareem, T.A. and A. Kaliani, Synthesis and thermal study of octahedral silver nano-plates in polyvinyl alcohol (PVA). *Arabian Journal of Chemistry*, 2011. **4**: p. 325-331.
21. Lim, S.P., et al., Silver/titania nanocomposite-modified photoelectrodes for photoelectrocatalytic methanol oxidation. *International Journal of Hydrogen Energy*, 2014. **39**(27): p. 14720-14729.
22. Kolobova, E., et al., Formation of silver active states in Ag/ZSM-5 catalysts for CO oxidation. *Fuel*, 2014. **138**: p. 65-71.
23. Chua, Y.S., et al., Alkali Metal Hydride Modification on Hydrazine Borane for Improved Dehydrogenation. *the journal of physical chemistry*, 2014. **118**(21): p. 11244-11251.
24. Soderberg, T. Section 16.4: Hydrogenation/dehydrogenation reactions of carbonyls, imines, and alcohols. *Organic Chemistry With a Biological Emphasis (Soderberg)*.
25. Hosseini, Z., M. Taghizadeh, and F. Yaripour, Synthesis of nanocrystalline γ - Al_2O_3 by sol-gel and precipitation methods for methanol dehydration to dimethyl ether. *Journal of Natural Gas Chemistry* 2011. **20**(2): p. 128-134.
26. Khom-in, J., et al., Dehydration of methanol to dimethyl ether over nanocrystalline Al_2O_3 with mixed γ - and χ -crystalline phases. *Catalysis Communications*, 2008. **9**(10): p. 1955-1958.
27. Chaitree, W., et al., Effect of nanocrystalline χ - Al_2O_3 structure on the catalytic behavior of $\text{Co}/\text{Al}_2\text{O}_3$ in CO hydrogenation. *Catalysis Today* 2011. **164**(1): p. 302-307.
28. Li, M.M.-J., et al., Enhanced CO_2 hydrogenation to methanol over CuZn nanoalloy in Ga modified Cu/ZnO catalysts. *Journal of Catalysis*, 2016. **343**: p. 157-167.
29. Introduction to acetaldehyde. 2000.
30. Acetaldehyde. in *American Conference of Governmental Industrial Hygienists*. 1998. United States National Library of Medicine.

31. Sam, k. Acetaldehyde Product Production from Organic Chemical Substance Acetylene. Synthetic Organic Chemicals 2012; Available from: <http://www.inclusive-science-engineering.com/acetaldehyde-product-production-from-organic-chemical-substance-acetylene/>.
32. Acetaldehyde, in Chemical Economics Handbook. 2013.
33. Eckert, M., et al., Acetaldehyde, in Ullmann's Encyclopedia of Industrial Chemistry. 2000, Wiley-VCH Verlag GmbH & Co. KGaA.
34. Wittayakhun, J. and N. Krisadanurak, Catalysis: Fundamentals and Application, in education. 2004, Thammasart university: Thammasart university publishing.
35. Book, g.d., Lower and Upper Explosive Limits for Flammable Gases and Vapors (LEL/UEL). 2001.
36. Acetaldehyde Market - Global Industry Analysis, Size, Share, Trends and Forecast 2015 - 2023. 2016; Available from: <http://www.transparencymarketresearch.com/acetaldehyde-market.html>.
37. Dutov, V.V., et al., Silica-supported silver-containing OMS-2 catalysts for ethanol oxidative dehydrogenation. Catalysis Today, 2016. **278, Part 1**: p. 164-173.
38. Khan, M.T., S. Halligudi, and S. Shukla, Hydration of acetylene to acetaldehyde using K [RuIII (EDTA-H) Cl] 2H₂O. Journal of molecular catalysis, 1990. **58(3)**: p. 299-305.
39. Mendelovici, L. and J.H. Lunsford, Partial oxidation of ethane to ethylene and acetaldehyde over a supported molybdenum catalyst. Journal of catalysis, 1985. **94(1)**: p. 37-50.
40. Taatjes, C.A., et al., Enols are common intermediates in hydrocarbon oxidation. Science, 2005. **308(5730)**: p. 1887-1889.
41. Matveev, K., et al., Kinetics of ethylene oxidation into acetaldehyde with phosphomolybdenovanadic heteropoly acids in the presence of Pd (2) aqua-complex. Kinetika i Kataliz, 1977. **18(2)**: p. 380-386.

42. Mao, C.-F. and M.A. Vannice, High surface area α -aluminas III. Oxidation of ethylene, ethylene oxide, and acetaldehyde over silver dispersed on high surface area α -alumina. *Applied Catalysis A: General*, 1995. **122**(1): p. 61-76.
43. JOSE, S. Acetaldehyde: A Global Strategic Business Report. Global Acetaldehyde Market to Reach 1.2 Million Tons by 2015, According to a New Report 2016 [cited 2016 Friday, July 1]; Available from: http://www.prweb.com/releases/acetaldehyde/acetice_ether_pyridine/prweb8070299.htm.
44. Acetaldehyde, in CHINA REPORT (CHINA). 2012.
45. Global Industry Analysts, I. ACETALDEHYDE - A GLOBAL STRATEGIC BUSINESS REPORT. 2015 [cited 2015 March 15]; Available from: <http://www.strategyr.com/pressMCP-2007.asp>.
46. Thuy, T.H.N., et al., Techno-economic and Environmental Assessment of Bioethanol Based Chemical Process: A Case Study on Ethyl Acetate. *Environmental Progress & Sustainable Energy* 2011. **30**(4): p. 675-684.
47. Volanti, D.P., et al., Insight into Copper-Based Catalysts: Microwave-Assisted Morphosynthesis, In Situ Reduction Studies, and Dehydrogenation of Ethanol. *ChemCatChem*, 2011. **3**: p. 839-843.
48. Sato, A.G., et al., Effect of the ZrO_2 phase on the structure and behavior of supported Cu catalysts for ethanol conversion. *Journal of Catalysis*, 2013. **307**: p. 1-17.
49. Janlamool, J. and B. Jongsomjit, Oxidative dehydrogenation of ethanol over $AgLi-Al_2O_3$ catalysts containing different phases of alumina. *Catalysis Communications*, 2015. **70**: p. 49-52.
50. M.J. Lippits, R.R.H. Boer Iwem, and B.E. Nieuwenhuys, A comparative study of oxidation of methanol on $\gamma-Al_2O_3$ supported group IB metal catalysts. *Catalysis Today*, 2009. **145**: p. 27-33.

51. Lippits, M.J. and B.E. Nieuwenhuys, Direct conversion of ethanol into ethylene oxide on gold-based catalysts Effect of CeO_x and Li_2O addition on the selectivity. *catalysis today*, 2010. **274**: p. 142-149.
52. Wannaborworn, M., P. Praserthdam, and B. Jongsomjit, A Comparative Study of Solvothermal and Sol-Gel-Derived Nanocrystalline Alumina Catalysts for Ethanol Dehydration. *Journal of Nanomaterials* 2015.
53. Goodarznia, S. and K.J. Smith, The effect of Cu loading on the formation of methyl formate and C_2 -oxygenates from CH_3OH and CO over K- or Cs-promoted Cu-MgO catalysts. *Journal of Molecular Catalysis A: Chemical*, 2012. **353–354**: p. 58-66.
54. Hao Zhang, G.W., Da Chen, Xiaojun Lv, and Jinghong Li, Tuning Photoelectrochemical Performances of Ag-TiO₂ Nanocomposites via Reduction/Oxidation of Ag. *CHEMISTRY OF MATERIALS*, 2008. **20**: p. 6543–6549.
55. Phung, T.K., et al., A study of commercial transition aluminas and of their catalytic activity in the dehydration of ethanol. *Journal of Catalysis*, 2014. **311**: p. 102-113.
56. Krutpijit, C. and B. Jongsomjit, Catalytic Ethanol Dehydration Over Different Acid-Activated Montmorillonite Clays. *Journal of Oleo Science*, 2016. **65(4)**: p. 347-355.
57. Hong-KuiWang, et al., Ag-Cu Bimetallic Nanoparticles Prepared by Microemulsion Method as Catalyst for Epoxidation of Styrene. *Journal of Nanomaterials*, 2012. **2012**.
58. Mamontov, G.V., et al., Ethanol dehydrogenation over Ag-CeO₂/SiO₂ catalyst: Role of Ag-CeO₂ interface. *Applied Catalysis A: General*, 2016. **528**: p. 161-167.
59. Kim, N.R., et al., Ag-Cu Bimetallic Nanoparticles with Enhanced Resistance to Oxidation: A Combined Experimental and Theoretical Study. *the journal of physical chemistry*, 2014. **118**: p. 26324-26331.

60. Lu, Z., et al., Methanol dehydrogenation to methyl formate catalyzed by SiO₂-, hydroxyapatite-, and MgO-supported copper catalysts and reaction kinetics. *Journal of Industrial and Engineering Chemistry*, 2015. **31**: p. 301-308.
61. Santacesaria, E., et al., Ethanol dehydrogenation to ethyl acetate by using copper and copper chromite catalysts. *Chemical Engineering Journal*, 2012. **179**: p. 209-220.
62. DeWilde, J.F., C.J. Czopinski, and A. Bhan, Ethanol Dehydration and Dehydrogenation on γ -Al₂O₃: Mechanism of Acetaldehyde Formation. *American Chemical Society*, 2014. **4**: p. 4425-4433.
63. Sun, J. and Y. Wang, Recent advances in catalytic conversion of ethanol to chemicals. *ACS Catalysis*, 2014. **4**(4): p. 1078-1090.
64. Hattori, H., Heterogeneous basic catalysis. *Chemical Reviews*, 1995. **95**(3): p. 537-558.



APPENDIX A

CALCULATION OF PHASE COMPOSITION OF ALUMINA

The γ - and χ - Al_2O_3 that used as support was resolved by the area of characteristic peak of chi phase at 43° . The calibration curve obtaining from the XRD patterns of the physical mixture between native γ - and χ -phase with different contents was shown below. The amount of chi-phase of synthesis sample was plotted and showed as a square dot at nearly 50% of calibration curve.

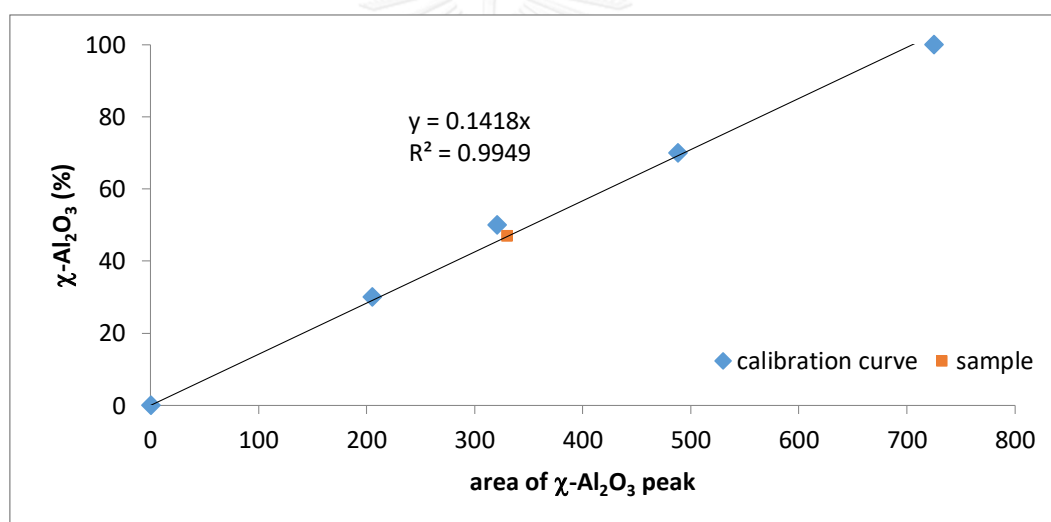


Figure A. 1 The calibration curve of chi-phase alumina obtained by XRD peaks at 2θ of 43° .

APPENDIX B

CALCULATION OF CATALYST PREPARATION

The catalysts were synthesis by incipient wetness impregnation method for different ratio of copper and silver including 100:0, 70:30, 50:50, 30:70, and 0:100. All catalysts contain 5 wt% of metal (Cu and Ag) and 0.7 wt% of Li. The calculation of the preparation are showed as follows:

<u>Reagent:</u>	-	Copper (II) nitrate ($\text{Cu}(\text{NO}_3)_2 \cdot 2.5 \text{H}_2\text{O}$)		
		Molecular weight	=	232.56 g/mol
		Copper (Cu) atomic weight	=	63.55 g/mol
	-	Silver (I) nitrate (AgNO_3)		
		Molecular weight	=	169.87 g/mol
		Silver (Ag) atomic weight	=	107.87 g/mol
	-	Lithium (I) nitrate (LiNO_3)		
		Molecular weight	=	68.95 g/mol
		Lithium (Li) atomic weight	=	6.94 g/mol

Calculation: Based on 1 g of the catalyst, so metal 5 wt% = 0.05 g
 Li 0.7 wt% = 0.007 g
 Al_2O_3 support = 1 - (0.05 + 0.007)
 = 0.0943 g

For Cu(100)Ag(0)Li/M-Al catalyst

Weight ratio of Cu:Ag = 100:0, so

There is 63.55 g. of Cu in 232.56 g. of $\text{Cu}(\text{NO}_3)_2 \cdot 2.5 \text{H}_2\text{O}$ reagent.

There is 0.05 g. of Cu in $\frac{0.05 \times 232.56}{63.55}$ g. of $\text{Cu}(\text{NO}_3)_2 \cdot 2.5 \text{H}_2\text{O}$ reagent.
 or in 0.183 g. of $\text{Cu}(\text{NO}_3)_2 \cdot 2.5 \text{H}_2\text{O}$ reagent.

There is 6.94 g. of Li in 68.95 g. of LiNO_3 reagent.

There is 0.007 g. of Li in $\frac{0.007 \times 68.95}{6.94}$ g. of LiNO_3 reagent.
 or in 0.0695 g. of LiNO_3 reagent.

For Cu(70)Ag(30)Li/M-Al catalyst

Weight ratio of Cu:Ag = 70:30, so

There is 63.55 g. of Cu in 232.56 g. of $\text{Cu}(\text{NO}_3)_2 \cdot 2.5 \text{H}_2\text{O}$ reagent.

There is (0.05×0.7) g. of Cu in $\frac{0.05 \times 0.7 \times 232.56}{63.55}$ g. of $\text{Cu}(\text{NO}_3)_2 \cdot 2.5 \text{H}_2\text{O}$ reagent.
or in 0.128 g. of $\text{Cu}(\text{NO}_3)_2 \cdot 2.5 \text{H}_2\text{O}$ reagent.

There is 107.87 g. of Ag in 169.87 g. of AgNO_3 reagent.

There is (0.05×0.3) g. of Ag in $\frac{0.05 \times 0.3 \times 169.87}{107.87}$ g. of AgNO_3 reagent.
or in 0.0236 g. of AgNO_3 reagent.

There is 6.94 g. of Li in 68.95 g. of LiNO_3 reagent.

There is 0.007 g. of Li in $\frac{0.007 \times 68.95}{6.94}$ g. of LiNO_3 reagent.
or in 0.0695 g. of LiNO_3 reagent.

For Cu(50)Ag(50)Li/M-Al catalyst

Weight ratio of Cu:Ag = 50:50, so

There is 63.55 g. of Cu in 232.56 g. of $\text{Cu}(\text{NO}_3)_2 \cdot 2.5 \text{H}_2\text{O}$ reagent.

There is (0.05×0.5) g. of Cu in $\frac{0.05 \times 0.5 \times 232.56}{63.55}$ g. of $\text{Cu}(\text{NO}_3)_2 \cdot 2.5 \text{H}_2\text{O}$ reagent.
or in 0.0915 g. of $\text{Cu}(\text{NO}_3)_2 \cdot 2.5 \text{H}_2\text{O}$ reagent.

There is 107.87 g. of Ag in 169.87 g. of AgNO_3 reagent.

There is (0.05×0.5) g. of Ag in $\frac{0.05 \times 0.5 \times 169.87}{107.87}$ g. of AgNO_3 reagent.
or in 0.0394 g. of AgNO_3 reagent.

There is 6.94 g. of Li in 68.95 g. of LiNO_3 reagent.

There is 0.007 g. of Li in $\frac{0.007 \times 68.95}{6.94}$ g. of LiNO_3 reagent.
or in 0.0695 g. of LiNO_3 reagent.

For Cu(30)Ag(70)Li/M-Al catalyst

Weight ratio of Cu:Ag = 30:70, so

There is 63.55 g. of Cu in 232.56 g. of $\text{Cu}(\text{NO}_3)_2 \cdot 2.5 \text{H}_2\text{O}$ reagent.

There is (0.05×0.3) g. of Cu in $\frac{0.05 \times 0.3 \times 232.56}{63.55}$ g. of $\text{Cu}(\text{NO}_3)_2 \cdot 2.5 \text{H}_2\text{O}$ reagent.
or in 0.0549 g. of $\text{Cu}(\text{NO}_3)_2 \cdot 2.5 \text{H}_2\text{O}$ reagent.

There is 107.87 g. of Ag in 169.87 g. of AgNO_3 reagent.

There is (0.05×0.7) g. of Ag in $\frac{0.05 \times 0.7 \times 169.87}{107.87}$ g. of AgNO_3 reagent.
or in 0.0551 g. of AgNO_3 reagent.

There is 6.94 g. of Li in 68.95 g. of LiNO_3 reagent.

There is 0.007 g. of Li in $\frac{0.007 \times 68.95}{6.94}$ g. of LiNO_3 reagent.
or in 0.0695 g. of LiNO_3 reagent.

For Cu(0)Ag(100)Li/M-Al catalyst

Weight ratio of Cu:Ag = 0:100, so

There is 107.87 g. of Ag in 169.87 g. of AgNO_3 reagent.

There is 0.05 g. of Ag in $\frac{0.05 \times 169.87}{107.87}$ g. of AgNO_3 reagent.
or in 0.0787 g. of AgNO_3 reagent.

There is 6.94 g. of Li in 68.95 g. of LiNO_3 reagent.

There is 0.007 g. of Li in $\frac{0.007 \times 68.95}{6.94}$ g. of LiNO_3 reagent.
or in 0.0695 g. of LiNO_3 reagent.

Pore volume of mixed-phase Al_2O_3 support is $0.546 \text{ cm}^3/\text{g}$.

Therefore, the amount of deionized water added to alumina support is 0.546 ml to 1 g. of catalyst.

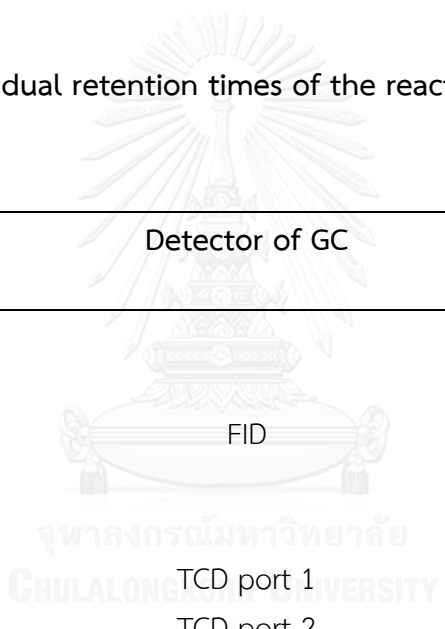
APPENDIX C

CALIBRATION CURVES

The composition and retention time of reactants, main product and byproducts gas were analyzed by a Shimadzu GC14B (DB5) gas chromatograph equipped with FID and a Shimadzu GC8A (molecular sieve 5A and Parapak Q) gas chromatography equipped with TCD.

The chromatogram distinguishes retention time of different chemicals that showed in **Table C.1**.

Table C. 1 The individual retention times of the reactant, main product, and byproducts.

Chemicals	Detector of GC	Retention time in chromatogram
Ethanol		4.4 min
Acetaldehyde		4.2 min
Ethylene		3.9 min
Acetone		4.6 min
Acetic acid		5.6 min
CO		5.8 min
CO ₂		1.9 min

The calibration curves were used for evaluating the mole of ethanol as a reactant gas, acetaldehyde as a main product, and ethylene, acetone, acetic acid, CO, and CO₂ as byproducts in both of oxidative dehydrogenation and dehydrogenation reactions. The calibration curves of their chemicals are illustrated in **Figure C.1-C.7** as follows;

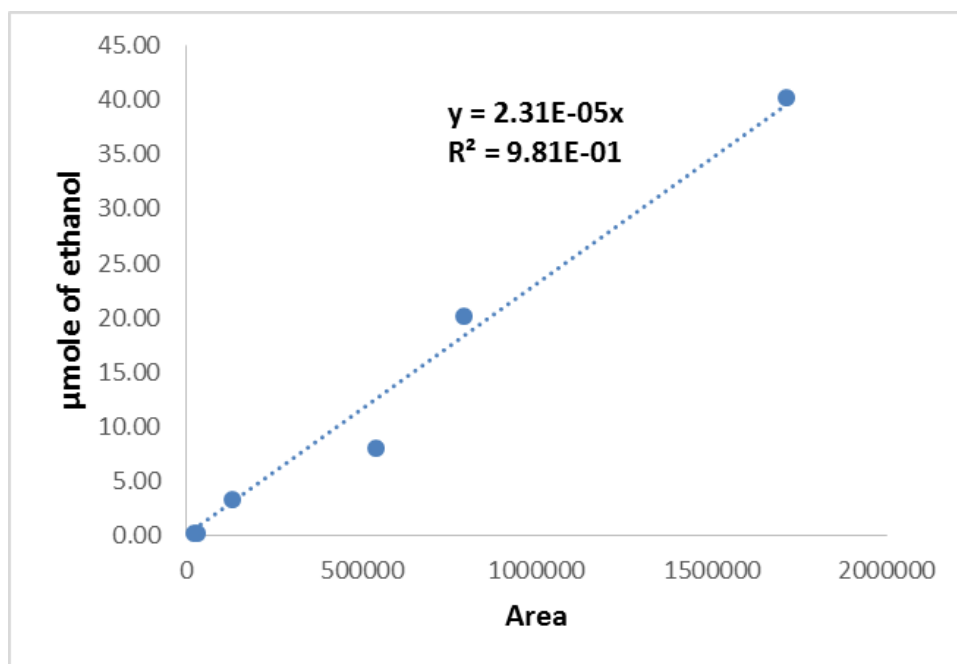


Figure C. 1 The calibration curve of ethanol.

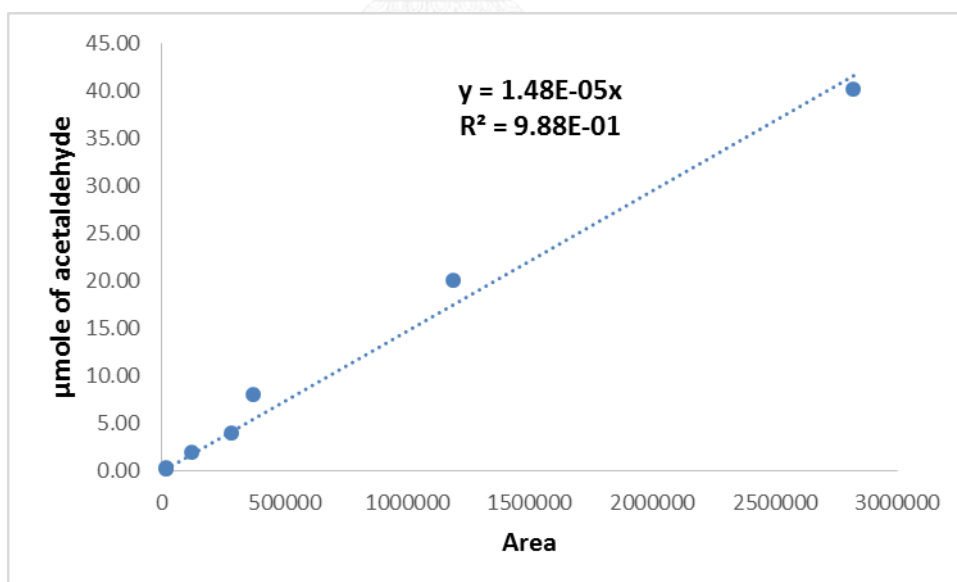


Figure C. 2 The calibration curve of acetaldehyde.

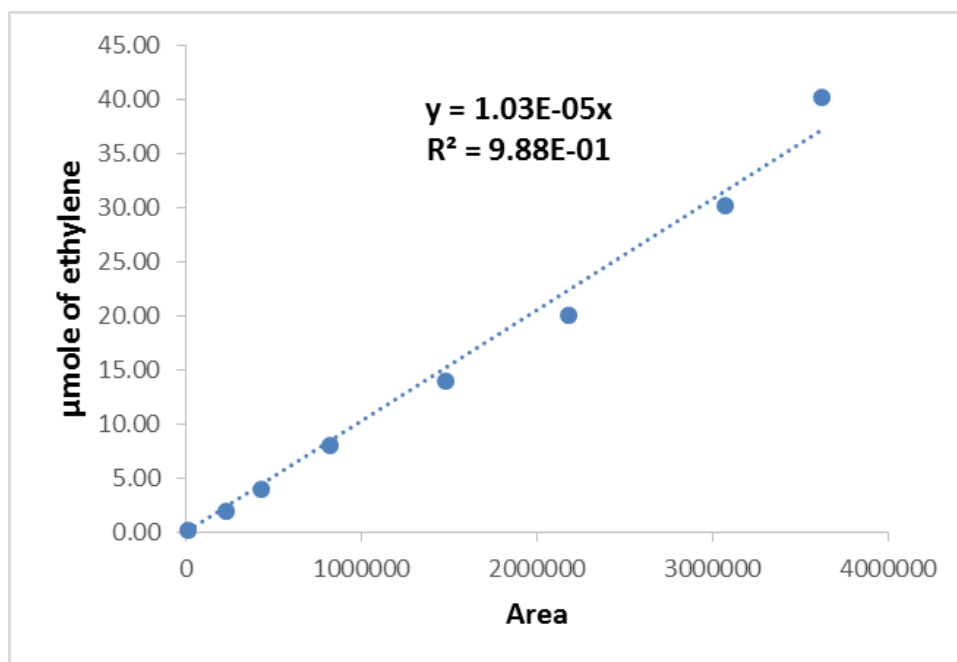


Figure C. 3 The calibration curve of ethylene.

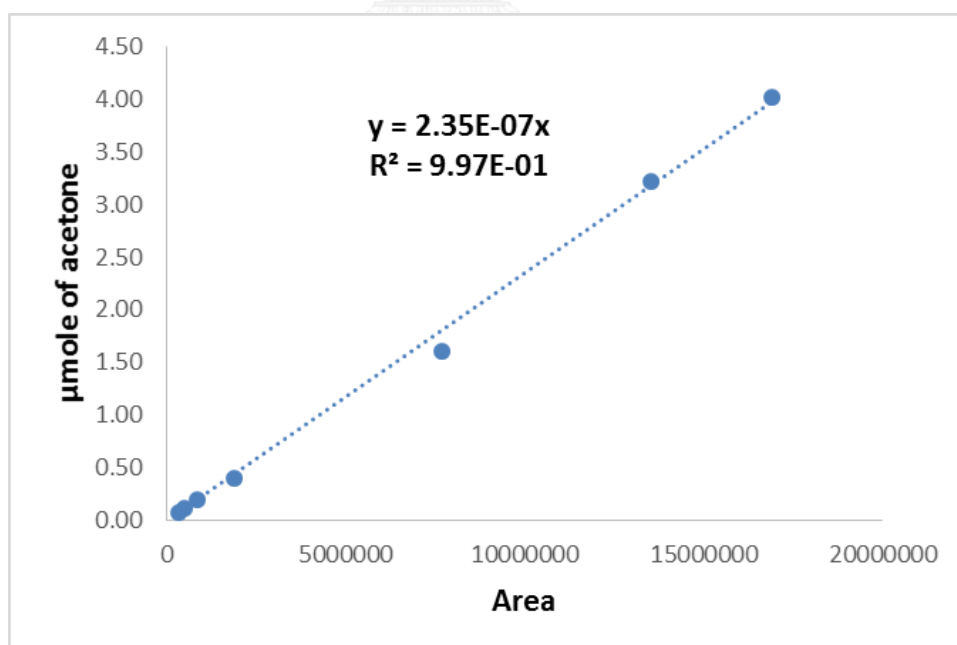


Figure C. 4 The calibration curve of acetone.

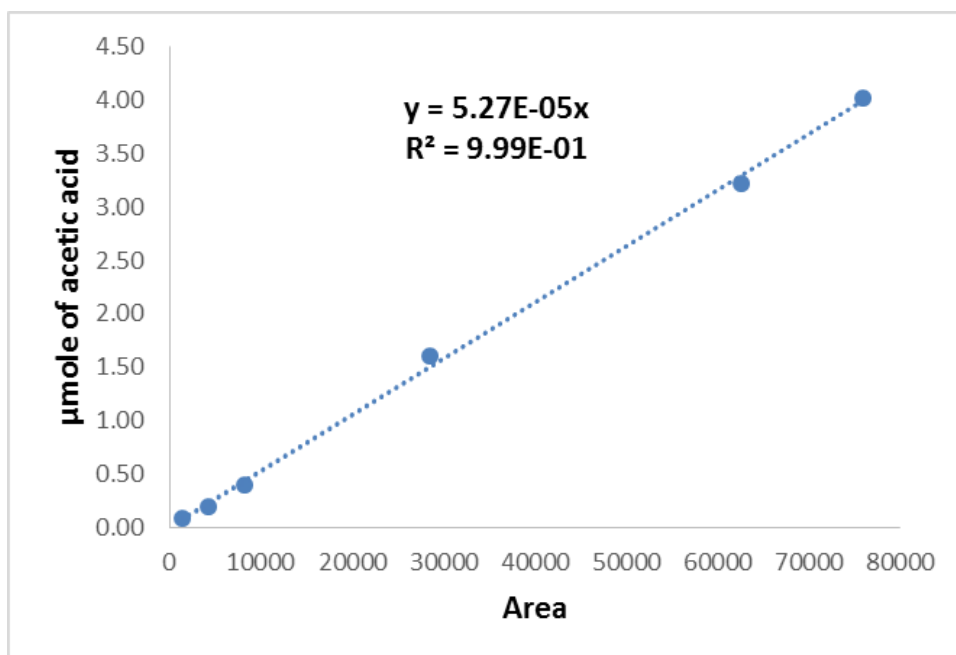


Figure C. 5 The calibration curve of acetic acid.

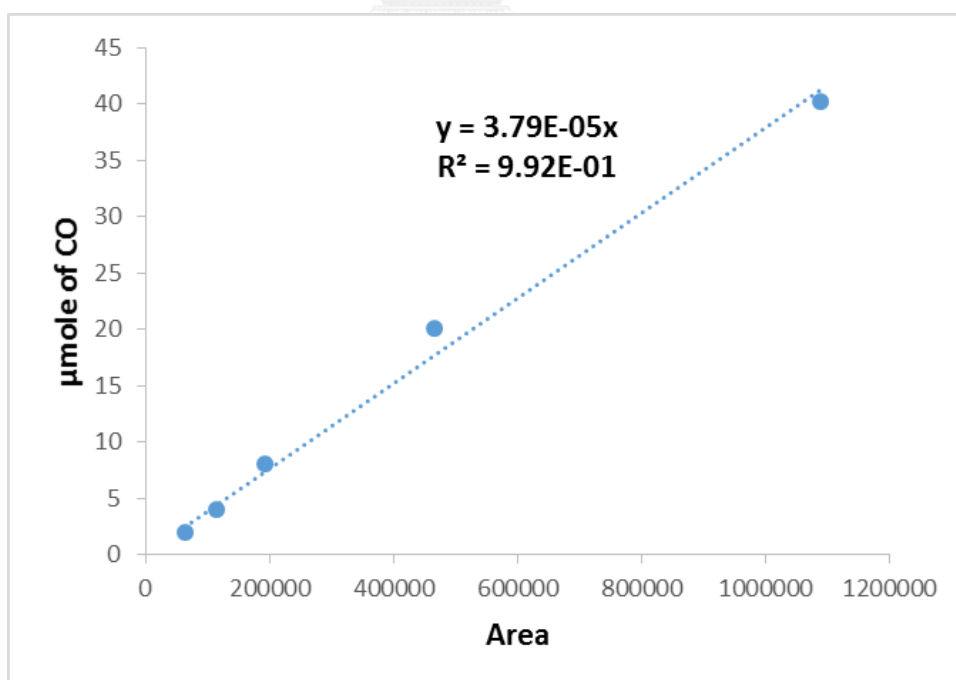


Figure C. 6 The calibration curve of carbon monoxide (CO).

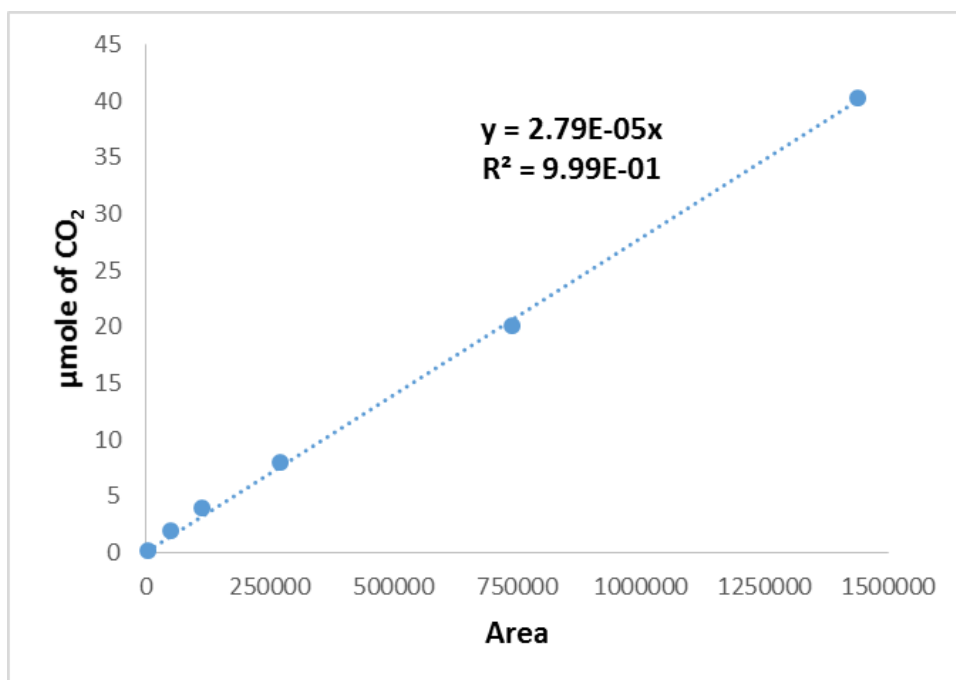
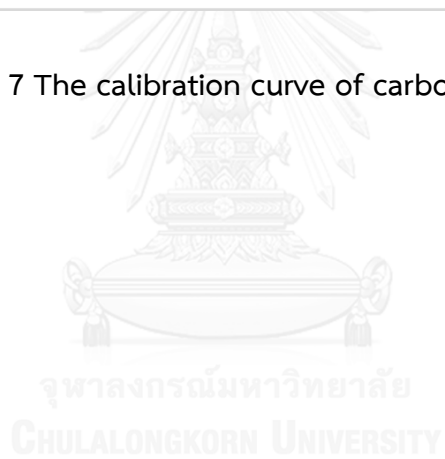


Figure C. 7 The calibration curve of carbon dioxide (CO₂).



APPENDIX D

CALCULATION OF TOTAL BASIC SITES OF CATALYSTS

The surface basicity and strength of basic site for catalysts can be computed from the CO₂-TPD profiles by following these steps.

Definition - the area of the CO₂-TPD profiles of each sample = A

The mole of CO₂ was determined from the calibration curve of CO₂ desorbed as following formula:

The mole of CO₂ (μmole) = 17.624 x A

Definition - Amount of each sample = B g.

The amount of basic sites of sample was determined in the range of temperature by this formula:

The basicity of sample (μmole CO₂/g cat.) = $\frac{\text{μmole of CO}_2 \text{ of the sample}}{\text{Amount of dry catalysts}}$
 = $\frac{17.624 \times A}{B}$

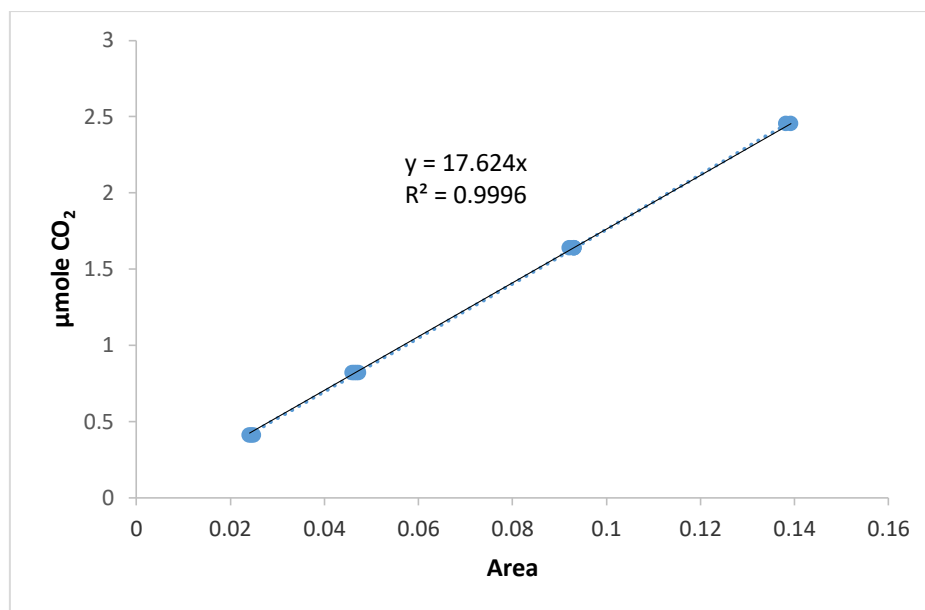
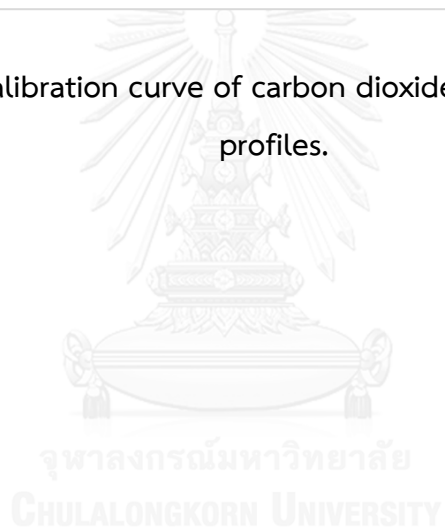


Figure D. 1 The calibration curve of carbon dioxide obtained from CO₂-TPD profiles.



APPENDIX E

CALCULATION OF CONVERSION, SELECTIVITY AND YIELD

The ethanol conversion was calculated as defined equations as follows:

$$\text{Conversion (\%)} = \frac{(\text{mole of ethanol feed} - \text{mole of ethanol reacted}) \times 100}{\text{mole of ethanol feed into the reactor}}$$

The activity of the catalysts in oxidative dehydrogenation and dehydrogenation reactions can be estimated by 2 choices; the first one is from the selectivity that defined as the moles of products formed with respect to total moles of all products, and another one is from the yield that defined as the results of selectivity and conversion. The selectivity and the yield were calculated as equations as follow:

$$\text{Acetaldehyde selectivity (\%)} = \frac{\text{mole of acetaldehyde produced}}{\text{mole of all products produced}} \times 100$$

$$\text{Acetaldehyde yield (\%)} = \frac{\text{selectivity of acetaldehyde} \times \text{conversion}}{100}$$

VITA

Miss Nasrada Sukarawan was born on September 1st, 1991 at Ramathibodi hospital, Phayathai district in Bangkok province, Thailand. She finished high school from Rittiyawannalai School in 2010 and graduated in Bachelor's degree from Department of Chemistry, Faculty of Science, Mahidol University, Thailand in April 2014. She has further studied in Master's degree at Department of Chemical Engineering, Faculty of Engineering, Chulalongkorn University since August 2014.

List of publication:

Nasrada Sukarawan, and Bunjerd Jongsomjit, "Effect of Copper Modification on Basicity of Silver-Lithium over Alumina Catalysts", proceeding of The 26th National Thai Institute of Chemical Engineering and Applied Science Conference (TICHE2016) and The 6th International Thai Institute of Chemical Engineering and Applied Science Conference (ITICHE2016), Bangkok, Thailand, 26-28 October, 2016.